COPI vesicle formation and *N*-myristoylation are targetable vulnerabilities of senescent cells

Domhnall McHugh[1,2], Bin Sun[1,2], Carmen Gutierrez-Muñoz[1,2], Fernanda Hernández-González[3,4,5], Massimiliano Mellone[6,+], Romain Guiho[7], Imanol Duran[1,2], Joaquim Pombo[1,2], Federico Pietrocola[8], Jodie Birch[1,2], Wouter W. Kallemeijn[9,10], Sanjay Khadayate[1,2], Gopuraja Dharmalingam[1,2], Santiago Vernia[1,2], Edward W. Tate[9,10], Juan Pedro Martínez-Barbera[7], Dominic J. Withers[1,2], Gareth J. Thomas[6], Manuel Serrano[3,11], and Jesús Gil[1,2,*]

[1]MRC London Institute of Medical Sciences (LMS), Du Cane Road, London, W12 0NN, UK.
[2]Institute of Clinical Sciences (ICS), Faculty of Medicine, Imperial College London, Du Cane Road, London W12 0NN, UK.
[3]Institute for Research in Biomedicine (IRB Barcelona), The Barcelona Institute of Science and Technology (BIST), Barcelona 08028, Spain.
[4]Department of Pulmonology, ICR, Hospital Clinic, August Pi i Sunyer Biomedical Research Institute (IDIBAPS), Universitat de Barcelona, Barcelona 08036, Spain.
[5]Instituto de Investigaciones Biomédicas August Pi i Sunyer (IDIBAPS), Barcelona 08036, Spain.
[6]School of Cancer Sciences, Faculty of Medicine, University of Southampton, Southampton SO16 6YD, UK.
[7]Developmental Biology and Cancer Programme, Birth Defects Research Centre, Great Ormond Street Institute of Child Health, University College London, 30 Guilford Street, London WC1N 1EH, UK.
[8]Karolinska Institute, Department of Biosciences and Nutrition, Huddinge 14183, Sweden.
[9]Department of Chemistry, Molecular Sciences Research Hub, 82 Wood Lane, London W12 0BZ, UK
[10]The Francis Crick Institute, 1 Midland Road, London NW1 1AT, UK
[11]Altos Labs, Cambridge Institute of Science, Granta Park CB21 6GP, UK

[+]Current address: AstraZeneca, Immuno-Oncology Discovery, Oncology R&D, Aaron Klug Building, Cambridge CB216GH, UK.

*Corresponding author: jesus.gil@imperial.ac.uk

KEYWORDS

Senescence, senolytics, genetic screens, COPI, *N*-Myristoylation, NMT inhibitors, UPR, lung fibrosis, NASH.

ABSTRACT

Drugs that selectively kill senescent cells, senolytics, improve the outcomes of cancer, fibrosis, and age-related diseases. Despite their potential, our knowledge of the molecular pathways that affect the survival of senescent cells is limited. To discover novel senolytic targets, we performed RNAi screens and identified COPI vesicle formation as a liability of senescent cells. Genetic or pharmacological inhibition of COPI results in Golgi dispersal, dysfunctional autophagy, and unfolded protein response-dependent apoptosis of senescent cells, and knockdown of COPI subunits improves outcomes of cancer and fibrosis in mouse models. Drugs targeting COPI have poor pharmacological properties, but we find that *N*-myristoyltransferase inhibitors (NMTi) phenocopy COPI inhibition and are potent senolytics. NMTi selectively eliminated senescent cells and improved outcomes in models of cancer and non-alcoholic steatohepatitis (NASH). Our results suggest that senescent cells rely on a hyperactive secretory apparatus and that inhibiting trafficking kills senescent cells with the potential to treat various senescence-associated diseases.

INTRODUCTION

Senescence is a cellular response induced by stresses such as replicative exhaustion, oncogenic activation, or genotoxic agents. Upon senescence induction, cells enter a stable cell cycle arrest, a process mediated by the upregulation of cyclin-dependent kinase inhibitors, such as $p16^{INK4a}$ and $p21^{CIP1}$ [1]. Senescent cells also undergo multiple phenotypic changes including altered morphology, chromatin remodelling, organelle reorganization, altered metabolism, and the production of a bio-active secretome known as the senescence-associated secretory phenotype (SASP) [2].

Cellular senescence hampers the replication of cells with DNA and macromolecular damage. As such, acute induction of senescence is a protective response that, by restricting the replication of damaged cells, limits cancer and fibrosis. In contrast, the accumulation of senescent cells during ageing contributes to a wide range of pathologies [3]. The selective killing of $p16^{INK4a}$-positive senescent cells (referred to as senolysis) in progeroid or aged normal mice improves healthspan [4], increases lifespan [5], and alleviates an array of pathologies that include atherosclerosis [6], osteoarthritis [7] and neurodegenerative diseases {Bussian, 2018 #6035}.

These observations have made the prospect of senolytic therapies attractive [8]. Several drugs that can selectively kill senescent cells have been identified, including dasatinib and quercetin (referred to as D+Q) [9], Bcl2 family inhibitors such as ABT-263 (also known as navitoclax) and ABT-737 [10-12], a modified FOXO4-p53 interfering peptide [13], HSP90 inhibitors [14], cardiac glycosides [15, 16] and β-galactosidase-activated nanoparticles and pro-drugs [17-19]. First-in-human studies have validated the potential of senolytics to decrease senescence burden in human patients [20-22]. However, the failure of the Phase 2 clinical trial of a senolytic MDM2 inhibitor against osteoarthritis [23] highlights the need to identify more effective and specific senolytics. To this end, we need to comprehensively uncover the molecular pathways that promote the survival of senescent cells.

Here, we performed unbiased genetic screens to discover novel senolytic pathways and targets. Our findings reveal COPI signalling and *N*-myristoylation as previously unknown and targetable vulnerabilities of senescent cells that can be exploited to treat senescence-associated pathologies.

RESULTS

Small interfering RNA screens identify novel senolytic targets

To discover novel and specific vulnerabilities associated with senescence, we performed large-scale small-interfering RNA (siRNA) screens in normal and senescent human cells (Fig. 1a). First, we used IMR90 fibroblasts expressing an ER:RAS fusion protein; in the presence of 4-hydroxytamoxifen (4OHT), ER:RAS becomes activated and induces oncogene-induced senescence (OIS, Extended Data Fig. 1a-d). We confirmed that siRNA transfection and associated knockdown were equally efficient in senescent and non-senescent cells. Moreover, siRNA-mediated knockdown of BCL2L1 (also known as Bcl-XL) preferentially killed cells undergoing OIS and could be used as a control for the screen (Fig. 1b and Sup Fig 1), in line with previous observations [12].

We employed IMR90 ER:RAS cells to screen a ‘‘druggable genome’’ siRNA library targeting around 5,500 genes, comparing the effects of siRNAs on the viability of normal and senescent cells, monitored using high-throughput microscopy. We identified 127 genes for which knockdown killed 4OHT-treated cells undergoing OIS (Fig. 1c-d); 62 of these genes were not essential for viability in control (DMSO-treated) cells (Extended Data Fig. 1e-f and Fig. 1d). We then performed a secondary screen with a new library comprising four independent siRNAs targeting each of the candidates (Fig. 1e-f) and confirmed 6 genes (BCL2L1, COPB2, COPG1, UBC, GNG8, and ALDOA) for which knockdown selectively killed cells undergoing OIS but not non-senescent cells (Fig. 1f).

Besides oncogenic activation, senescence can be triggered by other insults such as replicative stress, and exposure to irradiation or chemotherapeutic agents [1, 2]. We previously showed that sensitivity to senolytics depends on how senescence is induced [15]. To identify senolytic targets relevant to different types of senescence, we treated IMR90 cells with doxorubicin to model chemotherapy-induced senescence (TIS, Extended Data Fig. 1g-k). Similar to what we observed in OIS, the knockdown of BCL2L1 preferentially killed cells undergoing TIS (Fig. 1g). We screened a library targeting over 7,300 genes and identified that siRNAs against 121 genes killed cells undergoing doxorubicin-induced senescence (Fig. 1h-i). A secondary screen confirmed that siRNAs targeting 5 of those genes (BCL2L1, ARF1, UBB, TREM2, and APOC2) preferentially killed cells undergoing TIS when compared to normal cells (Fig. 1i-k). Overall, we identified 10 known or putative senolytic targets from

both screens. BCL2L1 together with ubiquitins (UBB and UBC) and components of the coatomer complex I (COPI) pathway (COPB2, COPG1, and ARF1) were commonly identified in both screens (Fig. 1l), suggesting that they constitute general vulnerabilities associated with senescence.

The Coatomer complex I (COPI) is a liability of senescent cells

COPI is best known for its involvement in the retrograde transport of vesicles from the Golgi to the ER, but it is also implicated in regulating other membrane trafficking events [24]. To confirm the COPI complex as a vulnerability of senescent cells, we used three independent shRNAs to deplete COPB2 (Sup Fig. 2a). Knockdown of COPB2 preferentially killed cells undergoing OIS (Fig. 2a-b). COPB2 depletion also killed IMR90 cells undergoing doxorubicin-induced senescence (Fig. 2c). COPI-coated vesicles consist of multiple subunits [25], and depletion of COPI subunit COPG1 (Sup Fig. 2b) also killed IMR90 cells undergoing OIS and doxorubicin-induced senescence (Fig. 2d and Sup Fig. 2c). Moreover, depletion of COPB2 is also senolytic in mixed cultures where normal and senescent cells co-exist (Fig. 2e-f).

The formation of COPI vesicles is regulated by the Arf family of GTPases [26]. Drugs such as brefeldin A (BFA, [27]) and golgicide A (GCA, [28]) interfere with COPI vesicle formation by inhibiting GBF1, a guanine nucleotide exchange factor required to activate Arf GTPases. We found that BFA and GCA treatments selectively killed cells undergoing OIS, as assessed by quantifying the effect of these drugs in senescent cells (as assessed by SA-β-Gal or IF against $p16^{INK4a}$ or $p21^{CIP1}$, Fig. 2g and Extended Data Fig. 2a-c). Similarly, SA-β-Gal staining performed after transfection of siRNAs targeting COPB2 or the corresponding controls also confirmed that COPB2 depletion targeted senescent (SA-β-Gal-positive) cells (Extended Data Fig. 2d).

Importantly, the EC_{50} values for BFA and GCA were around 60-fold and 11-fold lower, respectively, for senescent cells compared to normal cells (Fig. 2h and Extended Data Fig. 2e). BFA inhibits multiple guanine nucleotide exchange factors, whereas GCA is a specific GBF1 inhibitor [28]. To determine if the senolytic effects of GCA and BFA are due to on-target GBF1 inhibition, we took advantage of a previously described GBF1 mutant with reduced

binding to these drugs (GBF1^{M832L}) [28]. Expression of GBF1^{M832L} abrogated the senolytic effects of GCA and BFA, but not of the Bcl2 inhibitor ABT-263 (Fig. 2i).

Treatment of senescent cells with GBF1 inhibitors induced Caspase 3/7 activity (Fig 2j) and the death of senescent cells could be prevented by using the apoptosis pan-caspase inhibitor QVD, but not inhibitors of pyroptosis (YVAD or VX-765), necroptosis (Nec-1) or ferroptosis (Liprox, Sup. Fig 3a-b). We obtained similar results with the knockdown of COPB2 (Sup. Fig 3c-d), suggesting that COPI inhibition selectively induces apoptosis in senescent cells.

We took advantage of IMR90 cells undergoing senescence due to treatment with bleomycin, doxorubicin, or irradiation (Sup Fig 4a) to further confirm the senolytic potential of GBF1 inhibitors (Fig. 2k and Extended Data Fig. 2f). GCA and BFA also killed other cell types undergoing senescence due to bleomycin treatment, such as normal human lung fibroblasts (NHLFs, Sup Fig. 4b-c) or primary bronchial epithelial cells (PBECs, Sup Fig. 4d-e). Treatment with GCA (Fig. 2l) or BFA (Sup Fig. 4f) also eliminated senescent cells in mid-passage cultures of PBECs that contain a mixture of senescent (p16^{INK4a}-positive) and normal (p16^{INK4a}-negative) cells. Taken together these results demonstrate that COPI is a vulnerability of senescent cells and that drugs that inhibit GBF1 behave as broad-spectrum senolytics.

COPB2 knockdown causes Golgi disruption and triggers the unfolded protein response in senescent cells

COPI inhibition is known to disrupt the cis- and trans-Golgi compartments, and the early endosome, impairing protein secretion and autophagy [29]. To understand the reasons behind the selective sensitivity of senescent cells to COPI inhibition, we first conducted RNA-seq analysis of IMR90 cells undergoing OIS or bleomycin-induced senescence. While we did not observe any significant and substantial upregulation in the expression of COPI structural or regulatory subunits on senescent cells (Extended Data Fig 3a), gene set enrichment analysis (GSEA) found a COPI gene signature enriched on senescent cells, suggesting a higher reliance on the pathway (Fig 3a and Extended Data Fig 3b).

To examine the consequences of interfering with COPI in senescent cells, we knocked down COPB2 and examined the integrity and morphology of the Golgi using antibodies against

proteins in the trans-Golgi (TGN46, Fig. 3b) and the cis-Golgi (GM130, Fig. 3c). In agreement with previous observations [30], we found that cells undergoing OIS displayed an amplified Golgi (Fig. 3b). Importantly, COPB2 knockdown resulted in Golgi dispersal in senescent but not in normal cells. We performed automated high throughput microscopy and discovered an increase in the percentage of cells with a dispersed Golgi as assessed by TGN46 or GM130 staining (Fig. 3b-c). These results suggest that the expanded Golgi observed in cells undergoing OIS is disrupted upon COPB2 knockdown.

The expanded Golgi apparatus observed in senescent cells most likely reflects their enhanced need to produce, traffic, and recycle proteins required for the senescent program, including secreted factors as part of the SASP [30]. We reasoned that disrupting COPI-dependent Golgi expansion in senescent cells could trigger an accumulation of aberrant proteins, including intracellular accumulation of otherwise secreted factors. Cells undergoing OIS showed an increase in the intracellular levels of cytokines such as IL8 (Fig. 3d) or IL6 (Extended Data Fig. 3c), reflecting the production of SASP components. Strikingly, the intracellular levels of IL8 and IL6 were much higher in senescent cells upon COPB2 depletion (Fig. 3d and Extended Data Fig. 3c), and these changes were not due to a transcriptional increase of SASP components as mRNA levels of SASP components were unaffected by COPB2 knockdown (Extended data Fig 3d).

Treatment with glucocorticoids (such as beclomethasone or triamcinolone) inhibits the SASP [31] without preventing the induction of senescence (Sup Fig. 5a-d). Interestingly, glucocorticoids attenuated cell death induced by COPB2 knockdown, whereas cell death induced by BCLXL depletion was unaffected (Fig. 3e). We recently showed that knockdown of the alternative splicing regulator PTBP1 also results in SASP inhibition without affecting other senescence phenotypes ([32] and Sup. Fig 5e-g). Depletion of PTBP1 in senescent cells also prevented the cell death induced by the knockdown of COPB2 (Sup. Fig 5h).

We hypothesized that aberrant accumulation of SASP (and other misfolded proteins) on senescent cells could trigger the unfolded protein response (UPR), which may contribute to the senolytic effects associated with COPB2 knockdown. The UPR senses proteotoxic stress arising from the aberrant accumulation of proteins in the ER, and triggers increased expression of the transcription factors CHOP, ATF6, and XBP1 [33]. GSEA showed that signatures associated with activation of the UPR response or some of their key mediators (such as PERK and IRE1α) were found significantly upregulated in cells undergoing OIS or

bleomycin-induced senescence following COPB2 knockdown (Fig 3f and Sup Fig 6). To further investigate if COPI inhibition specifically activates the UPR in senescent cells, we assessed the frequency of cells with nuclear accumulation of these transcription factors. Using this approach, we found that COPB2 knockdown selectively activated the UPR in cells undergoing OIS but not in non-senescent cells (Fig 3g-h and Extended Data Fig 3e). Overall, these data suggest that the senolytic effects associated with COPB2 knockdown may relate to the selective activation of UPR response in senescent cells.

COPI inhibition triggers UPR and dysfunctional autophagy in senescent cells

Next, we decided to further investigate the mechanism behind the senolytic effect associated with COPI inhibition by taking advantage of GBF1 inhibitors that allow for an acute and sustained inhibition of the pathway by impeding COPI complex formation.

First, we analysed Golgi fragmentation and early endosome formation, known to be disrupted following COPI depletion. Treatment with GBF1 inhibitors GCA or BFA caused Golgi dispersal in both senescence and non-senescent cells (Fig. 4a) and prevented the expansion of early endosomes in senescent cells (Fig. 4b, and Extended Data Fig. 4a). Moreover, treatment with GBF1 inhibitors also resulted in intracellular accumulation of multiple SASP components, including IL-8 (Fig 4c and Sup Fig 7a), VEGF, GM-CSF and BMP2/4 in senescent cells (Sup Fig 7b). This intracellular accumulation of SASP components was not due to increased SASP transcription, as treatment with GBF1 inhibitors caused a decrease in mRNA levels of SASP components (Sup Fig 7c), likely due to a compensatory reduction in transcription following the triggering of UPR [34]. Interestingly, secretion of multiple SASP components was also significantly reduced in senescent cells treated with GBF1 inhibitors (Sup Fig 7d).

As we observed upon COPB2 knockdown in senescent cells, inhibition of SASP production prevented the senolytic effects of GBF1 inhibitors (Fig 4d and Extended data Fig 4b). We reasoned that intracellular accumulation of SASP components might reflect a wider trend for senescent cells to accumulate aberrant proteins upon COPI inhibition. To explore this possibility, we measured misfolded and aggregated proteins using proteostat [35]. Proteostat staining showed that senescence induction results in higher levels of misfolded/aggregated proteins, an increase that was exacerbated in senescent cells treated with GBF inhibitors (Fig 4e).

In accordance with what we observed upon COPB2 knockdown, GBF1 inhibitors also triggered a selective activation of the UPR response on cells undergoing OIS, as shown by increased expression of CHOP, XBP1, ATF6, and BiP (Fig 4f and Extended Data Fig 4c-f). Importantly, UPR activation was not limited to COPI inhibition in cells undergoing OIS, as similar results were observed in cells undergoing bleomycin-induced senescence (Sup. Fig 8). This happens even though the SASP in cells undergoing bleomycin-induced senescence is not induced to the same extent as in cells undergoing OIS (Sup. Fig 9a). The effects of GBF1 inhibitors on Golgi dispersal are known to be reversible [36]. Consistent with this reversibility, the senolytic effects of GBF1 inhibitors on IMR90 cells undergoing bleomycin-induced senescence could be prevented if the drugs were removed 24 h, but not 48 h, post-treatment (Sup. Fig 9b), while treatment with GBF1 inhibitors for 24 h was sufficient to trigger the death of cells undergoing OIS (Sup. Fig 9c), potentially due to its greater upregulation of SASP response.

COPI inhibition can result in an accumulation of non-degradative autophagosomes and impaired autophagy [29]. COPI inhibition resulted in the accumulation of LC3 and p62, suggesting a block in normal autophagic flux (Fig 4g and Extended Data Fig 4f-g). Glucocorticoid treatment, which inhibits SASP production, also reduced p62 accumulation in senescent cells treated with GBF1 inhibitors (Fig. 4h), suggesting that the autophagy defect may be driven in part by overwhelming of the autophagy machinery by the accumulation of aberrant proteins. Moreover, glucocorticoid treatment also prevented UPR as suggested by the lower frequency of nuclear ATF6 in senescent cells treated with GBF1 inhibitors (Fig. 4i). Finally, to assess whether UPR activation mediates the senolytic effects of GBF1 inhibitors, we inhibited the UPR effector kinase PERK. Treatment with two PERK inhibitors (GSK2656157 and GSK2606414), did not affect senescence (Sup. Fig 10), but importantly prevented the senolytic effects of the GBF1 inhibitors GCA and BFA (Fig. 4j). Together, our findings show that COPI inhibition causes Golgi dispersal, accumulation of aberrant proteins, early endosome disruption and dysfunctional autophagy in senescent cells, which results in proteotoxic responses and causes their selective killing (Fig. 4k).

Therapeutic benefits associated with COPI inhibition

Senescence induced by chemotherapeutic treatment determines the outcome of anticancer therapies. A two-step strategy combining senescence-inducing anti-cancer agents (such as

etoposide) followed by senolytics has been proposed [15, 37]. To determine if chemotherapy renders cancer cells sensitive to GBF1 inhibitors, we induced senescence by treatment with etoposide (Sup Fig. 11) and subsequently treated them with GCA or BFA (Fig. 5a and Extended Data Fig. 5a). Treatment with GCA (Fig. 5b-c) or BFA (Extended Data Fig. 5b-c) selectively killed cancer cells that were previously rendered senescent by etoposide.

The SASP of senescent cells can enhance the proliferative potential of cancer cells and promote tumor progression [38]. To investigate whether COPI inhibition in senescent cells compromises their ability to promote tumorigenesis, we used an experimental xenograft mouse model that monitors the effect of senescent fibroblasts on tumor growth [32, 39]. In addition, we took advantage of HFFF2 fibroblasts with doxycycline-inducible expression of shRNAs targeting either COPA or COPB2 (Sup Fig. 12a-e). We subcutaneously co-injected squamous cell carcinoma 5PT cells [40] with normal or senescent (irradiated) fibroblasts into immunodeficient mice (Fig. 5d) and confirmed that the presence of senescent fibroblasts enhanced tumor growth (Fig. 5e and Extended Data Fig. 5d). Depletion of COPA or COPB2, using two independent shRNAs targeting each gene, impaired the ability of irradiated, senescent fibroblasts to promote the growth of 5PT tumor cells in this setting (Fig. 5e, Sup Fig 12f and Extended Data Fig. 5d).

To examine whether COPI inhibition could have beneficial effects beyond cancer, we employed a model of lung fibrosis [16, 41]. In this model, normal or senescent (γ-irradiated, Extended Data Fig. 5g) human IMR90 fibroblasts, bearing doxycycline-inducible shControl or shCOPB2, were transplanted into the lung of immunodeficient mice (Fig. 5f). Mice were treated with doxycycline to induce shRNA expression. We took advantage of qPCR assessment of a human-specific gene (MMP3) to check that the different cells produce similar levels of engraftment (Extended Data Fig. 5h). Three weeks after intratracheal instillation, we assessed the expression of *CDKN2A* (the human gene encoding $p16^{INK4a}$) to detect senescent human fibroblasts in the lung. *CDKN2A* expression was lower in the lungs of mice transplanted with senescent fibroblasts expressing shCOPB2, suggesting that COPB2 depletion killed the transplanted senescent cells (Fig. 5g).

Interestingly, we observed increased expression of murine Cdkn1a, Col3A1 and Pai1 (Fig 5h-j) in lungs of mice transplanted with senescent fibroblasts that express shControl but not shCOPB2. These data suggest that senescent fibroblasts trigger senescence and lung fibrosis non-autonomously and that this consequence is attenuated by eliminating

senescent cells via COPI inhibition. To assess lung fibrosis, we measured hydroxyproline levels in the lung. This analysis confirmed that the injection of senescent cells, but not senescent shCOPB2 cells, increased lung fibrosis (Fig. 5k). We stained the lungs with Masson's trichome to further monitor fibrosis and observed increased fibrosis in the lungs from mice injected with senescent fibroblasts versus control fibroblasts, while fibrosis was reduced in the lungs of mice injected with senescent fibroblasts expressing shCOPB2 (Fig. 5l-m) as graded by Ashcroft scoring. In combination, these data suggest that inhibiting COPI can ameliorate the consequences associated with the presence of senescent cells in cancer and fibrosis.

Targeting *N*-myristoyltransferases (NMTs) phenocopies COPI inhibition to kill senescent cells

The poor pharmacological properties of existing drugs targeting the COPI complex (such as BFA) have hampered their use in the clinic [42]. Diverse post-translational modifications regulate the COPI pathway [43]. For example, the N-terminus of ARF1 is *N*-myristoylated co-translationally by *N*-myristoyltransferases (NMTs: NMT1 and NMT2) [44], and this modification is necessary for its function [45]. Recently, global analysis of *N*-myristoylated proteins identified several ARF GTPase family members [46, 47], suggesting that impairment of COPI function may be a key effect of pharmacologically inhibiting *N*-myristoylation.

To test this hypothesis, we treated control and senescent IMR90 ER:RAS cells with two different *N*-myristoyltransferase inhibitors (NMTi: IMP1088 and DDD86481) [48], which resulted in lower levels of ARF GTPases, as unveiled using a pan-ARF antibody (recognizing ARF1, ARF3, ARF5 and ARF6, Fig. 6a). This decreased expression likely reflects the increased proteasomal degradation which may be observed for proteins failing to undergo *N*-myristoylation [49]. Importantly, senescent cells treated with NMT inhibitors (IMP1088 and DD86481) displayed increased Golgi dispersal (Fig. 6b-c), endosomal disruption (Extended Data Fig. 6a), and intracellular accumulation of IL8 and IL6 (Fig. 6d and Extended Data Fig. 6b). Treatment with NMTi did not affect SASP transcription (Sup Fig 13a) but resulted in reduced secretion of multiple SASP components (Extended Data Fig 6c). GSEA showed an enrichment of signatures related to activation of the unfolded protein response in senescent cells treated with NMTi (Fig 6e and Sup Fig 13b-c). Moreover, as we observed upon COPB2 knockdown or GBF1 inhibition, senescent cells treated with

NMTi activated the UPR response (Fig 6f and Extended Data Fig 6d-e, as assessed by the accumulation of XBP1, ATF6, and CHOP) and displayed dysfunctional autophagy (Fig 6g). Interestingly, this is consistent with a previous report showing that NMTi induce ER stress in cancer cells [50]. We next assessed whether NMTi has senolytic properties. Treatment with three NMTi with different chemotypes (IMP1088, DD86481, and IMP1320) [48] selectively killed cells undergoing OIS (Fig 6h-j) by inducing apoptosis (Sup Fig 13d). NMTi also killed cells undergoing bleomycin-induced senescence (Extended Data Fig 6f-g), showing that their senolytic effects are not limited to OIS.

Recently the *Shigella* virulence factor IpaJ has been shown to induce the proteolytic cleavage of the *N*-myristoylated N-terminal glycine of ARF1 [51]. Importantly, substrate recognition makes IpaJ cleavage of *N*-myristoyl modifications selective for a limited number of proteins, including ARF1 [52]. We expressed wildtype IpaJ (WT) or an inactive C64A mutant on IMR90 cells and taking advantage of ω-alkynyl myristate (YnMyr) labelling [46, 53], we confirmed that while NMTi inhibited *N*-myristoylation of proteins with YnMyr, that is not the case when WT IpaJ is expressed (Sup Fig 14a). Indeed, western blot analysis followed by quantification shows that in contrast with NMTi, which reduced the expression of multiple *N*-myristoylated proteins, the expression of WT IpaJ reduced the expression of ARF1 but not of other *N*-myristoylated proteins (Sup Fig 14b-e). Interestingly, the expression of IpaJ WT but not the inactive IpaJ C64A mutant resulted in increased Golgi dispersal in senescent cells (Fig 6k) and was also senolytic (Fig. 6l). These experiments further suggest that reducing ARF1 *N*-myristoylation disrupts the COPI pathway. Overall, these results demonstrate that NMT inhibitors behave as senolytic agents, and phenocopy the effects of COPI inhibition.

NMT inhibitors are senolytic in different cancer models

Optimal NMT inhibitors display markedly superior *in vivo* pharmacokinetic properties to BFA and have been proposed as anticancer therapies [54]. To understand if NMTi could act as a senolytic in a ‘one-two punch’ strategy, we induced senescence in cancer cell lines by treatment with etoposide or doxorubicin (Sup Fig 15) and subsequently treated them with three different NMTi (Fig 7a). Treatment with IMP1088 (Fig 7b-d), DDD86481 (Extended Data Fig. 7a-b), or IMP1320 (Extended Data Fig. 7c-d) selectively killed cancer cells which were induced to senescence after treatment with etoposide or doxorubicin.

NMTi are tolerated at moderate doses both in mice [54] and human [55]. To confirm that our NMTi treatment regimens did not cause toxicities, we administered either DDD86481 or IMP1320 to mice and monitored several markers in blood without detecting any significant metabolic alterations (Sup Fig 16a-b). Similarly, we did not observe any changes in glucose, insulin levels, or cell type composition in the blood (Sup Fig 16c-d), further confirming that NMTi could be used *in vivo*.

To understand the potential benefit of NMTi in targeting senescent cells in the tumour microenvironment, we took advantage of the previously described experimental model that combines the xenograft of senescent fibroblasts and 5PT cancer cells [32, 39] (Fig. 5d-e). We co-injected 5PT cells alone or together with senescent, irradiated HFFF2 cells and assessed the effect of treatment with NMTi DDD86481 on tumour growth (Fig. 7e). While NMTi did not interfere with the growth of a xenograft caused by 5PT cells implanted alone, it abrogated the promotion of tumour growth associated with co-injection of senescent fibroblasts (Fig 7f and Extended Data Fig 7e).

To understand if NMTi could also eliminate preneoplastic senescent cells in the context of a tissue, we took advantage of a model of adamantinomatous craniopharyngioma (ACP), a WNT pathway-driven clinically relevant pituitary paediatric tumour, in which clusters of β-catenin+ pre-neoplastic senescent cells promote tumourigenesis in a paracrine manner [56]. We have previously used *ex vivo* pituitary cultures of this model to assess other senolytic drugs [15, 19]. Embryonic pituitaries at 18.5 days post-coitum (18.5 dpc) were dissected and cultured *ex vivo* with or without NMTi IMP1088 (Fig. 7g). Treatment with IMP1088 eliminated senescent cells as assessed by a significant decrease in β-catenin-positive and β-catenin-positive/$p21^{Cip1}$-positive cells (Fig 7h and Extended Data Fig 7f-g and Sup Fig 17a) by selectively inducing apoptosis (Fig 7i and Sup Fig 17b). IMP1088 did not affect other cell types in the pituitary, such as hormone-producing cells that are detected by the expression of synaptophysin (Extended Data Fig. 7h) [57].

To further investigate whether NMTi could act as senolytics *in vivo*, we employed a model of liver tumour initiation in which senescence is induced in hepatocytes by transposon-mediated transfer of oncogenic NRAS ($NRAS^{G12V}$) [58]. We expressed $NRAS^{G12V}$ in livers, taking advantage of hydrodynamic tail vein injection (HDTVI), and treated a cohort with NMTi IMP1320 (Fig. 7j). Mice treated with NMTi displayed reduced numbers of NRas-positive senescent hepatocytes, as assessed by reduced staining of NRas (Fig. 7k), SA-β-gal (Fig.

7l) and p21^{CIP1} (Fig. 7m) in liver sections. Together, these results imply that NMTi phenocopy COPI inhibition and can be used as senolytic drugs *in vivo*.

NMT inhibitors improve NASH-induced liver steatosis and fibrosis.

Elimination of senescent cells has a positive impact on many age-related phenotypes and diseases [5], including non-alcoholic steatohepatitis (NASH) [59]. To understand the potential of NMTi as a senotherapy for NASH, we fed 8-week-old males with a normal diet (chow) or a well-characterized Western-diet (WD)-based model of mouse NASH that is rich in fats and sugars (fructose and sucrose) for 19 weeks [60]. A cohort was treated with the NMTi DDD86481 for four consecutive days during weeks 5, 10, and 15 as summarized in Fig 8a. Assessment at the end of the experiment showed a significant increase in body weight in the WD-fed mice and a non-significant trend of lower weight in the NMTi-treated cohort when compared with the WD-fed, vehicle-treated group (Extended Data Fig 8a). To assess markers of metabolic health and liver damage, we measured levels of serum cholesterol, and ALT at week 15. While both WD-treated groups showed significantly higher levels of serum cholesterol, the cohort treated with NMTi had lower levels of serum ALT (Fig 8b), suggestive of reduced liver damage.

GSEA analysis showed an enrichment of senescence and SASP signatures in mice fed with WD when compared with the cohort fed with a chow diet (Extended data Fig 8b). Quantitative IHC of whole liver sections showed a significant increase in p21^{CIP1}-positive cells in the cohort fed with WD and a significant reduction in NMTi-treated mice (Fig 8c-d), suggesting that NMTi treatment caused a reduction of p21^{CIP1}-positive senescent cells. GSEA analysis confirmed that signatures of senescence and SASP were indeed downregulated in the NMTi-treated cohort when compared with WD-fed vehicle-treated mice (Fig 8e and Extended data Fig 8c).

H&E-stained liver sections showed increased hepatic steatosis in WD-fed mice that was less pronounced in the NMTi-treated cohort (Fig 8f, upper panels). To directly assess how NMTi affected lipid accumulation and liver steatosis, we stained lipids in liver sections using Oil Red O. Oil Red O staining revealed an increased accumulation of lipid deposits in the liver of WD-fed mice when compared with chow-fed mice that were reduced upon NMTi treatment (Fig. 8f, middle panels and Fig. 8g).

NASH is associated with chronic inflammation that results in the recruitment and activation of different immune cell populations that contribute to disease progression [61, 62]. To understand if NMTi treatment might affect the immune infiltration associated with NASH, we stained for CD68, a marker for Kupffer cells, and other infiltrating monocytes (Fig. 8f, lower panels). WD-fed mice displayed a significant increase in macrophages/monocytes (as assessed by CD68 staining), which was not observed in the NMTi-treated cohort (Fig. 8h), suggesting that NMTi treatment might reduce liver inflammation.

As fibrosis is a primary determinant of outcome in NASH [63], we assessed the effect of NMTi treatment on liver fibrosis. Using picrosirius red staining, we observed a significantly lower fibrotic area in liver sections from mice fed WD and treated with NMTi when compared with vehicle-treated counterparts (Fig 8i-j). Consistent with these results, the expression of collagens (*Col1a1* and *Col4a1*) was higher in mice fed with WD than in their chow diet-fed counterparts and was found significantly decreased in the NMTi treated group when compared with the WD+vehicle cohort (Fig 8k-l).

Finally, we took advantage of GSEA to corroborate these observations. GSEA suggested an increased presence of different immune cells including Kupffer cells, NKT cells, and CD8 T cells in the livers of mice fed with WD (Extended data Fig 8d). These immune cells have been linked with NASH progression [61, 62, 64]. Conversely, these immune gene signatures were found downregulated in the NMTi-treated cohort (Fig 8m and Extended Data Fig 8e). Moreover, gene signatures related to collagen were upregulated in the WD+vehicle cohort (Extended Fig 8f) but downregulated in their NMTi-treated counterparts (Fig 8n). Overall, the above results show that treatment with NMTi reduced senescence, inflammation, steatosis, and fibrosis in a WD-induced mouse model of NASH.

DISCUSSION

Senescent cells accumulate with age and contribute to cancer, fibrosis, and many age-related pathologies [3]. Their selective elimination, either by genetic or pharmacological means, results in widespread benefits such as increased lifespan, improved healthspan, and amelioration of their negative effects in many pathologies [4, 5]. Despite the clear benefits derived from eliminating senescent cells, only a handful of senolytic drugs are known, and only a few of those (such as the Bcl2-family inhibitor navitoclax or D+Q) have proven effective in multiple settings. However, concerns exist about the side effects of navitoclax [65] and the mechanism underlying the effects exerted by the D+Q combination is unclear. Therefore, there is a pressing need to discover novel senolytic drugs and identify targetable liabilities of senescent cells.

To fill this gap, we carried out screens to identify targetable liabilities of senescent cells. As senescence can be triggered by a variety of insults [1], we compared screens performed in models of oncogene- and therapy-induced senescence. Hits common to both screens were siRNAs targeting the BCL2-family protein BCL-XL (serving as an internal control) and genes encoding for ubiquitin. The latter likely relates to the enhanced protein degradation observed in senescent cells [66]. In addition, we identified components of the coatomer protein complex I (COPI) pathway. COPI participates in a variety of dynamic membrane-trafficking events, and it is well studied for its role in support of retrograde transport [24].

$KRAS^{mut}$/$LKB1^{mut}$ cancer cells have previously been shown to be addicted to COPI [67], suggesting that COPI inhibition might selectively kill cells expressing oncogenic RAS. However, we found that cells undergoing chemotherapy-, irradiation- and replicative senescence were also more sensitive to COPI inhibition than their control counterparts. These data suggest that drugs inhibiting COPI (such as golgicide A and brefeldin A) have broad senolytic properties.

Inhibition of COPI vesicle formation can block the transport of cargo both within the Golgi (intra-Golgi) and between Golgi and endoplasmic reticulum by disrupting intra-Golgi membrane dynamics and the ER-Golgi intermediate compartment (ERGIC). Cells undergoing senescence reorganize their endomembrane system to cope with the increase in secretion necessary for the SASP [30]. Depletion of COPB2 and inhibition of *N*-myristoyltransferases caused a more profound Golgi disruption in senescent cells compared to non-senescent cells, suggesting that their reorganized and enhanced Golgi might

increase their dependence on COPI. Importantly, interfering with the secretory apparatus by disrupting components of the COPI pathway results in the aberrant accumulation of SASP components and in general misfolded proteins in senescent cells, which saturates the autophagy machinery and activates the unfolded protein response (UPR), explaining the enhanced sensitivity of senescent cells to COPI inhibition.

Since senescence plays an important role in disease [3], we investigated whether COPI inhibition could be beneficial for the outcome of cancer and fibrosis. Senescence occurs at different stages of cancer evolution and treatment. Inhibiting COPI with BFA or GCA killed cancer cells that had been treated with chemotherapeutic agents. Moreover, COPB2 depletion prevented the senescence-fuelled increase in tumor growth in a xenograft cancer model. To test the senolytic effects of targeting COPB2 beyond cancer, we used a lung fibrosis model. In this model, senescent human fibroblasts implanted into the lung triggered fibrosis [16, 41], but depletion of COPB2 in senescent cells reduced the extent of lung fibrosis. These effects are consistent with the senolytic action associated with COPI inhibition. Since interfering with COPI (or NMT) also impairs the SASP, we speculate that the benefits associated with COPI inhibition in cancer and fibrosis might be the combined result of SASP suppression and selective killing of senescent cells.

Despite the promising therapeutic effects associated with COPI inhibition, the poor pharmacological properties of existing drugs targeting the pathway (such as BFA) have hampered their use in the clinic {Phillips, 1993 #6639}. Based on existing knowledge of COPI regulation [44-47], we hypothesized that NMTi would phenocopy COPI inhibition. Indeed, treatment with NMTi reduced the levels of Arf GTPases resulting in Golgi dispersal in senescent cells, intracellular accumulation of secreted cytokines, and UPR activation. More importantly, NMTi are potent senolytics. While our results suggest that the senolytic effect of NMTi might be explained by its effect on COPI signalling, it is worth noting that each of the different NMTi tested have a wider selective window than GBF1 inhibitors. This could reflect the different mechanisms of action of both drugs, with GBF1 inhibitors directly targeting GBF1 and affecting ARF function, while NMTi inhibits the myristoylation of newly synthesised proteins). But it also could suggest that additional targets besides the COPI pathway could contribute to explain the senolytic effects of NMTi.

In marked contrast with existing GBF1 inhibitors, NMT inhibitors are interesting candidates for *in vivo* use [68]. NMTi has been tested as an anticancer [54] and antiviral [68, 69] treatment. Our

results make the case for using the NMTi as senolytics. To evaluate their senolytic potential, we tested NMTi in different cancer models and a Western diet-induced model of NASH. Two different NMTi (IMP1088 or IMP1320) reduced the numbers of preneoplastic senescent cells in models of paediatric pituitary tumors and liver cancer while eliminating the tumour growth conferred by co-injected senescent cells in a xenograft cancer model. Moreover, treatment with NMTi in a Western diet-induced model of NASH, not only reduced senescence but also resulted in decreased inflammation, steatosis, and liver fibrosis. Therefore, our results show how NMTi treatment can eliminate senescent cells in vivo and encourages further development of NMTi to treat cancer and other senescence-associated pathologies.

In summary, our data identified COPI signalling and *N*-myristoylation as novel, targetable vulnerabilities of senescent cells. While existing GBF1 inhibitors (such as BFA and GCA, that target COPI signalling) are not appropriate for preclinical or clinical use, the most recent generation NMTi show exquisite senolytic potential and hold enormous promise for clinical development as senolytic medicines that could be used to target a wide range of senescence-associated pathologies.

REFERENCES

1. Herranz, N. & Gil, J. Mechanisms and functions of cellular senescence. *J Clin Invest* **128**, 1238-1246 (2018).
2. Gorgoulis, V. *et al.* Cellular Senescence: Defining a Path Forward. *Cell* **179**, 813-827 (2019).
3. Munoz-Espin, D. & Serrano, M. Cellular senescence: from physiology to pathology. *Nat Rev Mol Cell Biol* **15**, 482-496 (2014).
4. Baker, D.J. *et al.* Clearance of p16Ink4a-positive senescent cells delays ageing-associated disorders. *Nature* **479**, 232-236 (2011).
5. Baker, D.J. *et al.* Naturally occurring p16(Ink4a)-positive cells shorten healthy lifespan. *Nature* **530**, 184-189 (2016).
6. Childs, B.G. *et al.* Senescent intimal foam cells are deleterious at all stages of atherosclerosis. *Science* **354**, 472-477 (2016).
7. Jeon, O.H. *et al.* Local clearance of senescent cells attenuates the development of post-traumatic osteoarthritis and creates a pro-regenerative environment. *Nat Med* **23**, 775-781 (2017).
8. van Deursen, J.M. Senolytic therapies for healthy longevity. *Science* **364**, 636-637 (2019).
9. Zhu, Y. *et al.* The Achilles' heel of senescent cells: from transcriptome to senolytic drugs. *Aging Cell* **14**, 644-658 (2015).
10. Chen, Q. *et al.* ABT-263 induces apoptosis and synergizes with chemotherapy by targeting stemness pathways in esophageal cancer. *Oncotarget* **6**, 25883-25896 (2015).
11. Zhu, Y. *et al.* Identification of a novel senolytic agent, navitoclax, targeting the Bcl-2 family of anti-apoptotic factors. *Aging Cell* **15**, 428-435 (2016).
12. Yosef, R. *et al.* Directed elimination of senescent cells by inhibition of BCL-W and BCL-XL. *Nat Commun* **7**, 11190 (2016).
13. Baar, M.P. *et al.* Targeted Apoptosis of Senescent Cells Restores Tissue Homeostasis in Response to Chemotoxicity and Aging. *Cell* **169**, 132-147 e116 (2017).
14. Fuhrmann-Stroissnigg, H. *et al.* Identification of HSP90 inhibitors as a novel class of senolytics. *Nat Commun* **8**, 422 (2017).
15. Guerrero, A. *et al.* Cardiac glycosides are broad-spectrum senolytics. *Nat Metab* **1**, 1074-1088 (2019).
16. Triana-Martinez, F. *et al.* Identification and characterization of Cardiac Glycosides as senolytic compounds. *Nat Commun* **10**, 4731 (2019).
17. Gonzalez-Gualda, E. *et al.* Galacto-conjugation of Navitoclax as an efficient strategy to increase senolytic specificity and reduce platelet toxicity. *Aging Cell* **19**, e13142 (2020).
18. Munoz-Espin, D. *et al.* A versatile drug delivery system targeting senescent cells. *EMBO Mol Med* **10** (2018).
19. Guerrero, A. *et al.* Galactose-modified duocarmycin prodrugs as senolytics. *Aging Cell* **19**, e13133 (2020).
20. Justice, J.N. *et al.* Senolytics in idiopathic pulmonary fibrosis: Results from a first-in-human, open-label, pilot study. *EBioMedicine* (2019).
21. Ellison-Hughes, G.M. First evidence that senolytics are effective at decreasing senescent cells in humans. *EBioMedicine* **56**, 102473 (2020).

22. Hickson, L.J. *et al.* Senolytics decrease senescent cells in humans: Preliminary report from a clinical trial of Dasatinib plus Quercetin in individuals with diabetic kidney disease. *EBioMedicine* **47**, 446-456 (2019).
23. Roy, A.L. *et al.* A Blueprint for Characterizing Senescence. *Cell* (2020).
24. Beck, R., Adolf, F., Weimer, C., Bruegger, B. & Wieland, F.T. ArfGAP1 activity and COPI vesicle biogenesis. *Traffic* **10**, 307-315 (2009).
25. Bethune, J. & Wieland, F.T. Assembly of COPI and COPII Vesicular Coat Proteins on Membranes. *Annu Rev Biophys* **47**, 63-83 (2018).
26. Popoff, V. *et al.* Several ADP-ribosylation factor (Arf) isoforms support COPI vesicle formation. *J Biol Chem* **286**, 35634-35642 (2011).
27. Nebenfuhr, A., Ritzenthaler, C. & Robinson, D.G. Brefeldin A: deciphering an enigmatic inhibitor of secretion. *Plant Physiol* **130**, 1102-1108 (2002).
28. Saenz, J.B. *et al.* Golgicide A reveals essential roles for GBF1 in Golgi assembly and function. *Nat Chem Biol* **5**, 157-165 (2009).
29. Razi, M., Chan, E.Y. & Tooze, S.A. Early endosomes and endosomal coatomer are required for autophagy. *J Cell Biol* **185**, 305-321 (2009).
30. Narita, M. *et al.* Spatial coupling of mTOR and autophagy augments secretory phenotypes. *Science* **332**, 966-970 (2011).
31. Laberge, R.M. *et al.* Glucocorticoids suppress selected components of the senescence-associated secretory phenotype. *Aging Cell* **11**, 569-578 (2012).
32. Georgilis, A. *et al.* PTBP1-Mediated Alternative Splicing Regulates the Inflammatory Secretome and the Pro-tumorigenic Effects of Senescent Cells. *Cancer Cell* **34**, 85-102 e109 (2018).
33. Hetz, C. The unfolded protein response: controlling cell fate decisions under ER stress and beyond. *Nat Rev Mol Cell Biol* **13**, 89-102 (2012).
34. Hollien, J. *et al.* Regulated Ire1-dependent decay of messenger RNAs in mammalian cells. *J Cell Biol* **186**, 323-331 (2009).
35. Kitakaze, K. *et al.* Cell-based HTS identifies a chemical chaperone for preventing ER protein aggregation and proteotoxicity. *Elife* **8** (2019).
36. Ito, Y. *et al.* cis-Golgi proteins accumulate near the ER exit sites and act as the scaffold for Golgi regeneration after brefeldin A treatment in tobacco BY-2 cells. *Mol Biol Cell* **23**, 3203-3214 (2012).
37. Wang, L. & Bernards, R. Taking advantage of drug resistance, a new approach in the war on cancer. *Front Med* **12**, 490-495 (2018).
38. Krtolica, A., Parrinello, S., Lockett, S., Desprez, P.Y. & Campisi, J. Senescent fibroblasts promote epithelial cell growth and tumorigenesis: a link between cancer and aging. *Proc Natl Acad Sci U S A* **98**, 12072-12077 (2001).
39. Herranz, N. *et al.* mTOR regulates MAPKAPK2 translation to control the senescence-associated secretory phenotype. *Nat Cell Biol* **17**, 1205-1217 (2015).
40. Bauer, J.A. *et al.* Reversal of cisplatin resistance with a BH3 mimetic, (-)-gossypol, in head and neck cancer cells: role of wild-type p53 and Bcl-xL. *Mol Cancer Ther* **4**, 1096-1104 (2005).
41. Hernandez-Gonzalez, F. *et al.* Human senescent fibroblasts trigger progressive lung fibrosis in mice. *Aging (Albany NY)* **15** (2023).

42. Phillips, L.R., Supko, J.G. & Malspeis, L. Analysis of brefeldin A in plasma by gas chromatography with electron capture detection. *Anal Biochem* **211**, 16-22 (1993).
43. Luo, P.M. & Boyce, M. Directing Traffic: Regulation of COPI Transport by Post-translational Modifications. *Front Cell Dev Biol* **7**, 190 (2019).
44. Kahn, R.A., Goddard, C. & Newkirk, M. Chemical and immunological characterization of the 21-kDa ADP-ribosylation factor of adenylate cyclase. *J Biol Chem* **263**, 8282-8287 (1988).
45. Franco, M., Chardin, P., Chabre, M. & Paris, S. Myristoylation-facilitated binding of the G protein ARF1GDP to membrane phospholipids is required for its activation by a soluble nucleotide exchange factor. *J Biol Chem* **271**, 1573-1578 (1996).
46. Thinon, E. *et al.* Global profiling of co- and post-translationally N-myristoylated proteomes in human cells. *Nat Commun* **5**, 4919 (2014).
47. Goya Grocin, A., Serwa, R.A., Morales Sanfrutos, J., Ritzefeld, M. & Tate, E.W. Whole Proteome Profiling of N-Myristoyltransferase Activity and Inhibition Using Sortase A. *Mol Cell Proteomics* **18**, 115-126 (2019).
48. Kallemeijn, W.W. *et al.* Validation and Invalidation of Chemical Probes for the Human N-myristoyltransferases. *Cell Chem Biol* **26**, 892-900 e894 (2019).
49. Timms, R.T. *et al.* A glycine-specific N-degron pathway mediates the quality control of protein N-myristoylation. *Science* **365** (2019).
50. Thinon, E., Morales-Sanfrutos, J., Mann, D.J. & Tate, E.W. N-Myristoyltransferase Inhibition Induces ER-Stress, Cell Cycle Arrest, and Apoptosis in Cancer Cells. *ACS Chem Biol* **11**, 2165-2176 (2016).
51. Burnaevskiy, N. *et al.* Proteolytic elimination of N-myristoyl modifications by the Shigella virulence factor IpaJ. *Nature* **496**, 106-109 (2013).
52. Burnaevskiy, N., Peng, T., Reddick, L.E., Hang, H.C. & Alto, N.M. Myristoylome profiling reveals a concerted mechanism of ARF GTPase deacylation by the bacterial protease IpaJ. *Mol Cell* **58**, 110-122 (2015).
53. Kallemeijn, W.W. *et al.* Proteome-wide analysis of protein lipidation using chemical probes: in-gel fluorescence visualization, identification and quantification of N-myristoylation, N- and S-acylation, O-cholesterylation, S-farnesylation and S-geranylgeranylation. *Nat Protoc* **16**, 5083-5122 (2021).
54. Beauchamp, E. *et al.* Targeting N-myristoylation for therapy of B-cell lymphomas. *Nat Commun* **11**, 5348 (2020).
55. Sangha, R. *et al.* Novel, First-in-Human, Oral PCLX-001 Treatment in a Patient with Relapsed Diffuse Large B-Cell Lymphoma. *Curr Oncol* **29**, 1939-1946 (2022).
56. Gonzalez-Meljem, J.M. *et al.* Stem cell senescence drives age-attenuated induction of pituitary tumours in mouse models of paediatric craniopharyngioma. *Nat Commun* **8**, 1819 (2017).
57. Andoniadou, C.L. *et al.* Sox2(+) stem/progenitor cells in the adult mouse pituitary support organ homeostasis and have tumor-inducing potential. *Cell Stem Cell* **13**, 433-445 (2013).
58. Kang, T.W. *et al.* Senescence surveillance of pre-malignant hepatocytes limits liver cancer development. *Nature* **479**, 547-551 (2011).
59. Ogrodnik, M. *et al.* Cellular senescence drives age-dependent hepatic steatosis. *Nat Commun* **8**, 15691 (2017).

60. Gallage, S. *et al.* A researcher's guide to preclinical mouse NASH models. *Nat Metab* **4**, 1632-1649 (2022).
61. Huby, T. & Gautier, E.L. Immune cell-mediated features of non-alcoholic steatohepatitis. *Nat Rev Immunol* **22**, 429-443 (2022).
62. Anstee, Q.M., Reeves, H.L., Kotsiliti, E., Govaere, O. & Heikenwalder, M. From NASH to HCC: current concepts and future challenges. *Nat Rev Gastroenterol Hepatol* **16**, 411-428 (2019).
63. Angulo, P. *et al.* Liver Fibrosis, but No Other Histologic Features, Is Associated With Long-term Outcomes of Patients With Nonalcoholic Fatty Liver Disease. *Gastroenterology* **149**, 389-397 e310 (2015).
64. Reid, D.T. *et al.* Kupffer Cells Undergo Fundamental Changes during the Development of Experimental NASH and Are Critical in Initiating Liver Damage and Inflammation. *PLoS One* **11**, e0159524 (2016).
65. Wilson, W.H. *et al.* Navitoclax, a targeted high-affinity inhibitor of BCL-2, in lymphoid malignancies: a phase 1 dose-escalation study of safety, pharmacokinetics, pharmacodynamics, and antitumour activity. *Lancet Oncol* **11**, 1149-1159 (2010).
66. Deschenes-Simard, X. *et al.* Tumor suppressor activity of the ERK/MAPK pathway by promoting selective protein degradation. *Genes Dev* **27**, 900-915 (2013).
67. Kim, H.S. *et al.* Systematic identification of molecular subtype-selective vulnerabilities in non-small-cell lung cancer. *Cell* **155**, 552-566 (2013).
68. Mousnier, A. *et al.* Fragment-derived inhibitors of human N-myristoyltransferase block capsid assembly and replication of the common cold virus. *Nat Chem* **10**, 599-606 (2018).
69. Priyamvada, L. *et al.* Inhibition of vaccinia virus L1 N-myristoylation by the host N-myristoyltransferase inhibitor IMP-1088 generates non-infectious virions defective in cell entry. *PLoS Pathog* **18**, e1010662 (2022).

FIGURE LEGENDS

Figure 1. RNAi screens identify novel senolytic targets. a, Experimental design for the RNAi screens to identify senolytic targets. **b,** Quantification of cell survival (right) and representative DAPI stained IF pictures (left) of senescent (4OHT) and control (DMSO) IMR90 ER:RAS cells 3 days post-transfection with BCL2L1 siRNA (n=3). Scale bar, 100 μm. **c,** Results of the primary siRNA screen for senolytic targets in OIS. Normalized cell counts are shown as mean B-score. Candidate considered a hit if B-score in ≥2 replicates was <-3. **d,** Summary of the siRNA screen for senolytic targets in OIS. **e,** Re-test of OIS screen candidates. Data represented as percentage cell survival in control cells versus the "senolytic index" (difference in cell survival between control and senescent cells). Each point represents the mean of three replicates. The candidate was considered a hit if the senolytic index was>20 with siRNAs in ≥2 replicates. **f,** Percentage cell survival of best candidate senolytic siRNAs shown in the context of OIS (4OHT) and control cells (DMSO) (n=3). Data represents the deconvolution of values shown in Figure 1e. **g,** Quantification of cell survival (right) and representative DAPI stained IF pictures (left) of doxorubicin-induced senescent (Doxo) and control (DMSO) IMR90 cells 3 days post-transfection with BCL2L1 siRNA (n=3). The left panel shows representative DAPI-stained IF images. Scale bar, 100 μm. **h,** Results of the primary siRNA screen for senolytic targets in doxorubicin-induced senescence. Normalized cell counts are shown as B-score. Candidate considered a hit if B-score was <-3 in ≥2 replicates. **i,** Summary of the siRNA screen for senolytic targets in doxorubicin-induced senescence. **j,** Graph showing results of re-testing doxorubicin-induced senescence senolytic candidates with deconvoluted siRNAs. Data represented as percentage cell survival in control cells versus the difference in cell survival between control and senescent cells (senolytic index). Each point represents the mean of three replicates. Candidates were considered a hit if the senolytic index was>15 with siRNAs in ≥2 replicates. **k,** Percentage cell survival of best candidate senolytic siRNAs for doxorubicin-induced senescence (Doxo) and control cells (DMSO) (n=6, for DMSO and 4OHT treated cells, n=3 for BCLXL siRNA transfected cells). Data represents the deconvolution of values shown in Figure 1J with additional replicates. **l,** Common pathways identified in the siRNA screen for senolytic targets. Data represented in figure (b, f, g, and k) as mean±SD, with Unpaired, Two-tailed Student's T-test.

Figure 2. Coatomer complex I (COPI) is a vulnerability of senescent cells. a, Quantification of cell survival (right) and representative DAPI stained IF pictures (left) of senescent (4OHT) and control (DMSO) IMR90 ER:RAS cells infected with the indicated doxycycline-inducible shRNAs. Doxycycline (Dox) was added 7 days after senescence induction, and plates were fixed and stained 10 days after. (n=5). Scale bar, 100μm. **b,** Crystal violet staining. Dox was added 7 days after senescence induction, and plates were fixed and stained 9 days after. Representative image shown of three replicate experiments. **c,** Senolytic activity of COPB2 depletion in the context of doxorubicin-induced senescence in IMR90 cells (n=4 shCOPB2.1, n=5 other shRNAs). **d,** Senolytic activity of COPG1 depletion during OIS in IMR90 ER:RAS cells (n=6). Dox was added from day 0 of senescence induction and plates were fixed after 14 days. **e.** Schematic outlining strategy of co-culture senolytic testing of COPB2 siRNAs. **f,** Quantification of cell survival (right) and representative IF images (left) of the co-culture experiment of IMR90 GFP ER:RAS with IMR90 Cherry cells. Cells were transfected with the indicated siRNAs and cell numbers were determined from counts of mCherry or GFP-positive cells detected by IF. (n=3). **g,** Representative image of IMR90 ER:RAS cells 7 days post addition of 4OHT and stained for SA-β-galactosidase activity 72h after treatment with 2.5μM of golgicide A (GCA) treatment. Scale bar, 100μm. **h,** Dose-response curves for senolytic effect of GBF1 inhibitor golgicide A in the context of OIS (n=6). EC_{50}, half maximal effective concentration. **i,** Quantification of cell survival of control (RAS DMSO) and oncogene-induced senescent cells (RAS 4OHT) infected with the indicated vectors and treated with ABT-263, golgicide A (GCA) or brefeldin A (BFA) at indicated concentrations. (n=5 for GCA and BFA treated cells, n=3 for ABT-263 treated cells). **j**, Caspase-3/7 activity in control (DMSO) or oncogene-induced senescent (4OHT) cells after treatment with DMSO or 2.5μM golgicide A 7 days after senescence induction (n=3). **k,** Senolytic activity of golgicide A in senescence induced by irradiation (n=3), bleomycin (n=6), and doxorubicin treatment. (n=4). Data represented as mean±SD. Comparisons are to the corresponding DMSO-treated cells (grey bars) using two-way ANOVA. **l,** Representative pictures (left) of IF staining for $p16^{INK4a}$ in PBECs after treatment with golgicide A or vehicle (DMSO); $p16^{INK4a}$ is stained green. Scale bar, 50 μm. Quantification of $p16^{INK4a}$-positive and negative PBECs (right). (n=3). Data in all figures represent mean±SD. Unpaired, two-tailed, Student's t-test used unless otherwise stated.

Figure 3. COPB2 depletion causes Golgi disruption and triggers the unfolded protein response in senescent cells. a, GSEA plot for COPI transport is enriched in cells

undergoing OIS. NES, normalized enrichment score; FDR, false discovery rate. **b,** Quantification of cells with dispersed trans-Golgi (right) and representative TGN46 IF pictures (left). Senescent (4OHT) and control (DMSO) IMR90 ER:RAS cells were transfected with the indicated siRNAs (n=3). Quantification was performed using a threshold of organelle count (> 25) in the 'region growing' collar using multiscale-tophat segmentation for objects 1-3 pixels in size. The white arrow points to a cell with a normal trans-Golgi, while the yellow arrow indicates a cell with dispersed trans-Golgi. Scale Bar, 100 μm. **c,** Quantification of cells with dispersed cis-Golgi (right) and representative GM130 IF pictures (left). Senescent (4OHT) and control (DMSO) IMR90 ER:RAS cells were transfected with the indicated siRNAs (n=3). Quantification was performed using a threshold of the integrated intensity (Intensity x Area) in the 'region growing' collar. The white arrow points to a cell with a normal trans-Golgi, while the yellow arrow indicates a cell with dispersed cis-Golgi. Scale Bar, 100 μm. **d,** Quantification of intracellular levels of IL8 (right) and representative IL8 IF pictures (left) of senescent (4OHT) and control (DMSO) IMR90 ER:RAS cells after transfection with the indicated siRNAs (n=4). Scale Bar, 100μm. Statistical tests were performed using two-way ANOVA with Dunnett's correction for multiple comparisons against DMSO-treated cells. **e,** SASP inhibition caused by treatment with 10μM of glucocorticoids (Bec, beclomethasone; Tri, triamcinolone) prevents senolysis induced by COPB2 depletion. Quantification of cell survival of senescent (4OHT) and control (DMSO) IMR90 ER:RAS cells treated as indicated (n=3). **f,** GSEA plot showing that a UPR gene signature is enriched in IMR90 ER:RAS upon COPB2 depletion. NES, normalized enrichment score; FDR, false discovery rate. **g-h,** Quantification (right) of cells positive for nuclear CHOP (g, n=5 independent replicates per condition) and nuclear ATF6 (h, n=4 independent replicates per condition) 6 days after treating with 4OHT (to induce OIS) or DMSO (as control), cells were transfected with the indicated siRNAs. Cells were fixed, stained, and imaged 72 hours later. Representative images are shown (left). Scale bar, 100 μm. Unpaired two-tailed Student's t-test was used for statistical comparison. Data represented as mean±SD. Statistical tests are performed using two-way ANOVA against scrambled siRNA unless otherwise stated.

Figure 4. COPI inhibitors cause Golgi disruption, trigger UPR, and result in autophagy defects. a-c, Quantification of cell with fragmented trans-Golgi (a, right), early endosome numbers per cell (b) and intracellular levels of IL8 (c) in senescent (4OHT) and control (DMSO) IMR90 ER: RAS cells after treatment for 48 hours with 1.25μM of golgicide A (GCA),150nM of brefeldin A (BFA) or 1μM ABT-263 (n=3). Representative IF image for

TGN46 shown (a, left). Scale bar, 100 μm. **d,** SASP inhibition caused by treatment with 10μM of glucocorticoids (Bec, beclomethasone; Tri, triamcinolone) prevents senolysis induced by treatment with golgicide A (GCA) or brefeldin A (BFA). Quantification of cell survival of senescent (4OHT) and control (DMSO) IMR90 ER:RAS cells treated with either 1.25 μM of golgicide A (GCA) or 150 nM brefeldin A (BFA) (n=3). Cells were treated from day 4 after senescence induction with 10μM of beclomethasone or triamcinolone before the addition of senolytics. **e,** Quantification of relative levels of Proteostat signal intensity in senescent (4OHT) or control (DMSO) IMR90 ER: RAS cells after 48h treatment with 1.25μM of golgicide A (GCA) or 150nM of brefeldin A (BFA). (n=3). Representative IF images are shown (left). Scale bar, 100 μm. **f-g,** Quantification of cells positive for nuclear CHOP (f, right) or LC3B foci (g, right) 48 hours after either control (DMSO) or oncogene-induced senescent (4OHT) cells were treated with either 1 μM ABT-263, 1.25 μM of golgicide A (GCA) or 150 nM brefeldin A (BFA) (n=3). For (f) significance was determined using unpaired, two-tailed, Student's test with Holm-Šídák correction. Representative IF images for CHOP (f-left) and L3CB (g-left). Scale Bar, 100 μm. **h-i,** SASP inhibition caused by treatment with 10 μM of glucocorticoids (Bec, beclomethasone; Tri, triamcinolone) prevents p62/SQSTM1 (h) and ATF6 (i) induction caused by treatment with golgicide A (GCA) or brefeldin A (BFA). Quantification of p62/SQSTM1 and ATF6 positive senescent (4OHT) and control (DMSO) IMR90 ER:RAS cells treated with either 1 μM ABT263, 1.25 μM of golgicide A (GCA) or 150 nM brefeldin A (BFA). IF staining performed on plates fixed 48 hours after the addition of drugs. (n=3 independent replicates per condition). **j,** Survival of control (DMSO) or OIS cells (4OHT) pre-treated with 300 nM KIRA6, 1μM GSK2656157, or 1μM GSK2606414 before a 48-hour treatment with GCA or BFA at day 7 post-senescence induction (n=3). **k,** Scheme summarizing how COPI inhibition induces the death of senescent cells. All data represented as mean±SD. Two-way ANOVA was performed for statistical analysis of panels a, c, d, e, g, h, I, and j. Unpaired, two-tailed Student's t-test was used for statistical analysis of the data shown in b and f.

Figure 5. Therapeutic benefits of inhibiting the COPI pathway. a, Experimental design for the sequential treatment of cancer cells with chemotherapy and golgicide A (GCA). **b-c,** Quantification of cell survival of A549 cells (b) or SKHep1 cells (c) after treatment with the indicated drug combinations. (n=6) Unpaired, two-tailed, Student's t-test, Holm-Šídák correction. Data represented as mean±SD**. d,** Experimental design of tumor growth in NSG

cancer model with 5PT squamous cancer cells co-injected with HFFF2 fibroblasts. **e,** Tumor growth curves showing the tumour volume monitored over time (IR=irradiation). Data represented as Mean±SEM for all mice in each group. (n=7 per group). RM Two-way ANOVA with Greenhouse-Geisser correction & Dunnet's correction used for statistical analysis of day 20 timepoint relative to shControl+IR. Area under the curve (AUC) analysis for data pooled from two experiments shown in Extended Data Fig. 5d. All comparisons are to shControl + IR. **f,** Experimental design of the mouse model of lung fibrosis by intra-tracheal instillation of human senescent lung fibroblasts into nude mice. All analyses were performed 3 weeks after cell delivery (except those in Extended Data Fig. 5h, which were performed 48h post-instillation). **g-j,** Relative expression of the mRNAs coding for human CDKN2A (g), Cdkn1a (h), Col3a1 (i) and Pai1 (j) in lung samples from the experiment described in f. (n=5). Statistical analysis was performed using ordinary one-way ANOVA. Data represented as mean±SD. **k,** Lung hydroxyproline content in samples from mice of the experiment described in f. (n=5). Ordinary one-way ANOVA, multiple comparison Tukey test. Data represented as mean±SD. **l,** Ashcroft scoring for alveolar septal thickening in sections from lungs of mice grafted with IMR90 cells treated as indicated. (n=5). Ordinary One-way ANOVA, Multiple comparison Tukey test. Data represented as mean±SD. **m,** Representative pictures of lung sections stained with haematoxylin and eosin (H&E, top) and Masson's trichrome (bottom) from mice of the experiment described in f. Scale bar, 100 µm.

Figure 6. NMT inhibitors phenocopy COPI inhibition and are senolytic. a, Treatment with NMT inhibitors (NMTi) results in reduced levels of ARF GTPases. Control (DMSO) or senescent (4OHT) IMR90 ER:RAS cells were treated with 300nM IMP1088 or 1.5 µM DDD86481, 7 days after senescence induction. Protein extracts were collected 3 days later. Immunoblot of GAPDH is included as a loading control. Immunoblots of a representative experiment (out of three independent experiments) are shown. **b-d,** Quantification (right) of IF staining for trans-Golgi dispersal (TGN46, b), cis-Golgi dispersal (GM130, c), intracellular levels of IL8 (IL8, d). Control (DMSO) or senescent (4OHT) IMR90 ER:RAS cells were treated with 300nM IMP1088 or 1.5 µM DDD86481, 7 days after senescence induction for 5 days (n=3). Representative IF images are shown (left). Scale bar, 100µm. **e,** GSEA plot showing that an UPR gene signature is enriched in IMR90 ER:RAS treated with the NMTi IMP1088. NES, normalized enrichment score; FDR, false discovery rate. **f,** Quantification (right) of IF staining for XBP1. Control (DMSO) or senescent (4OHT) IMR90 ER:RAS cells

were treated with 300nM IMP1088 or 1.5 μM DDD86481 7 days after senescence induction for 5 days (n=3). Representative IF images are shown (left). Scale bar, 100μm. **g,** Quantification of IF staining for p62/SQSTM1. Control (DMSO) or senescent (4OHT) IMR90 ER:RAS cells were treated with 300nM IMP1088 or 1.5 μM DDD86481 7 days after senescence induction for 5 days (n=3). **h-j,** Dose-response curves for senolytic effect of NMT inhibitors. IMP1088 (h, n=8), DDD86481 (i, n=5), and IMP1320 (j, n=4). EC_{50}, half-maximal effective concentration. Control (DMSO) or Senescent (4OHT) IMR90 ER:RAS cells treated with inhibitors 7 days after senescence induction and fixed for cell counting 7 days after treatment. **k,** Quantification of dispersed trans-Golgi (right) and representative images (left) in C64A or WT IpaJ transduced control (DMSO) or senescent (4OHT) IMR90 ER:RAS cells(n=3 replicates per condition). Cells were fixed 7 days post-induction for IF staining. Scale bar, 50μm. **l,** Expression of WT IpaJ preferentially kills senescent cells. Survival of C46A or WT IpaJ transduced Control (DMSO) or Senescent (4OHT) IMR90 ER:RAS cells 7 days post-senescence induction. Survival was measured relative to vector-transduced cells. Unpaired, two-tailed, Student's, t-test. (n=3). Data represented as mean±SD. Statistical analysis is performed throughout the figure by ordinary two-way ANOVA unless otherwise specified.

Figure 7. NMT inhibitors target senescent cells in cancer models. a, Experimental design for the sequential treatment of cancer cells with chemotherapy and NMT inhibitors. **b,** Crystal violet staining of control (DMSO) and senescent (treated with doxorubicin or etoposide) HCT116 cells treated with 300nM IMP1088 7 days after senescence induction and treated for 7 days with the NMTi. The image is representative of two independent experiments. **c-d,** Dose-response curves for senolytic effect of IMP1088 treated HCT116 (c, n=4) or MCF7 (d, n=3 for DMSO and etoposide and n=2 for doxorubicin) cells treated with either doxorubicin or etoposide. EC_{50}, half-maximal effective concentration. **e,** Experimental design and timeline of tumor growth in NSG cancer model with 5PT squamous cancer cells co-injected with HFFF2 fibroblasts and treated with DDD86481. **f,** Area under the curve (AUC) analysis for tumor volume measured over time. Data represented as mean±SEM (n=6, 5PT+veh, n=8 other groups, see also Extended Data Fig 7e for the tumour growth curves). Ordinary One-way ANOVA, Dunnett's correction. **g,** Experimental design for the senolytic experiment in the *Hesx1*$^{Cre/+}$;*Ctnnb1*$^{lox(ex3)/+}$ mouse model of adamantinomatous craniopharyngioma (ACP). Tumoral pituitaries from 18.5dpc *Hesx1*$^{Cre/+}$;*Ctnnb1*$^{lox(ex3)/+}$

embryos were cultured in the presence of NMTi (600nM IMP1088; n=3) or vehicle (DMSO; n=5) and processed for histological analysis after 72 h. **h,** Quantification of βcatenin accumulating cells after NMTi treatment highlights the elimination of preneoplastic senescent lesions. Immunofluorescence staining against βcatenin (green) and cleaved caspase-3 (red) shows that oncogene-induced senescent βcatenin positive clusters of cells are undergoing apoptosis. Main scale bar, 50μm. Insert scale bar, 40μm. Data represented as mean±SD; n represents the number of pituitaries. (n=22 Vehicle, n=15, NMTi) Unpaired, two-tailed Student's t-test. **i,** Quantification of cleaved caspase-3 positive area (% of the pituitary surface) after NMTi treatment. (n=12 for all groups) Data represented as mean ± SD; ****p < 0.0001. Unpaired, two-tailed, Student's t-test. **j,** Experimental design for the oncogene-induced senescence experiment in the liver. **k-m,** Representative images (right) and quantification (left) of Nras-positive cells (e), SA-β-galactosidase (SA-β-Gal) staining (f) and $p21^{CIP1}$ staining by IHC (g) in the liver of mice treated with vehicle (n=9) or IMP1320 (n=9). Data represented as mean±SEM. Unpaired, two-tailed, Student's t-test. Arrows indicate examples of SA-β-galactosidase-positive cells. Scale bar, 100 μm (e-f); 50μm (g).

Figure 8. NMT inhibitors eliminate senescent cells and improve NASH-induced liver steatosis and fibrosis. a, Experimental design for the model of western diet (WD)-induced non-alcoholic steatohepatitis (NASH). **b,** Quantification of blood serum levels of cholesterol and ALT in normal, western-diet treated with vehicle (Chow + vehicle, n=15, WD + vehicle, n=14) or western-diet mice treated with DDD86481 (WD + NMTi, n=15). Ordinary One-way ANOVA. **c-d,** Representative images (c) and quantification (d) of $p21^{CIP1}$ staining of liver sections. Yellow arrows indicate examples of $p21^{CIP1}$-positive cells. Scale bar, 50 μm**. e,** GSEA plot showing that a senescence signature is downregulated in WD-fed mice treated with NMTi. NES, normalized enrichment score; FDR, false discovery rate. **f-h,** Representative images (f) of H&E (top), Oil red O (middle), and CD68 IHC (bottom) stained liver sections. Scale bar, 50μm (H&E), 20 μm (Oil red O and CD68). Quantification of Oil Red O staining (g) and CD68 staining (h) is shown. **i-j,** Representative images (i) for picrosirius red-stained liver sections from Chow (Chow + Veh, n=15) and western diet-fed mice treated with vehicle (WD+veh, n=14) or western diet-fed mice treated with NMTi (WD +NMTi, n=15). Scale bar, 50 μm. Picrosirius's red quantification is shown in (j). **k-l,** Levels of Col1a1 (k) and Col4a1 (l) mRNA from bulk liver extracts of chow-fed (Chow + Veh, n=15) and western diet-fed mice treated with vehicle (WD+veh, n=14) or NMTi (WD +NMTi, n=15). **m-n,** GSEA plot showing that senescence signature of Kupffer cells (m) and collagen

938 formation (n) are downregulated in WD-fed mice treated with NMTi. NES, normalized
939 enrichment score; FDR, false discovery rate. Data represented in this figure is Mean±SEM
940 with statistical analysis performed using Ordinary one-way ANOVA.
941

METHODS

Ethics. This research complied with all relevant ethical regulations and was approved and overseen by four ethics review boards. The lung fibrosis experiments were performed in compliance with guidelines established by the Barcelona Science Park's Committee on Animal Care (CEEA 10884). All other mouse procedures were performed under licence, according to UK Home Office Animals (Scientific Procedures) Act 1986, ARRIVE, and local institutional guidelines. The mouse pituitary experiments were approved by the UCL ethical review committee. Liver cancer initiation and the Western diet experiments were approved by the animal welfare and ethical review board at Imperial College London. Cancer xenograft experiments were performed by national and international guidelines and were approved by the author's institutional review board at Southampton University (PPL No. P81E129B7).

Drugs. The following compounds were used in the present study: ABT-263 (Selleckchem, S1001), Etoposide (Sigma-Aldrich, E1383), Palbociclib HCL (Selleckchem, S1116), Q-VD-OPh hydrate (Sigma-Aldrich, SML0063), 4-hydroxytamoxifen (4OHT) (Sigma-Aldrich, H7904), Doxycycline hyclate (Sigma-Aldrich, D9891), Doxorubicin hydrochloride (Cayman chemical, 15007), Triamcinolone (Selleckchem, S1933), Beclomethasone dipropionate (Selleckchem, S3078), GSK2606414 (Tocris, 5107), GSK2656157 (Selleckchem, S7033), Golgicide A (Selleckchem, S7266), Brefeldin A (Selleckchem, S7046), IMP1088 (Myricx), DDD86481 (Myricx), IMP1320 (Myricx), Bleomycin Sulfate (Generon, A10152)

Antibodies. The following primary antibodies were used in this study: mouse monoclonal anti-BrdU (3D4, BD Biosciences, 555627) 1:2000, mouse monoclonal anti-p16INK4a (JC8, CRUK) 1:1000, rabbit polyclonal anti-GAPDH (Abcam, ab22555) 1:2000, mouse monoclonal anti-IL8 (6217, R&D systems, MAB208) 1:100, goat polyclonal anti-IL6 (R&D Systems, AF-206-NA) 1:40-1:200, mouse monoclonal anti-ARF1/3/5/6 (1D9, Invitrogen, MA3-060) 1:500, rabbit monoclonal anti-COPB2 (899, Gifted from F. Weiland) 1:10000, mouse monoclonal anti-EEA1 (14, BD Biosciences, 610457) 1:200, rabbit polyclonal anti-XBP1 (Abcam, ab37152) 1:200, rabbit polyclonal anti-ATF6 (Abcam, ab37149) 1:500, sheep polyclonal anti-TGN46 (BioRad, AHP500G) 1:400, mouse monoclonal anti-GM130 (35, BD Biosciences, 610822) 1:500, mouse monoclonal anti-CHOP (L63F7, CST, 2895S) 1:1000, rabbit monoclonal anti-$p21^{CIP1}$ (12D1, CST, 2947S) 1:2000, rabbit monoclonal anti-$p21^{CIP1}$ (EPR18021, Abcam, ab188224) 1:700, mouse monoclonal anti-N-Ras (F155, Santa

Cruz, sc-31) 1:100, mouse monoclonal anti-β-Catenin (6F9, Sigma, C7082) 1:500, rabbit polyclonal anti-β-Catenin (Thermo, RB-9035-P1) 1:500, mouse monoclonal anti-Synaptophysin (27G12, Leica, SYNAP-299-L) 1:200, rabbit polyclonal anti-Cleaved-Caspase-3 (CST, 9661S) 1:1000, goat polyclonal anti-CXCL1 (R&D, AF-275) 1:100, mouse monoclonal anti-BMP2/4 (100230, R&D, MAB3552), mouse monoclonal anti-VEGF (23410, R&D MAB2931) 1:100. Mouse monoclonal anti-GM-CSF (3209, R&D, MAB215) 1:100, rabbit polyclonal anti-CD68 (Abcam, ab125212) 1:100. Rabbit polyclonal anti-ARF1 (10790-1-AP, Proteintech) 1:1000, rabbit polyclonal anti-ARL1 (16012-1-AP, Proteintech) 1:1000, rabbit polyclonal anti-PPM1B (HPA-016745, Cambridge Bioscience) 1:1000 and rabbit polyclonal, mouse monoclonal anti-TUBA (ab1729, Abcam), 1:1000.

We used the following secondary antibodies: goat anti-mouse IgG-HRP (Santa Cruz, sc-2005) 1:2000, goat anti-rabbit IgG-HRP (Santa Cruz, sc-2004) 1:2000, goat anti-mouse IgG (H+L) AlexaFluor488 conjugated (Invitrogen, A-11029) 1:2000, goat anti-mouse IgG (H+L) AlexaFluor594 conjugated (Invitrogen, A-11032) 1:2000, goat anti-rabbit IgG (H+L) AlexaFluor594 conjugated (Invitrogen, A-11037) 1:2000, donkey anti-sheep IgG (H+L) AlexaFluor594 conjugated (Invitrogen, A-11016) 1:2000, donkey anti-sheep IgG (H+L) AlexaFluor488 conjugated (Invitrogen, A-11015) 1:2000. For the IpaJ western blot experiments, we used the following secondary antibodies: IRDye 800CW goat anti-rabbit IgG (H+L, 926-32211, Li-Cor) and IRDye 800CV goat anti-mouse IgG (H+L, 926-32210, Li-Cor).

Cell lines. IMR90 (ATCC, CCL-186), SK-HEP-1 (ATCC, HTB-52), A549 (ATCC, CCL-185), HFFF2 (ECACC, 86031405), HCT-116(ATCC, CCL-247), MCF-7(ATCC, HTB-22), 5PT (Bauer et al., 2005, n/a), PBEC (ATCC, PCS-300-010), NHLF (Lonza, CC-2512). Primary bronchial airway epithelial cells (PBECs) were cultured in Airway Epithelial Cell Basal Medium (ATCC-PCS-300-030; ATCC) supplemented with Bronchial Epithelial Cell Growth Kit supplements (ATCC-PCS-300-040; ATCC) and 0.1% antibiotic–antimycotic solution (Gibco) with media replenished every 48 hours. Adult normal human lung fibroblasts (NHLFs) were cultured in Fibroblast Basal Medium (CC-3131; Lonza) supplemented with a SingleQuot Kit of supplements and growth factors (CC-4126; Lonza), with media replenished every 3-4 days as required. All other cells lines were maintained on Dulbecco's modified eagle medium (DMEM) (Gibco®) supplemented 1% 100X Gibco® Antimycotic-antibiotic and 10% (v/v) FBS (Labtech, Batch 41213) hereinafter referred to as DM10 media.

Passaging of cells was performed by enzymatic detachment using 0.05% Trypsin-EDTA (Gibco®) on cells for 5 minutes followed by inactivation in DM10 media and centrifugation at 180xg for 5 min. The supernatant was aspirated to remove dead cells and debris and the pellet was resuspended in fresh DM10. Cell viability and counts were determined by flow cytometry on a Guava EasyCyte platform (Millipore®) using Guava ViaCount Reagent to provide stains of dying and nucleated cells. In-built GuavaSoft software was used to gate live cells and remove cell debris/ dead cells from the final cell count. Experiments using IMR90 cells or cell lines generated from them were carried out using cells between passages 10 to 14. To generate ER:RAS^{GV12} and other derived cells, IMR90 or HFFF2 cells, retroviral and lentiviral infections were carried out as previously described in [32]. Treatment with 100nM 4-OHT (Sigma, in DMSO) was used to induce IMR90 ER:RAS cells to undergo OIS. Therapy-induced senescence, TIS was induced in IMR90 cells by treatment with 33 μM (50 μg/ml) Bleomycin sulfate (Generon, A10152) for 24 hours, 20 μM Palbociclib (Selleckchem, S1116) for 7 days or 100 nM Doxorubicin (Cayman chemical, #15007) for 7 days. Senescence was induced in A549 and SK-HEP-1 cells by treatment with 2 μM Etoposide (Sigma-Aldrich, E1383) for 7 days. HCT-116 senescence was induced by 100 nM treatment with doxorubicin (Cayman chemical, 15007) or 2μM etoposide for 3 days followed by 4 days culture in media without chemotherapy. Senescence was induced in MCF7 by 200nM treatment with doxorubicin or 2 μM etoposide for 7 days.

Mice. All mice were purchased from Charles River UK, Ltd except those noted differently. For Hydrodynamic tail vein injection (HDTVI) experiments female C57BL/6J mice aged 5-6 weeks were given 20 μg of a vector expressing Nras^{G12V} and Gaussia luciferase (Gluc) along with 5 μg of SB13 transposase-expressing plasmid. Experiments were performed as described previously in [58]. 4 days after HDTVI, mice were bled to assess the presence of Gaussia luciferase signal in the blood plasma and used to randomize groupings for vehicle and drug-treated groups. On day 5 mice were given 25 mg/kg of IMP1320 (n=9) or vehicle (n=9) (10mM Na_2HPO_4-$7H_2O$ & $NaH_2PO_4H_2O$ buffer, 0.2% Tween-80, pH 7.4) intraperitoneally (i.p.) daily for 4 days. 24 hours after last drug injection mice were culled and livers collected for paraffin embedding and frozen in Optimal cutting temperature (OCT).

For cancer xenograft experiments, $6.7x10^5$ 5PT cells ± $2x10^6$ HFFF2 cells were injected s.c. in the flanks of immunocompromised, male NSG mice (3-5 months old). For knockdown

experiments, HFFF2 fibroblasts expressing inducible shRNAs targeting COPA, COPB2, or control were irradiated with 10Gy using a MultiRad350 X-ray irradiation cabinet (from Precision X-ray) just before implantation. *In vivo,* expression of the shRNA was induced using doxycycline given in the drinking water throughout the experiment (2mg/ml with 5% sucrose in the drinking water). For inhibitor experiments, 10mg/Kg NMTi (DDD86481) was dissolved in water containing 5% DMSO, 20% PEG400, 10mM Na_2HPO_4-$7H_2O$ & $NaHPO_4H_20$ buffer, 0.5% Tween-80, pH 7.3, and administered t by IP injection as indicated in Fig 7e. Between 6-8 biological replicates were used per group. Tumour size was measured over time using an electronic caliper and calculated using the formula 4π/3 x r3 [radius (r) calculated from the average diameter, measured as the tumour width and length]. The area under the curve (AUC) for each tumour within a treatment group for single experiments was analyzed and statistical analysis comparing AUC was performed on pooling of multiple experiments.

For testing senolytics ex vivo in the ACP model of OIS, neoplastic pituitaries from 18.5dpc *Hesx1*$^{Cre/+}$*; Ctnnb1*$^{lox(ex3)/+}$ embryos [70] were dissected. Both male and female mice were used and numbers equalized in experimental and control groups.

For the lung fibrosis experiments, we used a previously described mouse model of lung fibrosis induced by intratracheal administration of senescent human cells [16, 41]. Normal proliferating (IMR90 vector) or gamma-irradiated senescent human fibroblasts IMR90 (IMR90 vector, IMR90 shCOPB2.1 or IMR90 shCOPB2.2) (500.000 cells) were delivered into the lungs of 6-8 weeks old athymic (nu/nu) mice (Envigo Laboratory). Two days before intratracheal instillation, these animals started treatment with doxycycline (1mg/ml in the drinking water) until the end of the experiment. Three weeks after intratracheal instillation, their lungs were removed and analyzed. For estimating the number of senescent IMR90 cells engrafted in the lung after 48h post-instillation, we first performed a calibration using a known amount of IMR90 cells mixed with lung homogenates. Specifically, the right lobes of nude mice were surgically dissected and placed into 1.5-mL tubes. Homogenates of the lung samples were performed by grinding the frozen samples with liquid nitrogen using a mortar and pestle. Tissues were then thawed, 1 mL of distilled water was added to the tissues, and the resulting suspensions were homogenized using a micro-sample homogenizer (Precellys). Different quantities of senescent shControl IMR90 cells (0, 1000,

5000, 10.000, 50.000, or 100.000 cells) were mixed with 1 mL of homogenized lung tissue. After Trizol extraction of RNA and cDNA synthesis using SuperScript™ III Reverse Transcriptase (Thermo Fisher, Waltham, MA, USA), real-time qPCR was performed using the PowerUp™ SYBR®Green Master Mix (Applied Biosystems, Foster City, CA, USA). Gene expression analysis was performed using predesigned primers and probes for human *MMP3*. Data were normalized using mouse actin b. The resulting calibration curve was used to interpolate the data obtained using lung samples 48h post-intratracheal instillation of shControl, shCOPB.1, and shCOPB.2 IMR90 cells (500,000 cells) in nude mice under doxycycline.

For western diet experiments, C57BL/6J male mice aged 8 weeks old were placed on chow or western diet (kcal 40% fat (non-trans-fat Primex Shortening), kcal 20% fructose, 2% cholesterol, D1602230i) for 4 weeks before the first round of injections. Mice were then injected with Vehicle (chow diet, n=15) (western diet, n=15) (10mM Na_2HPO_4-$7H_2O$ and $NaH_2PO_4H_2O$ buffer, 0.2% Tween-80, pH 7.4) or 10mg/kg DDD86481 (western diet, n=15) (5% DMSO, 20% PEG400, 10mM Na_2HPO_4-$7H_2O$) and NaH_2PO_4-H_2O buffer, 0.5% Tween-80, pH 7.3, dissolved by cold water bath sonication) i.p. daily for 3 days, then given 2 rounds of 4 week rest period and 3-day daily i.p. injection. Blood was collected before the final round of injection for physiological assessments. Mice were allowed to rest for 4 weeks before being culled and organs were collected for freezing in OCT, paraffin embedding, blood collection for physiological measurements, and tissue snap-freezing for RNA extraction.

Vector construction. pLNC-ER:RAS-neo has been previously described in [71]. The mutant $GBF1_{M832L}$ construct was a gift from F.J.M. van Kuppeveld (Utrecht University). Cloning of $GBF1_{M832L}$ intro retroviral expression vector (pBabe-puro,) was performed by PCR amplification using Human5SnaBIGBF1 (5'-CGTACGTAGCCATGGTGGATAAGAATATTT-3') and Human3SalIGBF1 (5'-CGGTCGACGCCTTAGTTGACCTCAGAGGTG-3') primers with Q5® High-Fidelity DNA Polymerase (New England Biosciences) according to manufacturer's instructions. Amplified $GBF1_{M832L}$ was subcloned into pBabe-puro using standard cloning with SnaBI and SalI restriction enzymes. Gaussia luciferase (Gluc) containing plasmid was a gift from U. Griesenbach (Imperial College London). To generate Gluc expressing HDTVI construct (CaNiGluc), Gluc was PCR amplified using: 5BmgBIsogLUX: (5'-GATTAAGACG TGGTTTTCCT TTGAAAAACA CGATGATAAT ATGGGAGTGA AGGTGCTGTT-3') and 3sogLUXAge1 (5'-TTTGTTACCG GTCTCATCAA

TCTCCCCCAGCT-3') primers and Q5® High-Fidelity DNA Polymerase (New England Biosciences) according to manufacturer's instructions. Amplified Gluc was subcloned into HDTVI construct (CaNiG) by restriction enzyme excision of GFP and annealing of Gluc amplicon processed with BmgBI and AgeI into CaNiG plasmid. IpaJ construct was a gift from Ed Tate (Imperial College London). Cloning of $IpaJ_{WT/C64A}$ was performed by PCR amplification of IpaJ using 5'EcoRIKozIpaJ (5'-tggtggaattcgccaccATGTCGGAACAACGGAAG-3') and 3'IpaJPmeI (5'-agcaggtttaaacTTACAAAGCCTCATTAGT-3') and subcloning into pLenti-puro vector (Addgene #39481) with EcoRI and PmeI restriction enzymes. Tetracycline inducible (Tet-ON all-in-one) shRNA vector (LT3GEPIR) was a gift from J. Zuber (IMP, Vienna). The generation of miRE-based inducible shRNA vectors was performed as previously described [32]. The following shRNA sequences were used against the following genes: *COPB2* (#1-TTAAATATCTTTACAATGCTGT, #2- TAATTGAACACTCTAATCTGCA and #5-TCAATCATCCAAAATATCTTCA) *COPA* (#1- TTCACTTTAGAAATCTTCACAG, #2-TTGAATTTGAACTCAGTGGGAT, #3- TTATATTTTTATTAGAGACGGG and #4-TTGAAATTTAAATGTCTAAGGA) *COPG1* (#1- TTTTCAATACAGAAGCTTGGGA, #4-TTCATTGTCATCATCCATCACA and #5- TTTTGAATGTGATCAGCTACAG) and *BCL2L1* (#1- TAGTATATCATCTTCACAAGGA). *PTBP1 (*#53- AGACCAGAGATTTTATTTT, #86-GGATTCAAGTTCTTCCAGA)

Immunofluorescence and high throughput microscopy. Immunofluorescence staining was carried out by first fixing wells of 96 well plates at desired timepoint for 1 hour using 4% PFA (w/v, in PBS) followed by washing 3 times with PBS. Wells were then permeabilized using 0.2% Triton® X-100 (v/v, PBS) for 10 min and then washed twice with PBS to halt permeabilization. Non-specific antibody binding was blocked by incubation with a blocking solution for 1 hour at RT. The blocking solution contained 1% BSA (w/v, PBS) supplemented with 0.4% Fish Skin Gelatin (v/v, PBS). Primary antibodies were diluted in blocking solution and wells were incubated with primary antibody solution for 1 hour at RT. For BrdU staining primary antibody solution is supplemented with 0.5U/µl DNase (Sigma) and 1mM $MgCl_2$ and incubation times are reduced to 30 minutes. Following incubation, the primary antibody was then removed by washing 3 times with PBS. Secondary antibodies conjugated to Alexa-594 or Alexa-488 fluorophores were then diluted in blocking solution and added to wells to be incubated in the dark for 1 hour. The secondary antibody was then removed by washing 3

times with PBS and nuclei counterstaining with 1μg/mL DAPI (w/v, PBS) for 10 minutes. Wells were then washed with PBS three times.

Immunofluorescence image acquisition was performed using an automated InCell Analyzer 2000 high-throughput microscope. Multiple 96-well plates were placed into stacks from which a KiNEDx Robotic arm (PAA) running Overlord™ software so that plates could be sequentially loaded, imaged, and removed with the InCell microscope. Wells were imaged using a 20x objective except for wells stained only with DAPI or Golgi-related staining, which were performed at 10x and 40x respectively. 2x2 binning of images was used to reduce image file sizes. Fluorophores were imaged using pre-set 'DAPI', 'Texas Red' & 'FITC' wavelengths on the microscope for DAPI stain, AlexaFluor® 594, and AlexaFluor® 488 respectively. 8, 24, and 18 fields per well were captured for 10x, 20x, and 40x objectives respectively.

High-content image analysis was carried out using the InCell Investigator 2.7.3 software (GE Healthcare®). DAPI nuclear counterstain was used to segment cells using a Top-hat method and used to provide a mask for nuclear-localized stains. For cytoplasmic stains, a 6μm collar was applied around the cell and for detection of cytoplasmic organelles such as Golgi, a 'region growing' collar was used. Quantification for nuclear staining was measured as average pixel intensity (greyscale) for the wavelength of fluorophore across the area of the nuclear mask. Cytoplasmic staining quantification was of either the average pixel intensity or the coefficient of variance of pixel intensities within the collar area. Golgi structural analysis utilized a multiscale top-hat segmentation method to detect organelle structures between 1 and 3 pixels in size within a region-growing collar. Cells with >25 Golgi organelle structures per cell were classified as cells with dispersed Golgi.

Growth assays. BrdU incorporation and colony formation assays were performed as previously described in [39]. Briefly, for BrdU incorporation assays, cells were incubated with 10μM BrdU for 18 hours before being fixed using 4% Paraformaldehyde (v/v, PBS). BrdU incorporation was assessed via immunofluorescence and high-content analysis. For crystal violet staining, cells were seeded at low density in 10 cm dishes and cultured for 10-14 days or until proliferating cells had reached 80-90% confluency. To assess senolysis, cells were seeded in 10cm plates at high density. Senolytic drugs were added at their indicated concentration in DMSO (< 0.5% v/v final concentration) and cultured for a further 3 days. If longer drug treatment was required fresh drug and media were added on day 3 and cultured

for a further 4 days. At the endpoint, plates were fixed with 0.5% (w/v, PBS) glutaraldehyde (Sigma) for 1 hour, washed twice with dH_2O, and left to dry overnight. Dried plates were then stained with a 0.2% (w/v, PBS) solution of crystal violet (Sigma, C6158).

Senolytic assays. Senolytic assays were performed as described before [15]. Briefly, at the indicated points, confluent senescent or control cells in 96-well plates were switched to DMEM 0.5% FBS and drugs in DMSO were added (<5% v/v final concentration). Drugs were replenished after 3 days if the assay length was longer than 72h. For therapy-induced senescence of primary bronchial airway epithelial cells (PBECs) (ATCC PCS-300-010) were seeded at passage 3 and treated with Bleomycin (100ng/ml), or vehicle, for 5 days followed by wash-out. 7 days post-senescence induction, cells were treated with the indicated drugs for 72 hours. Adult normal human lung fibroblasts (NHLFs) (Lonza CC-2512) at passage 4-5 were seeded into 96-well plates and induced to senesce by treatment with Bleomycin (50mg/ml), or vehicle, for 24 hours. 7 days post-induction of senescence, cells were treated with the indicated drug concentrations for 72 hours. Cells were fixed and stained with DAPI followed by assessment by automated microscopy. The percentage survival was calculated by dividing the number of cells post-drug treatment by the corresponding number of cells treated with the vehicle at the same time.

For senolytics assays during replicative senescence, PBECs were serially passaged until passage 4-6, whereby a mixed population of senescent and growing cells can be distinguished. PBECs were plated into 96-well plates and treated with the indicated drug for 72 hours. Cells were fixed and stained with anti-p16 antibody and DAPI followed by assessment by automated microscopy. The percentage survival for p16-negative and p16-positive fractions was calculated by dividing the number of cells post-drug treatment by the number of cells treated with the vehicle.

Tissue processing. Organs were fixed in 4% PFA overnight before being transferred to 70% Ethanol. Tissue processing before paraffin embedding was performed on a Sakura Tissue-Tek VIP® 6 automated tissue processor. Briefly, specimens in embedding cassettes were dehydrated by progressing through steps of 70% Ethanol for 45min at 37°C, 80% Ethanol for 45min at 37°C, 90% Ethanol for 30min at 37°C, 96% Ethanol for 45min at 37°C, 100% Ethanol for 30min at 37°C, 100% Ethanol for 1hr at 37°C, 100% Ethanol for 1hr at 37°C. Dehydrated samples are then cleared by three washes in Xylene for 30min, 45min, and 1hr at 37°C. Finally, specimens are infiltrated by two immersions in 62°C paraffin wax

for 45 min and 1hr, followed by two immersions in 62°C paraffin wax for 30min. The specimen was then embedded in a paraffin block on an embedding centre (Leica EG1160 Embedding Centre) and 4μm sections were made using ThermoFisher scientific Microtome Microm HM355S and attached to slides.

Immunohistochemical staining. Slides were deparaffinized by washing slides twice in Histoclear™ for 5 minutes each, followed by 5-minute washes in decreasing concentrations of ethanol with 100%, 75%, 50%, and 25% ethanol before a final wash of 5 min in dH_2O. Heat-induced epitope retrieval (HIER) was then performed in a pressure cooker for 20 min using either antigen-unmasking solution, Citrate-based at pH 6.0 (VectorLab, H-3300-250), or antigen-unmasking solution, Tris-based at pH 9.0 (VectorLab, H-3301-250) depending on antibody manufacturer's instructions. Following HIER, slides were cooled on ice for 10min and then washed in PBS for 5 min. For intracellular stains, sections were permeabilized with 0.2% Triton X-100 in PBS for 10min and washed twice in PBS for 5 min. For NRAS staining Liver slides were washed in 0.1% H_2O_2 in PBS for 15 min followed by washing twice in PBS to reduce endogenous peroxide activity. Sections were marked using a hydrophobic pen and Non-specific antigen binding was blocked by incubating slides with CAS-Block™ Histochemical reagent (ThermoFisher, 008120) for 30-45 min in a humidified chamber. Slides were then incubated with primary antibody overnight in a humidified chamber at 4°C. Slides were washed twice in PBS for 5 min and incubated with secondary antibody SignalStain® Boost IHC detection reagent with Mouse HRP (Cell Signalling Technology, 8125) or Rabbit HRP (Cell Signalling Technology, 8114) for 30-45 min. Next, slides were washed twice in PBS for 5 min and incubated for 2-10min with SignalStain® DAB substrate kit (CST, 8059) to detect HRP signal. Signal development was stopped when visible positive cells could be detected on a microscope, by washing slides in dH_2O. To counterstain the DAB signal, slides were incubated for the 30s in Modified Mayer's Haematoxylin (Lillie's Modification) (DAKO), washed in dH_2O, and incubated for 30s in 0.05% Ammonium solution (PBS) followed by washing in dH_2O. Before mounting coverslips with VectaMount aqueous mounting media (VectorLab, H-5501-60) slides were dehydrated by washing for 1 minute in 75% Ethanol, 5 minutes in 100% Ethanol, and 5 minutes in Histoclear®. Slide images were acquired using a 20x brightfield objective on a Zeiss AxioScan Z.1 slide scanner and analysis was performed on fields using QuPath version

0.2.0-m9 using an inbuilt positive cell detection tool to segment Haematoxylin-stained nuclei and quantify the mean intensity of DAB.

Histologic analysis of the mouse fibrosis experiment. Left lung tissue was fixed in a 10% neutral buffered formalin solution for 24 hours and subsequently transferred into tissue cassettes and placed into PBS for a minimum of 24 hours. Tissues were then shipped to Institute for Research in Biomedicine (IRB, Barcelona) Histopathology Facility for paraffin embedding, sectioning, and Masson's Trichrome and Hematoxilin-Eosin staining. Samples were examined first in a blinded fashion and in a second round in an unblinded fashion. Semiquantitative histological scoring of fibrosis was scored at 20-40x using the following scale: 1, x1; 2, x2; 3, x3 increase the thickening of alveolar walls; 4, >x3 thickening of alveolar walls and focal areas of single fibrotic masses. If there was difficulty in deciding between two scores, the intervening number was given.

Hydroxyproline Assay. Superior and middle lung lobes were surgically dissected, weighed, and placed into 1.5-mL sterile tubes and flash-frozen until all the samples were collected. Homogenates of the lung samples were performed grinding the frozen samples with liquid nitrogen using a mortar and pestle. On the day of the assay, tissues were thawed, and 1 mL of distilled water was added to the tissues. Tissues were homogenized using a micro-sample homogenizer (Precellys). 200 µL of 12N hydrochloride was added to 200 µL of homogenized tissues. Samples were placed into a preheated oven set to 120ºC and incubated overnight. The next morning, samples were cooled and vortexed. Biochemical quantification of hydroxyproline was performed using a hydroxyproline assay kit (Amsbio).

Senescence-associated β-galactosidase assay. Cells grown in 6-well plates were fixed with a solution of 0.5% glutaraldehyde (w/v, PBS) (Sigma) for 10 min and washed twice in a solution of 1mM $MgCl_2$/PBS (pH 6.0). To stain plates were incubated with X-gal staining solution for 18h at 37ºC. Images were acquired by brightfield microscopy using an inverted microscope (Olympus CKX41) with an attached digital camera (Olympus DP20). Cells were counted using ImageJ software to determine the percentage of positive cells.

Liver samples frozen in optimal cutting temperature (OCT) were cryosectioned (15µM) and frozen sections were fixed in ice-cold 0.5% Glutaraldehyde (w/v, PBS) for 15 min and washed 1mM $MgCl_2$/PBS (pH 6.0) for 5 min. β-galactosidase activity was stained for with X-

gal staining solution (1mg ml^{-1} X-gal, Thermo Scientific™, 5mM $K_3(Fe(CN)_6)$, 5mM $K_4(Fe(CN)_6)$) diluted in 1mM $MgCl_2$/PBS (pH 6.0) for 18h at 37°C. Slides were dehydrated and coverslips mounted before being imaged using 20x brightfield objective on Zeiss AxioScan Z.1 slide scanner. ImageJ was used to quantify staining by measuring the SA-β-gal-stained area as a percentage of the total tissue area excluding luminal spaces.

Sirius Red staining. Sirius red staining was carried out for collagen I / III fiber containing connective tissue on paraffin-embedded sections using Picro-Sirius Red Stain Kit (Abcam, ab150681). Before staining, sections were deparaffinized in Histoclear and graded ethanol washes as described above (*see Immunohistochemical staining)* and hydrated in distilled water. Sections were then incubated with Picro-Sirius red solution for 60 min at RT and then rinsed twice with 0.5% glacial acetic acid solution (in dH_2O). Excess water was then removed by shaking slides and then rinsing in 100% ethanol. Sections were then dehydrated by two washes of 100% ethanol for 2 min each and two washes in Histoclear for 2 min each. Coverslips were mounted and slides were imaged on Zeiss AxioScan Z.1. Staining was quantified by thresholding the collagen-stained area for detection of fibers (red) and measuring this area relative to the total tissue area.

Blood chemistry and immune cell composition analysis. For analysis of immune cell composition in whole blood, tail-vein blood was collected 2 days after the last treatment. Whole blood was diluted in saline to a volume of 200 μL and ran on a Sysmex XE2100 automated cell counter. Blood glucose levels were determined by collecting whole blood from the tail vein into heparinized tubes (Abraxis), 120-140μL of whole blood to be loaded onto a comprehensive diagnostic profile reagent rotor (Abraxis) or Mammalian Liver Profile reagent rotor and run on a VetScan VS2 Chemistry Analyzer (Abraxis, 500-7123).

Oil Red O staining. Staining for lipids was carried out on liver tissue in OCT was snap-frozen in liquid N2 and cryosectioned (15μm). Sections were equilibrated to RT for 10 min and then stained with 0.5% Oil Red O solution (w/v, in isopropanol, Sigma, O1391) for 5 min, rinsed in tap water and counterstained with Mayer's hematoxylin for the 30s. Then sections were again rinsed in tap water for 30 min and coverslips mounted. Images were acquired on Zeiss AxioScan Z.1 and ImageJ quantification of the Oil-red stain area relative to the background tissue area.

***Ex vivo* culture of mouse pituitaries.** Neoplastic pituitaries from 18.5dpc *Hesx1*$^{Cre/+}$;*Ctnnb1*$^{lox(ex3)/+}$ embryos were dissected and placed on top of 5 µM Nuclepore membranes (VWR) in 24 well plates containing 500 µl of media (DMEM-F12, Gibco, 1% Pen/Strep, Sigma and 1% FBS, Thermo Fisher Scientific) supplemented with either IMP1088 or vehicle (DMSO). Media was changed every 24h, pituitaries were processed for analysis after 72 hours. Immunofluorescence staining was performed as previously described in [56]. The proportion of β-catenin-accumulating cells was calculated as an index out of the total DAPI-stained nuclei. Over 120,000 DAPI nuclei were counted from 15 to 22 histological sections per sample, in a total of eight neoplastic pituitaries. The proportion of cleaved-caspase-3 and synaptophysin-positive cells was calculated as an index out of the total tissue area, from 6 to 12 histological sections per sample.

Immunoblotting. Cells were collected for protein extraction by first washing twice with ice-cold PBS, scraping and centrifugation performed at 180g for 5 min at 4°C. Cell pellets were then resuspended in RIPA lysis buffer (Thermo Scientific™, 89900) supplemented with one tablet of PhosSTOP® (Roche) and one tablet of cOmplete™, Mini, EDTA-free Protease inhibitor (Roche). Lysis was performed on ice for 30 min with periodic vortexing. After lysis samples were centrifuged at 13,000g for 20min at 4°C and protein-containing supernatant was transferred to a fresh tube. RIPA lysed samples quantification was then performed using Pierce BCA assay (Thermo Scientific™) and equal amounts of sample resuspended in required volumes of 4x Laemili sample Buffer (Bio-Rad, #1610747) and boiled at 95°C for 10 min. To immunoblot proteins, samples were separated by size on pre-cast polyacrylamide gradient gels (Bio-Rad, #4561084) and transferred onto 0.2µm nitrocellulose membranes (Bio-Rad). Efficient transfer and correct gel loading were verified by Ponceau S staining before 1hr blocking of membranes with 5% milk (w/v) diluted in TBS supplemented with 0.1% Tween-20 (v/v) (TBST). Primary antibodies were diluted in 5% milk (w/v, TBST) and incubated with membranes overnight at 4°C. This was then followed by three washes with TBST followed by 1hr incubation with horseradish peroxidase-conjugated secondary antibody. Secondary antibody binding was visualized using Amersham ECL Prime Western Blotting Detection Reagent (Cytiva) and imaged on Amersham Imager 680 blot and gel imager (Cytiva).

RNA extraction. Total RNA from tissues was extracted by bulk way of by bead disruption in 800 µL of TRIzol® reagent (Invitrogen) using TissueLyser (Qiagen) followed by further homogenization using QIAshredder kit (Qiagen) according to manufacturers' instructions. Homogenized tissue in TRIzol® was then mixed with 160µL of Chloroform (Sigma) and vortexed for 15s, then centrifuged at 15,000rpm at 4ºC for 30-45 min. The top aqueous phase containing RNA was then column purified using RNAeasy®Mini Kit (Qiagen) and subjected to DNase treatment as per the manufacturer's instructions. RNA concentration was determined using NanoDrop® ND-1000 UV-Vis spectrophotometer at 260nm wavelength.

For extraction of total RNA from cells, 6-well plates were scraped in 800 µL of TRIzol® reagent (Invitrogen), mixed with 160 µL of Chloroform (Sigma), vortexed, and centrifuged as stated above. The aqueous phase was then transferred to a new tube and processed from step 2 onwards of the manufacturers' instructions for RNAeasy® Mini Kit (Qiagen).

cDNA synthesis and quantitative RT-PCR. To generate cDNA, total RNA was diluted in nuclease-free water to the same concentration across samples of the same experiment and 1-5 µg amplified using SuperScript® II Reverse Transcriptase kit (Invitrogen) combined with 1 µL of random hexamer primers (50 ng/µL, Invitrogen), 1 µL dNTP mix (10 mM, Bioline) and made up to a final volume of 11 µL in nuclease-free water. Mix was then added to thermocycler for one cycle of 10 min at 25 ºC, 50 min at 42ºC, and 15 min at 70ºC. cDNA samples were then diluted at 10 ng/µL based on input RNA concentration.

mRNA expression analysis was carried out using real-time quantitative PCR (RT-qPCR) by way of amplification of cDNA using SYBR® Green PCR Master Mix (Applied Biosystems) run on a CFX96™ Real-Time PCR Detection system (Bio-Rad). RT-qPCR primers were selected from PrimerBank [72] spanning exon-exon junctions. Relative gene expression in human cell lines was determined using the ΔΔCt method by measuring the RT-qPCR signal relative to the signal of housekeeping gene RPS14 and normalization to control samples. For mouse mRNA expression, the ΔΔCt method was again used but the signal was measured relative to GAPDH.

For the mouse fibrosis experiments, tissues were homogenized in Trizol and the cDNA was synthesized using the SuperScript™ III Reverse Transcriptase (Thermo Fisher, Waltham, MA, USA). Real-Time PCR was performed using the PowerUp™ SYBR®Green Master Mix (Applied Biosystems, Foster City, CA, USA). Gene expression analysis was performed

using the indicated primers. The results were then normalized using the housekeeping gene Gapdh, Actin b, or Hprt.

Human primer pairs are:

COPG1: CACCTTGAGAAGAGTGCGGTA, GGCACATTTCCGAGGGTTG

COPB2: CTTCCTGTTCGAGCTGCAAAG, CACTCTAATCTGCATGTCATCCG

RPS14: CTGCGAGTGCTGTCAGAGG, TCACCGCCCTACACATCAAACT

GAPDH: TTCACCACCATGGAGAAGGC, CCCTTTTGGCTCCACCCT

CDKN2A: GATCCAGGTGGGTAGAAGGTC, CCCCTGCAAACTTCGTCCT

Mouse primer pairs are:

Cdkn1a: TCCCGACTCTTGACATTGCT, TGCAGAAGGGGAAGTATGGG

Gapdh: AACTTTGGCATTGTGGAAGG, ACACATTGGGGGTAGGAACA

Actin b: ATGGAGGGGAATACAGCCC, TTCTTTGCAGCTCCTTCGTT

Cdkn1a: GTGGGTCTGACTCCAGCCC, CCTTCTCGTGAGACGCTTAC

Col3a1: ACAGCAAATTCACTTACAC, CTCATTGCCTTGCGTGTTT

Cxcl2: CTGCCAAGGGTTGACTTCAA, TTTTGACCGCCCTTGAGAGT

Pai-1 (Serpine1): CCAACATCTTGGATGCTGAA, GCCAGGGTTGCACTAAACAT

Col1a1: GAGAGGTGAACAAGGTCCCG, AAACCTCTCTCGCCTCTTGC

Col4a1: CTGGCACAAAAGGGACGAG, ACGTGGCCGAGAATTTCACC

Hprt: CACAGGACTAGAACACCTGC, GCTGGTGAAAAGGACCTCT

RNA-Seq and GSEA. Total RNA extracted and purified from tissues or cell extraction was analyzed on a 2100 Bioanalyzer (Agilent) using RNA 6000 Nano Kit (Agilent) to verify RNA purity and integrity before library preparation. RNA from tissue samples with an RNA integrity number (RIN) corresponding to the ratio of 18S to 28S rRNA peaks on bioanalyzer trace of less than 3 were not submitted for library processing. Library preparation to generate cDNA was performed by MRC – LMS genomics core facility with 200ng of starting RNA using the NEBNext® Poly(A) mRNA magnetic isolation kit (NEB, E7490) to isolate mRNA from the total RNA sample. Purified samples were then processed using the NEBNext® Ultra™ II. Directional RNA Library Prep Kit for Illumina (NEB, E7760). Libraries were then assessed on a 2100 Bioanalyzer and concentration was determined using a Qubit® Fluorometer and the Qubit dsDNA HS Assay kit (Thermo Scientific™). Indexed libraries were then run on 2 lanes of a NextSeq 2000 sequencer (Illumina) with > 10 million single-end 75bp reads being generated per sample. Human RNA-seq reads were assessed for

quality using FASTQC and then aligned to human genome hg19 by Tophat (v. 2.0.11) using '-library-type- fr-firststrand' parameters along with gene annotation from Ensembl (v.67). Gene set enrichment analysis (GSEA) was carried out on the differential expression between vehicle and drug-treated aged tissues using "wald statistics" parameters in DESeq2 and all curated gene sets in MSigDB.

Live-cell microscopy. To analyse live-cell induction of apoptosis, cells were incubated with IncuCyte caspase-3/7 reagent (1:500, Essen Bioscience) following reverse transfection with senolytic siRNAs or drug treatment. Four images per well of a 96-well plate were collected every 2h for 3-4 days using a 10x objective on an IncuCyte microscope and fluorescence images were analyzed in IncuCyte Zoom software (Essen Bioscience).

Druggable-genome siRNA screening and siRNA transfection. Druggable genome-siRNA libraries were purchased from Qiagen (Human Druggable Genome siRNA Set V4.1, 2 siRNA per gene) and Dharmacon™ (siGenome human druggable genome, 4 siRNA per gene). Individual siRNAs were purchased from the siGenome reagent family of Dharmacon™ (Horizon Discovery) and came lyophilized in tube format or coated onto 96-well plates. Before transfection, plates containing 0.1nM of lyophilized siRNA were resuspended in 100µL of nuclease-free water and 3.6µL of siRNA aliquoted into daughter plates. For large-scale libraries, daughter plates were aliquoted using Laboratory Automation Workstation Biomek® NX^P (Beckman Coulter). Transfection mix containing 0.2 µL DharmaFECT™ 1 with 17.4 µL of DMEM only or 0.4 µL DharmaFECT™ 1 with 17.2 µL of DMEM was added to daughter siRNA plates for IMR90 ER:RAS or IMR90 experiments respectively. To reverse transfect cells, 100 µL suspensions of proliferating or senescent cells in media with DMEM supplemented with 10% FBS only were added to plates with combined transfection mix and siRNA (final siRNA concentration 30nM). After 18 hours when cells had been allowed to adhere, media was replaced with DMEM supplemented with 0.5% (w/v) FBS and 1% antibiotic-antimycotic solution. Plates were then fixed in 4% PFA (w/v) 72 hours after media change, to then be processed for quantitative IF. For analysis of mRNA, the protocol was scaled to a 6-well plate format and cells were collected by the addition of TRIzol ® RNA isolation reagent (Invitrogen) to the well followed by scraping and collection. siRNAs targeting the following genes were used in this study:
ARF1 (#1- GACCACCAUUCCCACCAUA and #3- CGGCCGAGAUCACAGACAA)
COPB2 (#1- CAACAGCAUUGUAAAGAUA, #2- GGACACACCCAUUAUGUUA, #3-

GGUCAAACAAUGUCGCUUU and #4- GGUUGUGACAGGAGCGGAU), *COPG1* (#1- GAGGGUGGCUUUGAGUAUA and #4- GGAGGCCCGUGUAUUUAAU), *TREM2* (#1- GGACACAUCCACCCAGUGA and #4- GGGCUGAGAGACACGUGAA), *GNG8* (#1- CCAACAACAUGGCCAAGAU and #2- GAAGGUGUCGCAGGCAGCA), *UBB* (#2- GUAUGCAGAUCUUCGUGAA and #4- CCCAGUGACACCAUCGAAA), *UBC* (#3- GAAGAUGGACGCACCCUGU and #4- GUAAGACCAUCACUCUCGA), *ALDOA* (#1- GGACAAAUGGCGAGACUAC and #3- GGCGUUGUGUGCUGAAGAU), *APOC2* (#1- AGGAAUCUCUCUCCAGUUA and # 2- CAGCAGCCAUGAGCACUUA)

B-score normalization analysis. To analyse the siRNA screen, cell counts were normalized by B-score using R package, CellHTS2 (https://doi.org/doi:10.18129/B9.bioc.cellHTS2) [73]. Cell count normalization was performed using the plate-averaging method and on separate batches for control and senescent cells in addition to separate normalization performed for each batch of plate transfections.

ELISA. For detection of secreted factors in conditioned media of IMR90 ER: RAS cells, 100µL of media (DMEM supplemented with 0.5% (w/v) FBS and 1% antibiotic-antimycotic solution) incubated with cells and inhibitors for 48-72h was collected and filtered using a 0.2µm cellulose acetate membrane (Gilson). Filtered samples were then subject to an ELISA kit according to manufacturer's instructions (R&D: IL-6, DY206; IL-8, DY208; VEGF, DY293B; CXCL1, DY275; G-CSF, DY214; GM-CSF, DY215; CCL2, DY279; CCL20, DY360; LIF, DY7734). Cell numbers were calculated using high throughput microscopy and used to normalize levels of secreted factors.

Proteostat Assay. Relative levels of protein aggregates were measured using the PROTEOSTAT® Protein aggregation assay (ENZ-51023) according to the manufacturer's instructions. Briefly, cells plated in 96 well formats and treated with the drug were incubated with PROTEOSTAT® detection reagent for 15 min at room temperature and red on a FLUOstar® Omega plate reader at $_{ex}$550nm and $_{em}$600nm. The background was subtracted and intensity values normalized to cell counts from fixed DAPI stained plates using high throughput microscopy.

Visualization of IpaJ effects on *N*-myristoylation with YnMyr and immunoblot analysis. In triplicate for each condition, IMR90 cells (controls, and cells transduced with

IpaJ WT and IpaJ C64A constructs) were seeded in 6 well plates and grown to 70-80% confluence. IMR90 control cells were incubated for 1 h with DMSO or 100 nM IMP-1088. All conditions, including IpaJ variant-expressing cells, were thereafter metabolically labeled with 20 μM YnMyr for 18 h. Thereafter, cells were washed with PBS, harvested by trypsinization, and cell pellets were stored at -80°C until further analysis. Cell pellets were lysed, YnMyr-labelled proteins functionalized with fluorescent capture reagent and resolved by fluorescence scanning after separation on 15% (w/v) SDS-PAGE gels as previously described [48, 53]. Immunoblotting was performed on ARF1, ARL1, PPM1β , and TUBA, read-out on a Li-Cor Odyssey CLx using IRDye 800CW-functionalized secondary antibodies. Fluorescence intensities were quantified by ImageJ and normalized to TUBA loading control.

Statistics and reproducibility. Statistical analyses were performed and plotted using GraphPad Prism 9 software. Details of the test used are given in the corresponding figure legends and the source data. Statistical analysis was performed using either an Unpaired, two-tailed t-test with Holm-Sidak multiple comparison correction or with Ordinary one or two-way ANOVA with Dunnet's or Tukey's multiple comparison correction. Tumor growth curves were analyzed using RM Two-way ANOVA with Greenhouse Geisser Correction and Dunnet's correction. P values and Adjusted P values are shown for values lower than p=0.1. P values for other comparisons can be found in the source data. *, $p < 0.05$.**, $p \leq 0.01$.***, $p \leq 0.001$.****, $p \leq 0.0001$.

Reporting Summary. Further information on research design is available in the Nature Research Reporting Summary.

DATA AVAILABILITY

Source data and full membranes for the western blot experiments have been included as supplementary information in this manuscript. The RNA-seq data generated in this study have been deposited in the GEO database under accession numbers GSE224070 (token **gvipekuqlxydbet**), GSE224071 (token **ovgzggauxritzyn**) and GSE224069 (token **knepucqafnidxeb**).

METHODS REFERENCES

70. Gaston-Massuet, C. *et al.* Increased Wingless (Wnt) signaling in pituitary progenitor/stem cells gives rise to pituitary tumors in mice and humans. *Proc Natl Acad Sci U S A* **108**, 11482-11487 (2011).
71. Acosta, J.C. *et al.* Chemokine signaling via the CXCR2 receptor reinforces senescence. *Cell* **133**, 1006-1018 (2008).
72. Wang, X., Spandidos, A., Wang, H. & Seed, B. PrimerBank: a PCR primer database for quantitative gene expression analysis, 2012 update. *Nucleic Acids Res* **40**, D1144-1149 (2012).
73. Pelz, O., Gilsdorf, M. & Boutros, M. web cellHTS2: a web application for the analysis of high-throughput screening data. *BMC Bioinformatics* **11**, 185 (2010).

ACKNOWLEDGEMENTS

We are grateful to members of J. Gil's laboratory for reagents, comments, and other contributions to this project. We thank M. Latreille (MRC LMS) and S. Gallage (DKFZ) for their feedback. We thank Neus Prats (IRB) for scoring the pathological state of mouse lung fibrosis. We thank F.J.M. van Kuppeveld (Utrecht University) for the GBF1 constructs and F. Wieland (Heidelberg University Biochemistry Centre) for anti-COPI antibodies, U. Griesenbach (Imperial College London) for the Gaussia luciferase plasmid and J. Zuber (IMP Vienna) for the LT3GEPIR plasmid. Some figures were designed using elements from Smart Servier medical art that are licensed under creative commons BY 3.0. terms. Core support from MRC (MC_U120085810) and grants from Unity Biotechnology, Worldwide Cancer Research (18-0215), CRUK (C15075/A28647) and Imperial Confidence in Concept funded research in J. G.'s laboratory. D.J.W. was funded by a Wellcome Trust Strategic Award (098565) and core support from MRC (MC-A654-5QB40). J.P.M.-B. was funded by Cancer Research UK (A27727), the Brain Tumour Charity (EVEREST (GN-000382) and GN-000522), Children with Cancer UK (CwCUK 15-190) and National Institute of Health Research Biomedical Research Centre at the Great Ormond Street Hospital for Children NHS Foundation Trust, and the University College London. J.P.M.-B. is a Great Ormond Street Hospital for Children's Charity Principal Investigator. Work in the laboratory of M.S. was funded by the IRB and "la Caixa" Foundation, and by grants from the Spanish Ministry of Science co-funded by the European Regional Development Fund (ERDF) (SAF2017-82613-R), European Research Council (ERC-2014-AdG/669622), and Secretaria d'Universitats i Recerca del Departament d'Empresa i Coneixement of Catalonia (Grup de Recerca consolidate 2017 SGR 282). F.P. is supported by a Karolinska Institute Starting Grant and a starting grant from the Swedish Research Council (2019_02050_3). F.H.-G. was funded by the PhD4MD Programme of the IRB, Hospital Clinic and IDIBAPS. W.W.K. and E.W.T. acknowledge support from the European Commission (Marie Sklodowska Curie Individual Fellowship grant 752165 to W.W.K), Myricx Pharma Ltd., and Cancer Research UK, with support from the Engineering & Physical Sciences Research Council, (C29637/A21451, C29637/A20183 and DRCNPG-Nov21\100001 to E.W.T.). Work in E.W.T.'s laboratories is supported by the Francis Crick Institute, which receives its core funding from Cancer Research UK, the UK Medical Research Council, and the Wellcome Trust (FC001057 and FC001097). G.J.T was funded by CRUK (A27989).

AUTHOR CONTRIBUTIONS

F.H.-G., F.P. and M.S. contribution relate to the mouse lung fibrosis; M.M. and G.J.T. to the cancer xenograft; R.G. and J.P. M.-B., to the craniopharyngioma murine model; E.W.T. and W.W.K. to NMTi; S.V. and D.J.W. to the mouse models; J.B. to the PBEC and NHLF experiments; B.S. and J.P. to the liver cancer initiation and NASH models. C.G.-M. to the NASH model. I.D. to senescence in cancer cells. D.M.'s contribution relates to the liver cancer models and all other cell culture experiments. D.M., B.S., F.H.-G., M.M., R.G., J.P., F.P., J.B., C.G.-M., I.D., and W.W.K. performed, designed, and analyzed experiments. G.D. and S.K. analyzed experiments. D.M. and J.G. conceived the project and wrote the manuscript with the input of all authors. S.V., J.P. M.-B., G.J.T., E.W.T., M.S., and D.J.W. designed experiments and secured funding. J.G. supervised the project and secured funding.

COMPETING INTERESTS

J. G. has acted as a consultant for Unity Biotechnology, Geras Bio, Myricx Pharma Ltd., and Merck KGaA; owns equity in Geras Bio and share options in Myricx Pharma Ltd. and is a named inventor in an MRC patent related to senolytic therapies (unrelated to the work described here). J.G. receives current funding from Pfizer (unrelated to this research). Unity Biotechnology funded research on senolytics in J.G.’s laboratory. E.W.T. is a founding director and shareholder of Myricx Pharma Ltd. and a named inventor on patents covering NMT inhibitors (WO2017001812A1, PCT/GB2019/053613), is an advisor of Sasmara Therapeutics, and receives current or recent funding from Myricx Pharma Ltd, Pfizer Ltd, Kura Oncology, AstraZeneca, Merck & Co., GSK. D.M., E.W.T., W.W.K., and J.G. are named inventors on an Imperial College patent related to this work. M.S. is a shareholder of Senolytic Therapeutics, Inc., Life Biosciences, Inc, Rejuveron Senescence Therapeutics, AG, and Altos Labs, Inc, and it was an advisor of Rejuveron Senescence Therapeutics, AG and Altos Labs, Inc.

ADDITIONAL INFORMATION

Correspondence and requests for materials should be addressed to J.G.

EXTENDED DATA FIGURE LEGENDS

Extended Data Figure 1. Models for oncogene- and therapy-induced senescence. a, Outline of IMR90 ER:RAS system for modelling oncogene-induced senescence (OIS). The addition of 4-OHT induces the activation of ER:RAS, triggering OIS. **b,** Quantification of IF staining for BrdU incorporation in IMR90 ER: RAS cells 5 days after treatment with 4-OHT or DMSO (n = 3). **c,** Quantification (left) of the percentage of cells staining positive for SA-βgalactosidase activity in IMR90 ER:RAS cells 5 days after treatment with 4-OHT or DMSO (n = 3). The right panels show representative brightfield images. Scale bar, 100μm. **d,** Quantification (left) of the percentage of cells staining positive for $p16^{INK4a}$ in IMR90 ER:RAS cells 5 days after treatment with 4-OHT or DMSO (n = 3). The right panels show representative IF images for $p16^{INK4a}$ staining. Scale bar, 100 μm. **e,** B score normalization of cell numbers shown for the siRNA screen performed on control, non-senescent (DMSO treated) IMR90 ER: RAS cells. Points show normalized values for 3 replicates. Red box indicates samples with a B-score < 3. **f**, Screen results for control (DMSO-treated IMR90 ER:RAS) and OIS (4OHT-treated IMR90 ER:RAS). Graph displays B-score in OIS versus the negative of the difference in B score between OIS and control screens. Points show normalized values for 3 replicates with cut-offs shown for OIS B-score < -3 and a difference in B score of > 2 between control and OIS cells. **g,** Model of therapy-induced senescence (TIS). Senescence was induced by 7 days of doxorubicin treatment in IMR90 cells. **h,** Quantification of IF staining for BrdU incorporation in IMR90 cells 2 days after treatment with doxorubicin or DMSO (n = 3).**i,** Quantification (left) of the percentage of cells staining positive for SA-β-galactosidase activity in IMR90 cells 7 days treating with doxorubicin or DMSO (n = 3). The right panels show representative brightfield images. Scale bar, 100 μm. **j-k**, Quantification (left) of the percentage of cells staining positive for $p21^{CIP1}$ (j) or $p16^{INK4a}$ (k) in IMR90 cells 6 (j) or 3 (k) days after treating with doxorubicin or DMSO (n = 3). The right panels show representative IF images for $p21^{CIP1}$ staining. Scale bar, 100 μm. Data represented as mean±SD unless otherwise stated. Statistical tests are performed using unpaired, Student's t-test unless otherwise stated.

Extended Data Figure 2. COPI inhibitors are senolytic. a-c, IMR90 ER:RAS cells were treated 7 days after senescence induction with either DMSO (D), 2.5μM golgicide A (G), or 150nM brefeldin A (B) for 72h, and cells fixed and stained as indicated. Percentage of either

total cells or cells positive for SA-β-galactosidase (a), $p16^{INK4a}$ (b), and $p21^{CIP1}$ (c) relative to the total number of DMSO-treated cells. (n=3 replicates per condition). Two-way ANOVA, Dunnett's Correction. The significance of total cell comparisons is shown in black, while the significance for comparisons of positive for SA-β-galactosidase (a), $p16^{INK4a}$ (b), and $p21^{CIP1}$ (c) are shown in blue, green, and red respectively. Percentage cells represent a fraction of cells compared to the total number of cells in the DMSO-treated sample for each replicate. **d,** IMR90 ER:RAS cells were transfected with the indicated siRNAs 7 days after treatment with 4OHT (senescent) or DMSO (controls). Cells were fixed and stained for SA-β-galactosidase activity 72 h after transfection. Representative images (left). Scale bar, 100 μm.Quantification (right) of a relative number of senescent cells. Shown are the percentage of total or SA-β-gal-positive cells relative to the total number of DMSO-treated cells. (n=3 replicates per condition). Scr. scrambled. Two-way ANOVA, Dunnett's Correction. Percentage cells represent a fraction of cells compared to the total number of cells in the DMSO-treated sample for each replicate. **e,** Dose-response curves for senolytic effect of GBF1 inhibitor brefeldin A in the context of OIS (n=3-6 replicates per point). EC_{50}, half maximal effective concentration. **f,** Senolytic activity of brefeldin A in the context of senescence induced by irradiation (n=3, n=2 for ABT-263 & 40nM BFA treatment), bleomycin (n=6) or doxorubicin (n=4). Data represented as mean±SD. Comparisons are to the corresponding DMSO-treated cells (gray bars) using two-way ANOVA with Dunnet's correction. Data represented as mean±SD unless otherwise stated.

Extended Data Figure 3. Effects of COPB2 depletion on senescent cells. a, Heatmap derived from RNA-Seq data showing the relative mRNA levels of COPI components (in black) in senescent cells. As a reference, we included the relative levels of MMP3 and CXCL8 (upregulated during senescence, in red) and MKI67 and COL15A1 (downregulated during senescence, in blue). Represented are the log_2Fold change (FC) in oncogene-induced senescent (RAS) or therapy-induced senescent (BLEO) IMR90 ER:RAS or IMR90 cells transduced with shRNA vector, induced to senesce for 10 days and measured relative to respective cell lines treated with DMSO. **b,** GSEA plot showing that a COPI-mediated transport signature is upregulated during bleomycin-induced senescence. NES, normalized enrichment score; FDR, false discovery rate. **c,** Quantification of intracellular levels of IL6 (right) and representative IL6 IF pictures (left) of senescent (4OHT) and control (DMSO) IMR90 ER:RAS cells after transfection with the indicated siRNAs (n=4). Scale Bar, 100μm.

Statistical tests were performed using two-way ANOVA with Dunnett's correction for multiple comparisons. **d,** Heatmap derived of RNA-Seq data showing the relative mRNA levels of SASP components in the indicated cells. Data represented as row z-score normalized. **e,** Quantification of percentage positive for nuclear XBP1 (right) and representative XBP1 IF pictures (left) of senescent (4OHT) and control (DMSO) IMR90 ER:RAS cells after transfection with the indicated siRNAs (n=3). Scale Bar, 100μm. Unpaired two-tailed, student's t-test. Data is represented throughout the figure as Mean±SD.

Extended Data Figure 4. Effects of COPI inhibition in the unfolded protein response and autophagy. a, Representative IF images of EEA1 staining in control (DMSO) and senescent (4OHT) IMR90 ER:RAS treated with either DMSO or 1.25μM of golgicide A (GCA) 48h, 7 days after senescence induction. Scale bar, 100 μm. **b,** SASP inhibition caused by the knockdown of PTBP1 prevents the senolytic effect of GBF1 inhibitors. Quantification of cell survival of senescent (4OHT) and control (DMSO) IMR90 ER:RAS cells treated as indicated (n=3). Ordinary Two-way ANOVA, Dunnett's Correction. Comparison is to the corresponding IMR90 ER: RAS vector +4OHT condition. **c-d,** Quantification (right) of cells positive for nuclear XBP1 (c) and ATF6 (d), 48 hours after either control (DMSO) or oncogene-induced senescent (4OHT) cells were treated with either 1 μM ABT-263, 1.25 μM of golgicide A (GCA) or 150 nM brefeldin A (BFA) (n=3). Representative IF images (left) for XBP1 (c) and ATF6 (d) immunostaining are shown. Scale Bar, 100 μm. Significance was calculated using unpaired, two-tailed, Student's t-test. **e-f,** Quantification (e) of the level of BiP protein (relative to α-tubulin) as assessed by western blot of either control (DMSO) or senescent (4OHT) 48h after treatment with either 1.25 μM of golgicide A (GCA) or 150 nM brefeldin A (BFA) (n=3). Unpaired, two-tailed, Student's t-test, Holm-Šídák correction. A representative image of one of three western blots (f) shown for BiP, α-tubulin, and LC3 is shown. Immunoblot of α-tubulin is included as a loading control. **g**, Representative IF images for p62/SQSTM1 immunostaining are shown for control (DMSO) and senescent (4OHT) IMR90 ER: RAS treated with 1.25μM Golgicide A for 48h 7 days post senescence induction. Scale bar, 100 μm.

Extended Data Figure 5. Therapeutic benefits of inhibiting the COPI pathway. a, Experimental design for the sequential treatment of cancer cells with chemotherapy and brefeldin A (BFA). **b-c,** Quantification of cell survival of A549 cells (b) or SKHep1 cells (c) after treatment with the indicated drug combinations. (n=6) Unpaired, two-tailed, Student's

t-test, Holm-Šídák correction. **d,** Area under the curve (AUC) analysis for tumour volume measured over time in two independent experiments (Experiment A and B; see Fig. 5e for the tumor growth curves of Experiment A and Supplemental Figure 12F for Experiment B). Data represented as Mean±SEM (n=14 Vector, Vector+Irrd & shCOPB2.2 + Irrd, n=13 shCOPB2.1+Irrd, n=7 for both COPA shRNA + Irrd samples). Ordinary two-way ANOVA was used for the statistical comparison of groups to Vector+Irrd. **e,** Experimental design (left) of tumor growth in NSG cancer model with 5PT squamous cancer cells co-injected with HFFF2 fibroblasts (Right) Tumor growth curves showing the tumour volume monitored over time (IR=irradiation). Data represented as mean±SEM (n=6-8 per group). RM Two-way ANOVA with Geisser Greenhouse correction and Dunnet's correction used for comparisons to 5PT + HFFF2 shControl used for the statistical test. P values are shown for the final time point. **f,** Representative images of staining for in vitro SA-β-gal in irradiated IMR90s transduced with shRNAs against COPB2 with positive cells staining blue. Scale bar, 200 μm. **g,** Quantification of the initial engraftment of human fibroblasts in the lungs of nude mice measured 48 hours after the instillation of 500.000 of the indicated cells. Engraftment was assessed by the expression levels of mRNAs coding for human MMP3. Ordinary one-way ANOVA and posthoc multiple comparisons Tukey tests. Data represented as mean±SD.

Extended Data Figure 6. NMT inhibitors phenocopy the effects of inhibiting COPI in senescent cells. a, Quantification (right) of IF staining for EEA1 vesicles in control (DMSO) or senescent (4OHT) IMR90 ER:RAS cells were treated with 300nM IMP1088 or 1.5 μM DDD86481 for 7 days after senescence induction for 5 days (n=3). Ordinary Two-way ANOVA, Dunnett's correction. Representative IF images are shown (left). Scale bar, 100μm. **b,** Quantification (right) of intracellular levels of IL8 in control (DMSO) or senescent (4OHT) IMR90 ER:RAS cells treated with 300nM IMP1088 or 1.5 μM DDD86481 7 days after senescence induction for 5 days (n=3). Ordinary Two-way ANOVA, Dunnett's correction. Representative IF images are shown (left). Scale bar, 100μm. **c,** Relative fold change of IL6, IL8, G-CSF, and CCL2 in the supernatant of (DMSO) or day 7 senescent cells (4OHT+DMSO) treated with NMTi (4OHT+IMP1088/DDD8641) for 5 days. Concentration determined by ELISA normalized to cell counts and shown relative to senescent cells (4OHT+DMSO) n=3. Comparisons are to senescent cells (4OHT+DMSO). Significance was calculated using ordinary two-way ANOVA, Dunnett's correction. **d-e,** Quantification (right) of IF staining nuclear ATF6 (d) and nuclear CHOP (e) in control (DMSO) or senescent (4OHT) IMR90 ER:RAS cells treated with 300 nM IMP1088 or 1.5 μM DDD86481, 7 days

after senescence induction for 5 days (n=3). Ordinary two-way ANOVA, Dunnett's correction. Representative IF images are shown (left). Scale bar, 100μm. **f-g,** Dose-response curves for senolytic effect of NMT inhibitors in bleomycin-induced senescence. IMP1088 (f, n=6), DDD86481 (g, n=5). EC_{50}, half-maximal effective concentration. Control (DMSO) or senescent (Bleomycin) IMR90 was treated with inhibitors 7 days after senescence induction and fixed for assessing cell number 7 days after treatment. Data represented as mean ± SD throughout the figure.

Extended Data Figure 7. NMT inhibitors target senescent cells in cancer models. a-b, Dose-response curves for assessing the senolytic activity of DDD86481 treated HCT116 (a, n=4 replicates for all groups) or MCF7 (b, n=3 for DMSO, n=3 for etoposide, n=2 for doxorubicin) cells induced to senesce with either doxorubicin or etoposide. **c-d,** Dose-response curves for assessing the senolytic activity of IMP1320 treated HCT116 (c, n=4 replicates for all groups) or MCF7 (d, n=3 for DMSO, n=3 for etoposide, n=2 for doxorubicin) cells induced to senesce with either doxorubicin or etoposide treatment. EC_{50}, half-maximal effective concentration. **e,** Tumor growth curves showing the tumour volume monitored over time (IR=irradiation). Data represented as mean±SEM (n=6 5PT+Veh, n=8 per group all other groups; see the fig 7f for the relative AUC analysis. RM Two-way ANOVA with Geisser Greenhouse correction and Dunnet's correction used for to 5PT/IR HFFF2 + vehicle used for the statistical test. p values are shown as the final timepoint. **f-g,** Quantification of βcatenin positive (f) and $p21^{Cip1}$ positive/ βcatenin positive (g) cells in the pituitary gland at 0, 24, 48, and 72h after treatment with 600nM IMP1088 *ex vivo* (n=5 per timepoint). Data is represented as min to max plots; n represents the number of pituitaries. (f, 0h n=42, 24h n=19. 48h, n=30, 72h, n=15) (g, 0h n=42, 24h n=19, 48h, n=30, 72h n=21) Ordinary One-way ANOVA with Dunnett's correction. **h,** Synaptophysin is a marker of the normal hormone-producing cells in the pituitary gland, quantification of synaptophysin positive area (purple; % of the pituitary surface) after NMTi treatment highlights no significant effect of the treatment on normal cells. The left panel shows representative images. (each group n=6) Data represented as mean ± SD. ns, not significant. Unpaired, two-tailed, Student's t-test. Scale bar, 50 μm.

Extended Data Figure 8. NMT inhibitors eliminate senescent cells and improve NASH-induced liver steatosis and fibrosis. a, Body weight of chow-fed (n=15) and western diet (WD)-fed mice treated with vehicle (n=14) or NMT inhibitor (n=15) following the last round

of treatment. Ordinary One-way ANOVA. Dunnett's test. **b-f,** GSEA plots showing the enrichment of the indicated signatures in mice fed WD (WD+veh) as compared with mice fed with chow diet (Chow+veh; b, d,f) or in mice fed with WD and treated with NMTi (WD+NMTi) as compared with mice fed with WD and treated with vehicle (WD+vehicle; c, e). NES, normalized enrichment score; FDR, false discovery rate.

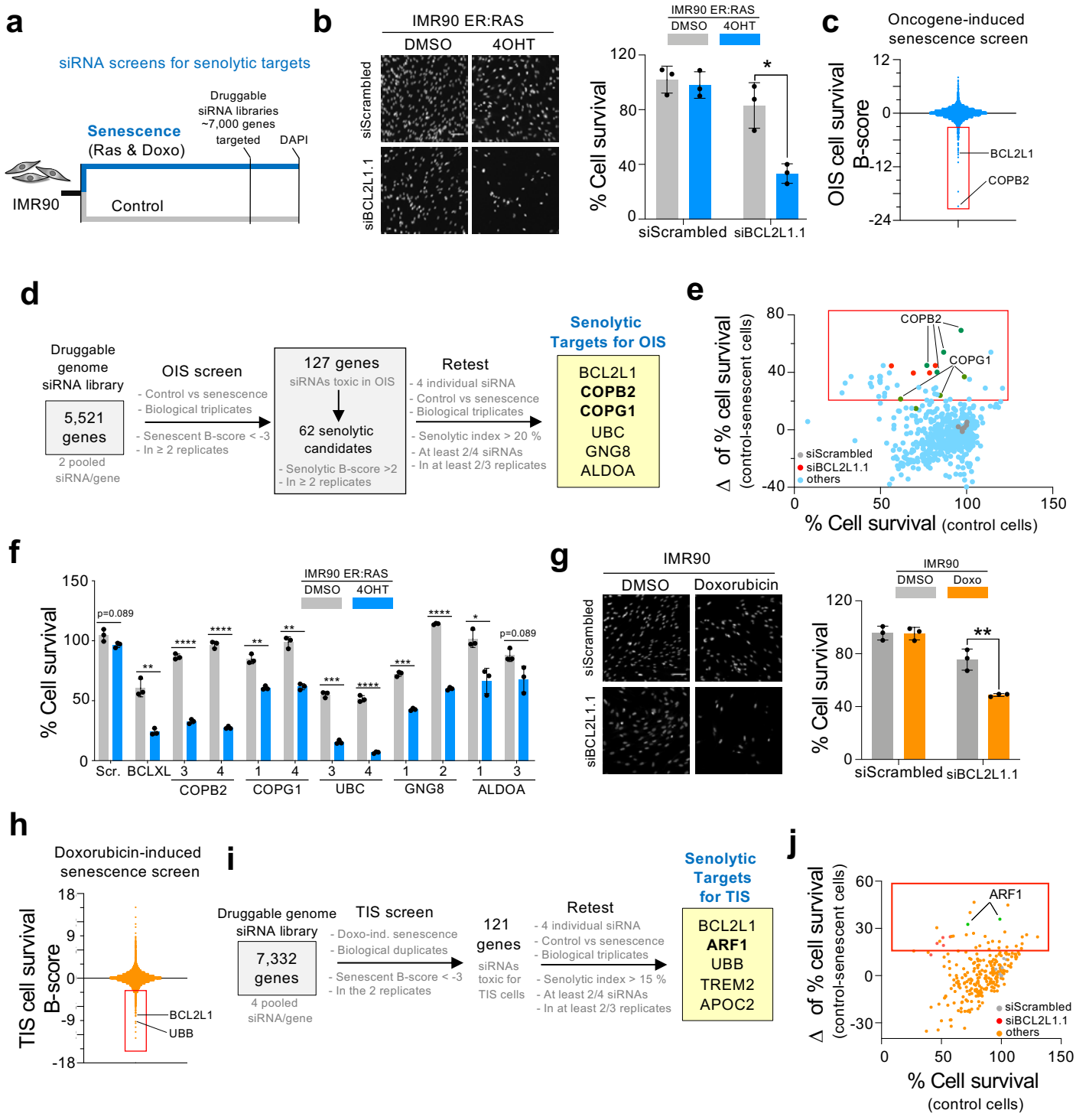
a
siRNA screens for senolytic targets
Druggable siRNA libraries ~7,000 genes
Senescence (Ras & Doxo)
targeted
DAPI
IMR90
Control
b
IMR90 ER:RAS
DMSO
4OHT
siScrambled
siBCL2L1.1
% Cell survival
c
Oncogene-induced senescence screen
OIS cell survival B-score
BCL2L1
COPB2
d
Druggable genome siRNA library
5,521 genes
2 pooled siRNA/gene
OIS screen
- Control vs senescence
- Biological triplicates
- Senescent B-score < -3
- In ≥ 2 replicates
127 genes
siRNAs toxic in OIS
62 senolytic candidates
- Senolytic B-score >2
- In ≥ 2 replicates
Retest
- 4 individual siRNA
- Control vs senescence
- Biological triplicates
- Senolytic index > 20 %
- At least 2/4 siRNAs
- In at least 2/3 replicates
Senolytic Targets for OIS
BCL2L1
COPB2
COPG1
UBC
GNG8
ALDOA
e
Δ of % cell survival (control-senescent cells)
COPB2
COPG1
siScrambled
siBCL2L1.1
others
% Cell survival (control cells)
f
IMR90 ER:RAS
DMSO
4OHT
% Cell survival
p=0.089
Scr.
BCLXL
COPB2
COPG1
UBC
GNG8
ALDOA
g
IMR90
DMSO
Doxorubicin
siScrambled
siBCL2L1.1
Doxo
h
Doxorubicin-induced senescence screen
TIS cell survival B-score
BCL2L1
UBB
i
Druggable genome siRNA library
7,332 genes
4 pooled siRNA/gene
TIS screen
- Doxo-ind. senescence
- Biological duplicates
- Senescent B-score < -3
- In the 2 replicates
121 genes
siRNAs toxic for TIS cells
Retest
- 4 individual siRNA
- Control vs senescence
- Biological triplicates
- Senolytic index > 15 %
- At least 2/4 siRNAs
- In at least 2/3 replicates
Senolytic Targets for TIS
BCL2L1
ARF1
UBB
TREM2
APOC2
j
Δ of % cell survival (control-senescent cells)
ARF1
siScrambled
siBCL2L1.1
others
% Cell survival (control cells)
k
% Cell survival
p=0.084
Scr.
BCLXL
ARF1
UBB
TREM2
APOC2
IMR90
DMSO
Doxo
l
- **BCL2 family** (*BCLXL*)
- **Ubiquitin** (*UBB*, *UBC*)
- **COPI** (*COPG2*, *COPB1*, *ARF1*)

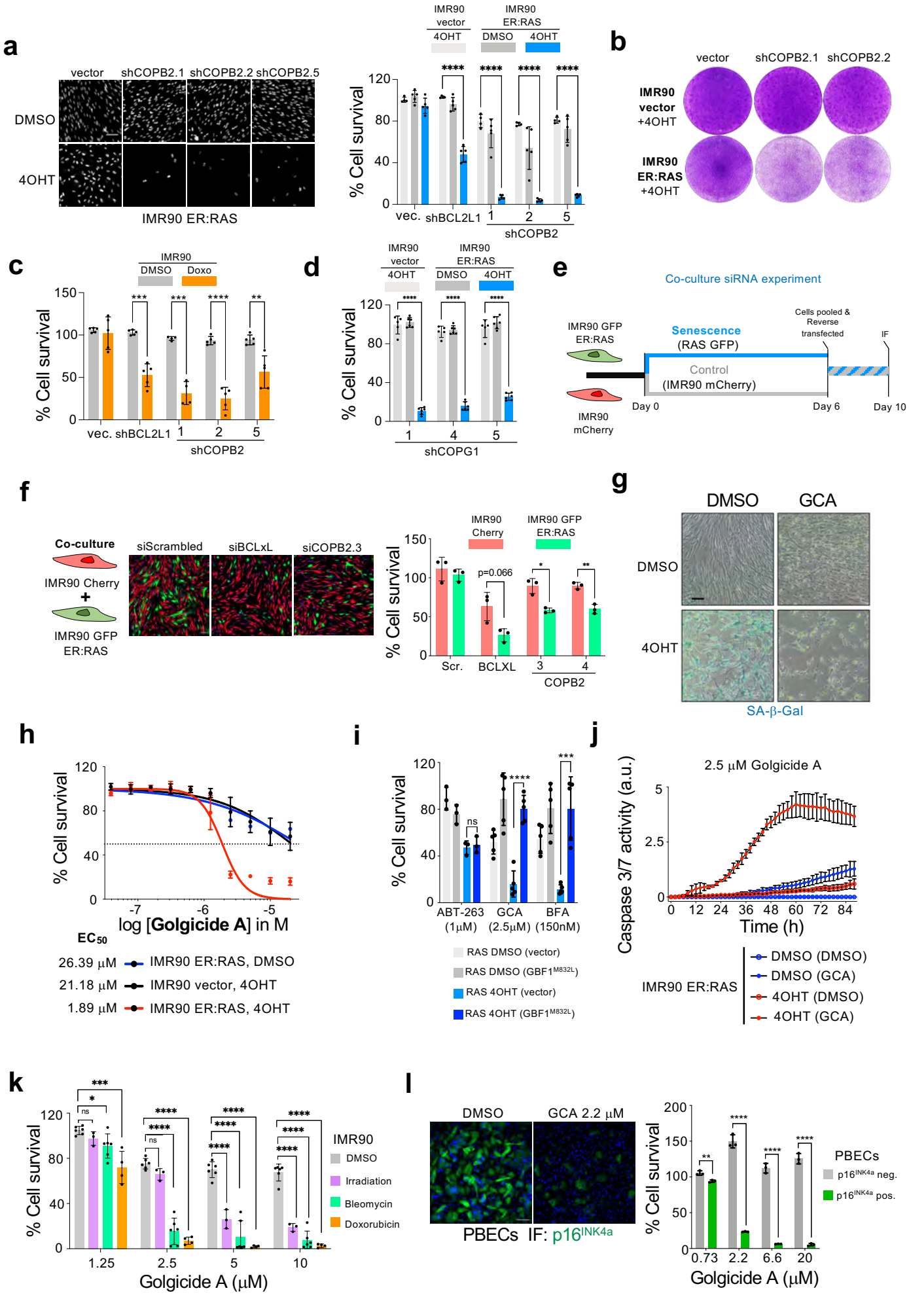
a
vector
shCOPB2.1
shCOPB2.2
shCOPB2.5
DMSO
4OHT
IMR90 ER:RAS
IMR90 vector
IMR90 ER:RAS
4OHT
DMSO
4OHT
% Cell survival
vec.
shBCL2L1
1
2
5
shCOPB2
b
vector
shCOPB2.1
shCOPB2.2
IMR90 vector +4OHT
IMR90 ER:RAS +4OHT
c
IMR90
DMSO
Doxo
% Cell survival
vec.
shBCL2L1
1
2
5
shCOPB2
d
IMR90 vector
IMR90 ER:RAS
4OHT
DMSO
4OHT
% Cell survival
1
4
5
shCOPG1
e
Co-culture siRNA experiment
IMR90 GFP ER:RAS
IMR90 mCherry
Senescence (RAS GFP)
Control (IMR90 mCherry)
Cells pooled & Reverse transfected
IF
Day 0
Day 6
Day 10
f
Co-culture
IMR90 Cherry
+
IMR90 GFP ER:RAS
siScrambled
siBCLxL
siCOPB2.3
IMR90 Cherry
IMR90 GFP ER:RAS
% Cell survival
p=0.066
Scr.
BCLXL
3
4
COPB2
g
DMSO
GCA
DMSO
4OHT
SA-β-Gal
h
% Cell survival
log [Golgicide A] in M
EC50
26.39 μM IMR90 ER:RAS, DMSO
21.18 μM IMR90 vector, 4OHT
1.89 μM IMR90 ER:RAS, 4OHT
i
% Cell survival
ns
ABT-263 (1μM)
GCA (2.5μM)
BFA (150nM)
RAS DMSO (vector)
RAS DMSO (GBF1M832L)
RAS 4OHT (vector)
RAS 4OHT (GBF1M832L)
j
2.5 μM Golgicide A
Caspase 3/7 activity (a.u.)
Time (h)
IMR90 ER:RAS
DMSO (DMSO)
DMSO (GCA)
4OHT (DMSO)
4OHT (GCA)
k
% Cell survival
IMR90
DMSO
Irradiation
Bleomycin
Doxorubicin
Golgicide A (μM)
l
DMSO
GCA 2.2 μM
PBECs IF: p16INK4a
% Cell survival
PBECs
p16INK4a neg.
p16INK4a pos.
Golgicide A (μM)

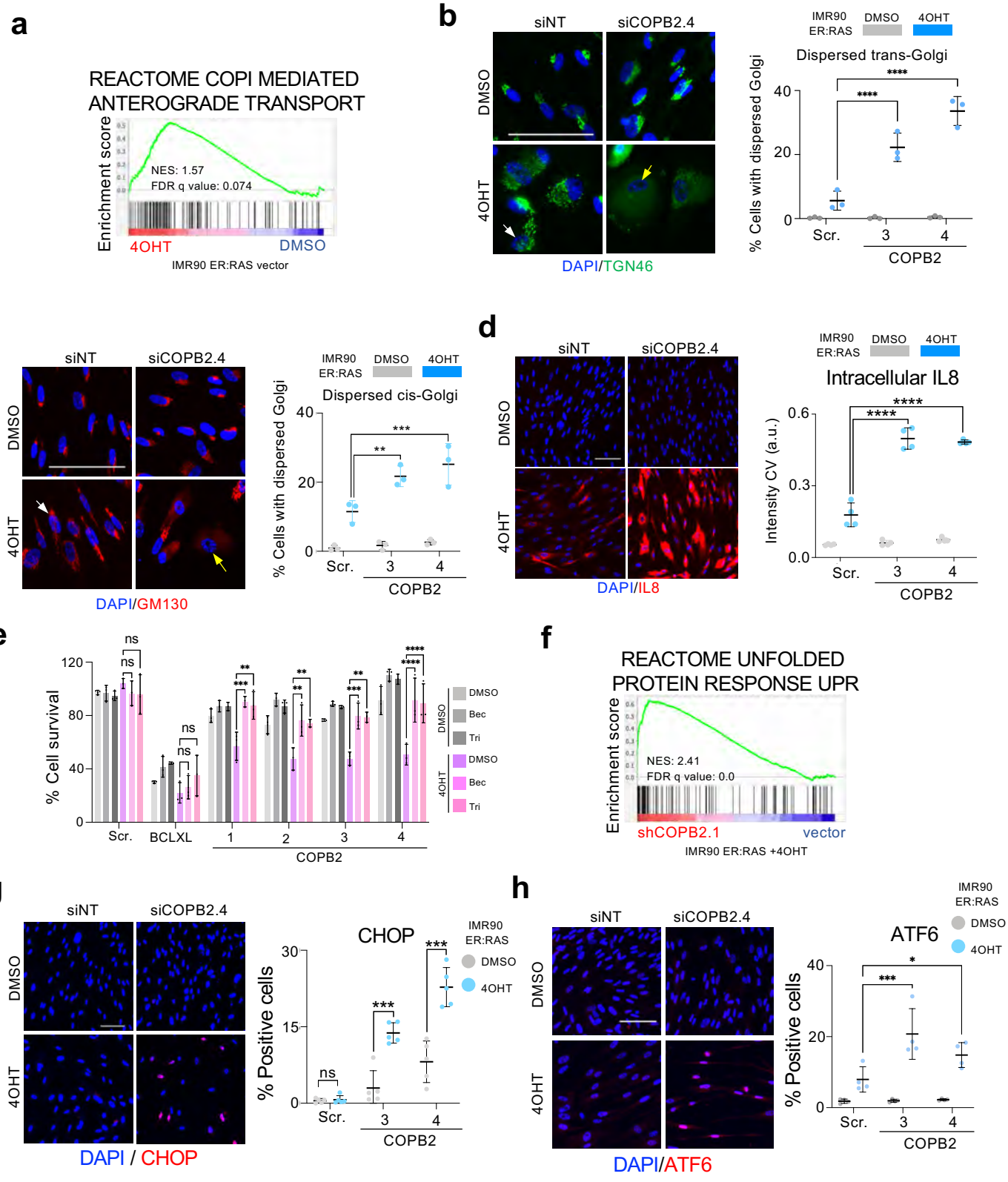
a
REACTOME COPI MEDIATED ANTEROGRADE TRANSPORT
Enrichment score
NES: 1.57
FDR q value: 0.074
4OHT
DMSO
IMR90 ER:RAS vector
b
siNT
siCOPB2.4
DMSO
4OHT
DAPI/TGN46
IMR90 ER:RAS
DMSO
4OHT
Dispersed trans-Golgi
% Cells with dispersed Golgi
Scr.
3
4
COPB2
c
siNT
siCOPB2.4
DMSO
4OHT
DAPI/GM130
IMR90 ER:RAS
DMSO
4OHT
Dispersed cis-Golgi
% Cells with dispersed Golgi
Scr.
3
4
COPB2
d
siNT
siCOPB2.4
DMSO
4OHT
DAPI/IL8
IMR90 ER:RAS
DMSO
4OHT
Intracellular IL8
Intensity CV (a.u.)
Scr.
3
4
COPB2
e
% Cell survival
Scr.
BCLXL
1
2
3
4
COPB2
DMSO
Bec
Tri
DMSO
Bec
Tri
4OHT
f
REACTOME UNFOLDED PROTEIN RESPONSE UPR
Enrichment score
NES: 2.41
FDR q value: 0.0
shCOPB2.1
vector
IMR90 ER:RAS +4OHT
g
siNT
siCOPB2.4
DMSO
4OHT
DAPI / CHOP
CHOP
% Positive cells
Scr.
3
4
COPB2
IMR90 ER:RAS
DMSO
4OHT
h
siNT
siCOPB2.4
DMSO
4OHT
DAPI/ATF6
ATF6
% Positive cells
Scr.
3
4
COPB2
IMR90 ER:RAS
DMSO
4OHT

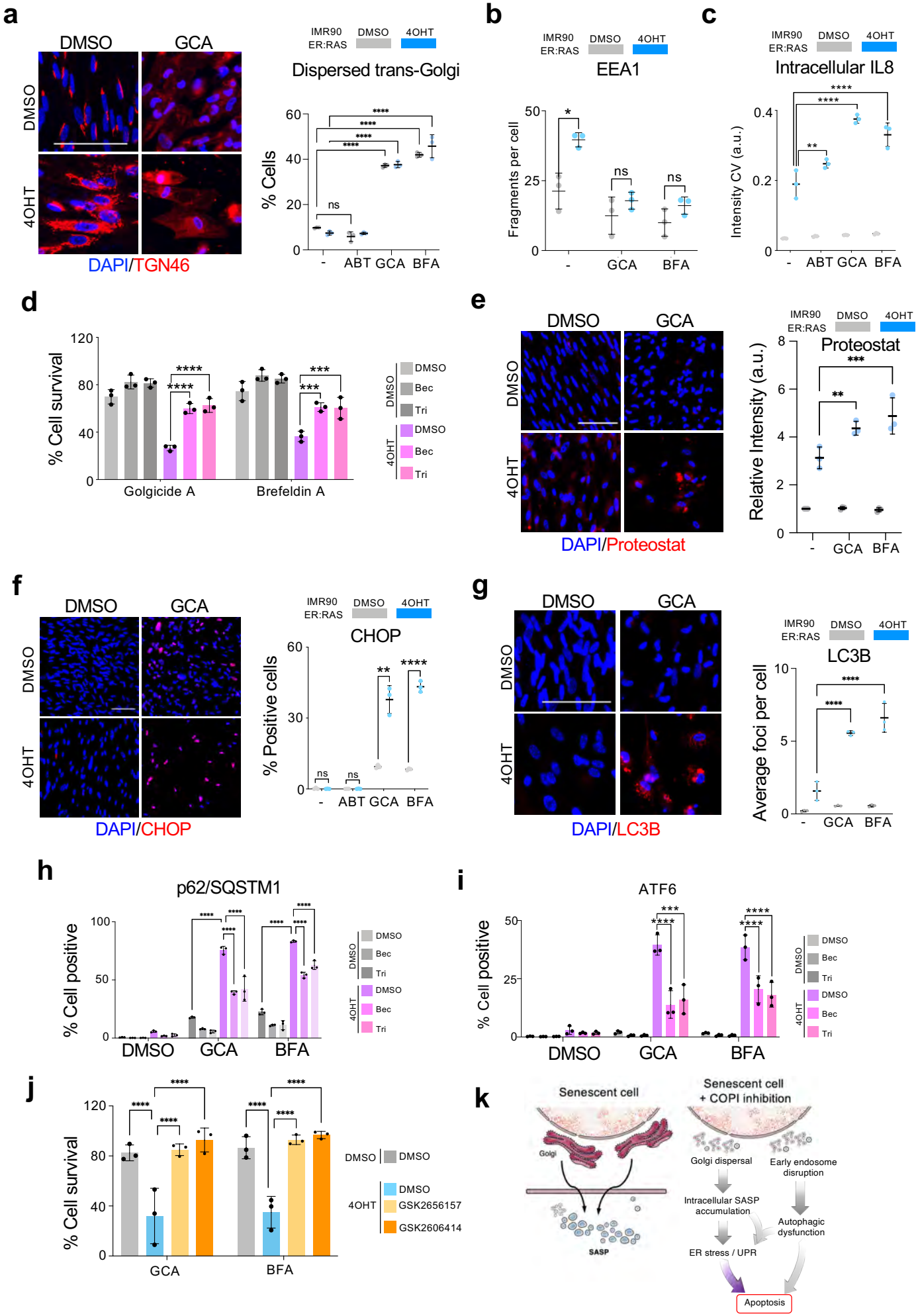
a
DMSO
GCA
DMSO
4OHT
DAPI/TGN46
IMR90 ER:RAS
DMSO
4OHT
Dispersed trans-Golgi
% Cells
ns
ABT
GCA
BFA
b
EEA1
Fragments per cell
c
Intracellular IL8
Intensity CV (a.u.)
d
% Cell survival
Golgicide A
Brefeldin A
Bec
Tri
e
Proteostat
Relative Intensity (a.u.)
DAPI/Proteostat
f
CHOP
% Positive cells
DAPI/CHOP
g
LC3B
Average foci per cell
DAPI/LC3B
h
p62/SQSTM1
% Cell positive
i
ATF6
j
GSK2656157
GSK2606414
k
Senescent cell
Senescent cell + COPI inhibition
Golgi
Golgi dispersal
Early endosome disruption
Intracellular SASP accumulation
Autophagic dysfunction
ER stress / UPR
SASP
Apoptosis

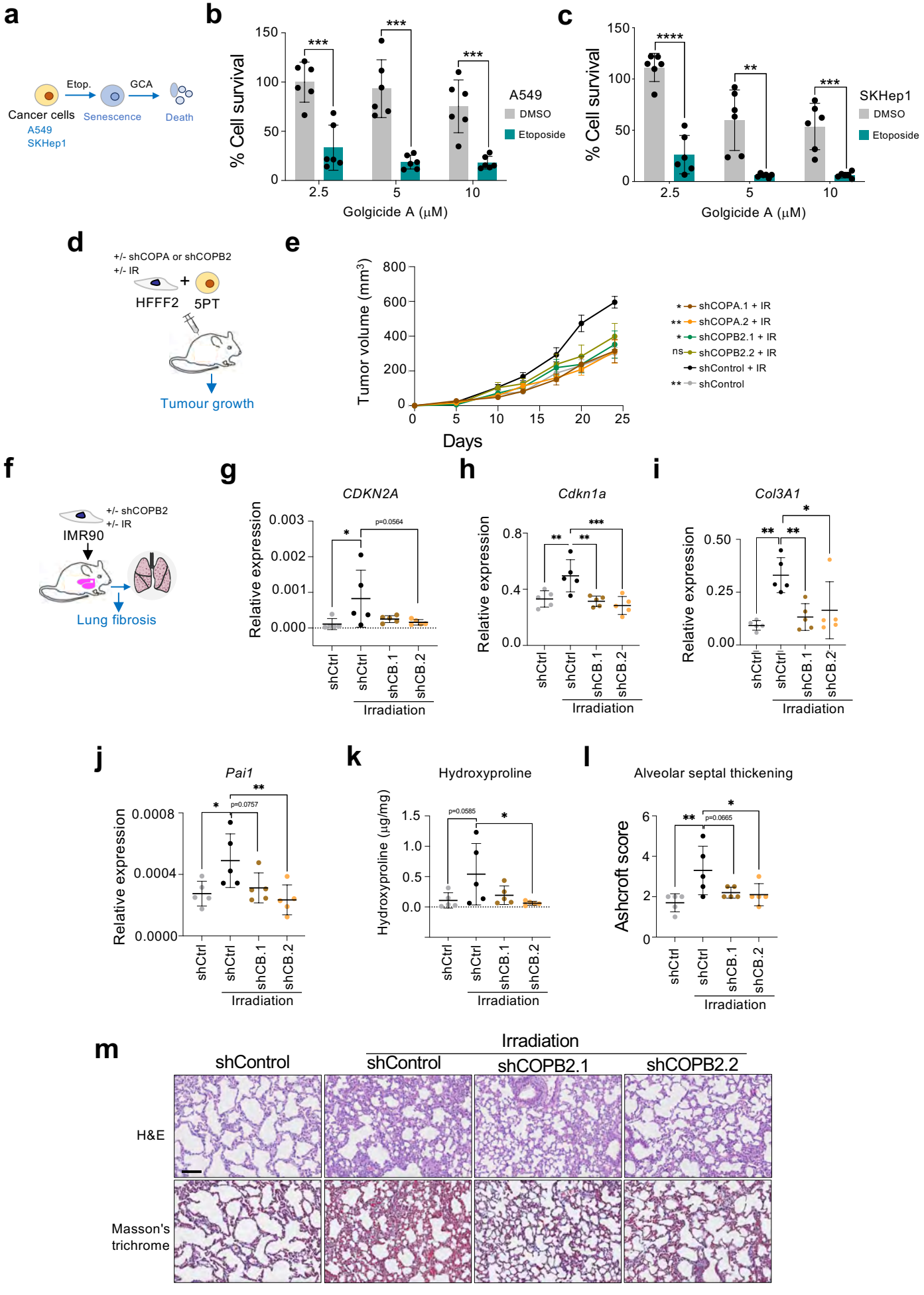
a
Etop.
GCA
Cancer cells
Senescence
Death
A549
SKHep1
b
% Cell survival
A549
DMSO
Etoposide
Golgicide A (μM)
c
% Cell survival
SKHep1
DMSO
Etoposide
Golgicide A (μM)
d
+/- shCOPA or shCOPB2
+/- IR
HFFF2
5PT
Tumour growth
e
Tumor volume (mm3)
Days
shCOPA.1 + IR
shCOPA.2 + IR
shCOPB2.1 + IR
shCOPB2.2 + IR
shControl + IR
shControl
f
+/- shCOPB2
+/- IR
IMR90
Lung fibrosis
g
CDKN2A
Relative expression
p=0.0564
shCtrl
shCB.1
shCB.2
Irradiation
h
Cdkn1a
Relative expression
i
Col3A1
Relative expression
j
Pai1
Relative expression
p=0.0757
k
Hydroxyproline
Hydroxyproline (μg/mg)
p=0.0585
l
Alveolar septal thickening
Ashcroft score
p=0.0665
m
Irradiation
shControl
shControl
shCOPB2.1
shCOPB2.2
H&E
Masson's trichrome

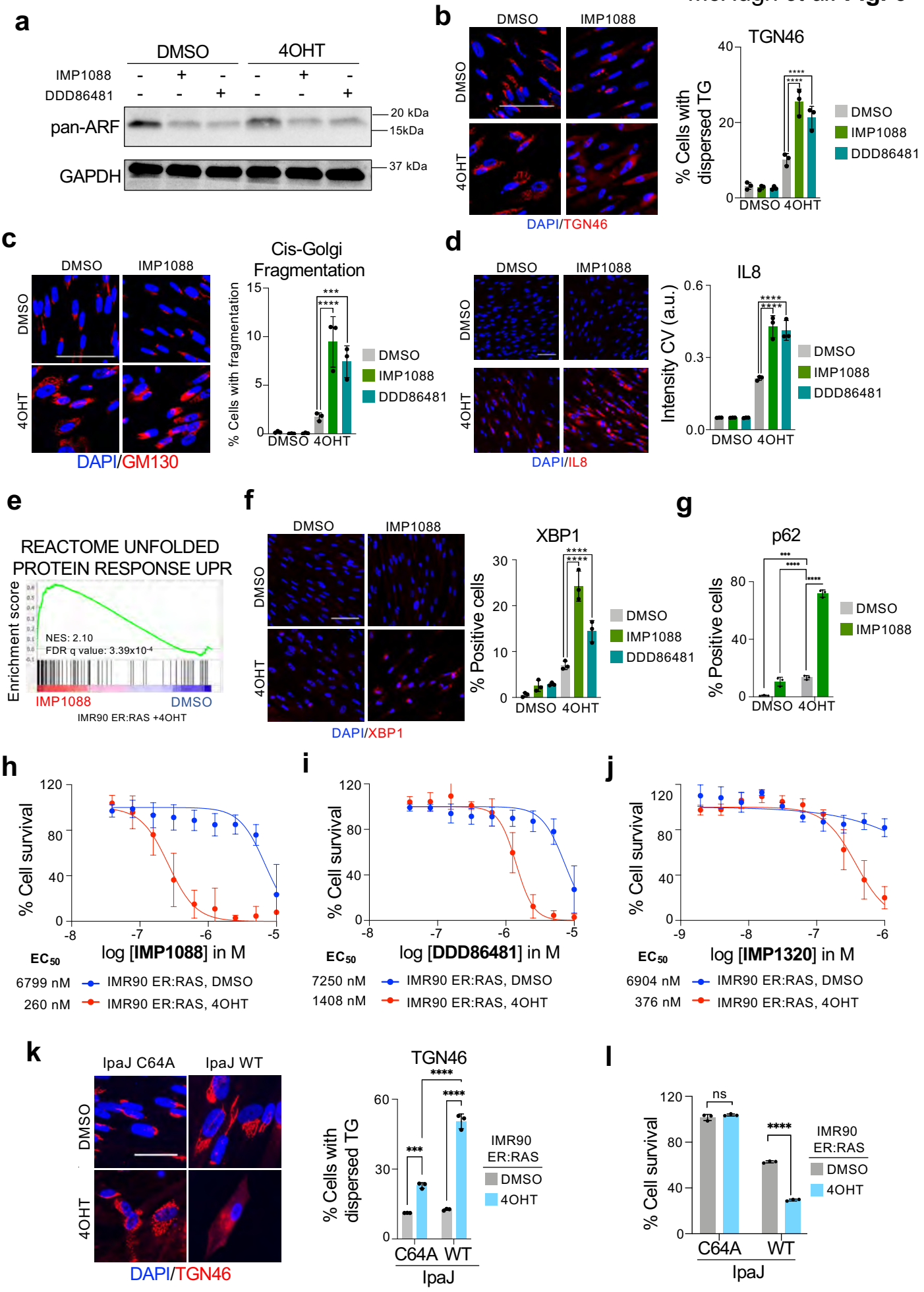
a
DMSO
4OHT
IMP1088
DDD86481
pan-ARF
GAPDH
20 kDa
15kDa
37 kDa
b
DMSO
IMP1088
DAPI/TGN46
TGN46
% Cells with dispersed TG
DMSO
IMP1088
DDD86481
c
Cis-Golgi Fragmentation
% Cells with fragmentation
DAPI/GM130
d
IL8
Intensity CV (a.u.)
DAPI/IL8
e
REACTOME UNFOLDED PROTEIN RESPONSE UPR
Enrichment score
NES: 2.10
FDR q value: 3.39x10-4
IMP1088
DMSO
IMR90 ER:RAS +4OHT
f
XBP1
% Positive cells
DAPI/XBP1
g
p62
% Positive cells
h
% Cell survival
log [IMP1088] in M
EC50
6799 nM IMR90 ER:RAS, DMSO
260 nM IMR90 ER:RAS, 4OHT
i
log [DDD86481] in M
7250 nM IMR90 ER:RAS, DMSO
1408 nM IMR90 ER:RAS, 4OHT
j
log [IMP1320] in M
6904 nM IMR90 ER:RAS, DMSO
376 nM IMR90 ER:RAS, 4OHT
k
IpaJ C64A
IpaJ WT
DAPI/TGN46
TGN46
% Cells with dispersed TG
IMR90 ER:RAS
C64A
WT
IpaJ
l
% Cell survival
ns

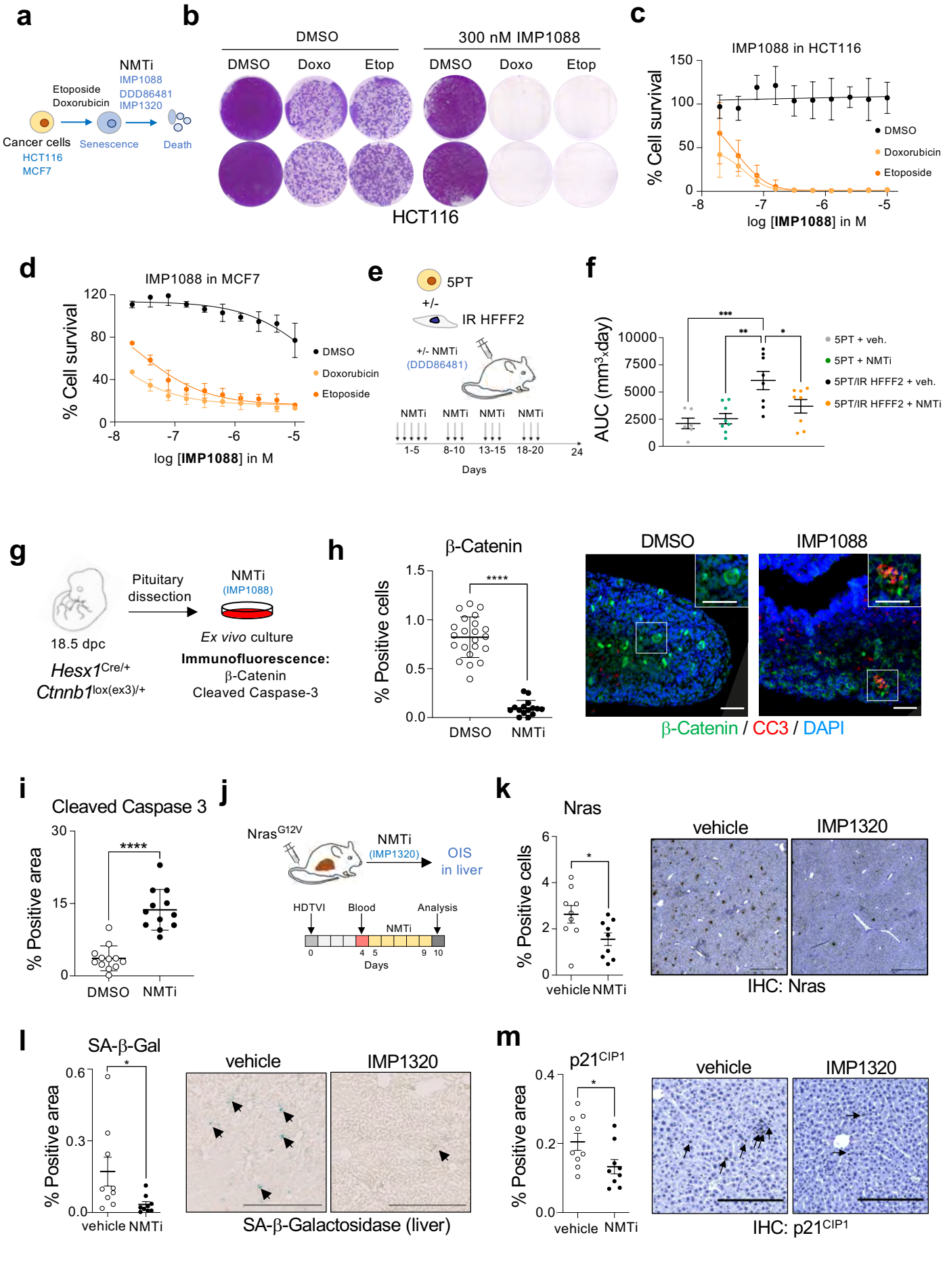
a
NMTi
IMP1088
DDD86481
IMP1320
Etoposide
Doxorubicin
Cancer cells
HCT116
MCF7
Senescence
Death
b
DMSO
300 nM IMP1088
DMSO
Doxo
Etop
DMSO
Doxo
Etop
HCT116
c
IMP1088 in HCT116
% Cell survival
log [IMP1088] in M
DMSO
Doxorubicin
Etoposide
d
IMP1088 in MCF7
% Cell survival
log [IMP1088] in M
DMSO
Doxorubicin
Etoposide
e
5PT
+/-
IR HFFF2
+/- NMTi
(DDD86481)
NMTi
1-5
8-10
13-15
18-20
24
Days
f
AUC (mm³xday)
5PT + veh.
5PT + NMTi
5PT/IR HFFF2 + veh.
5PT/IR HFFF2 + NMTi
g
Pituitary
dissection
NMTi
(IMP1088)
18.5 dpc
Hesx1Cre/+
Ctnnb1lox(ex3)/+
Ex vivo culture
Immunofluorescence:
β-Catenin
Cleaved Caspase-3
h
β-Catenin
% Positive cells
DMSO
NMTi
DMSO
IMP1088
β-Catenin / CC3 / DAPI
i
Cleaved Caspase 3
% Positive area
DMSO
NMTi
j
NrasG12V
NMTi
(IMP1320)
OIS
in liver
HDTVI
Blood
Analysis
NMTi
Days
k
Nras
% Positive cells
vehicle
NMTi
vehicle
IMP1320
IHC: Nras
l
SA-β-Gal
% Positive area
vehicle
NMTi
vehicle
IMP1320
SA-β-Galactosidase (liver)
m
p21CIP1
% Positive area
vehicle
NMTi
vehicle
IMP1320
IHC: p21CIP1

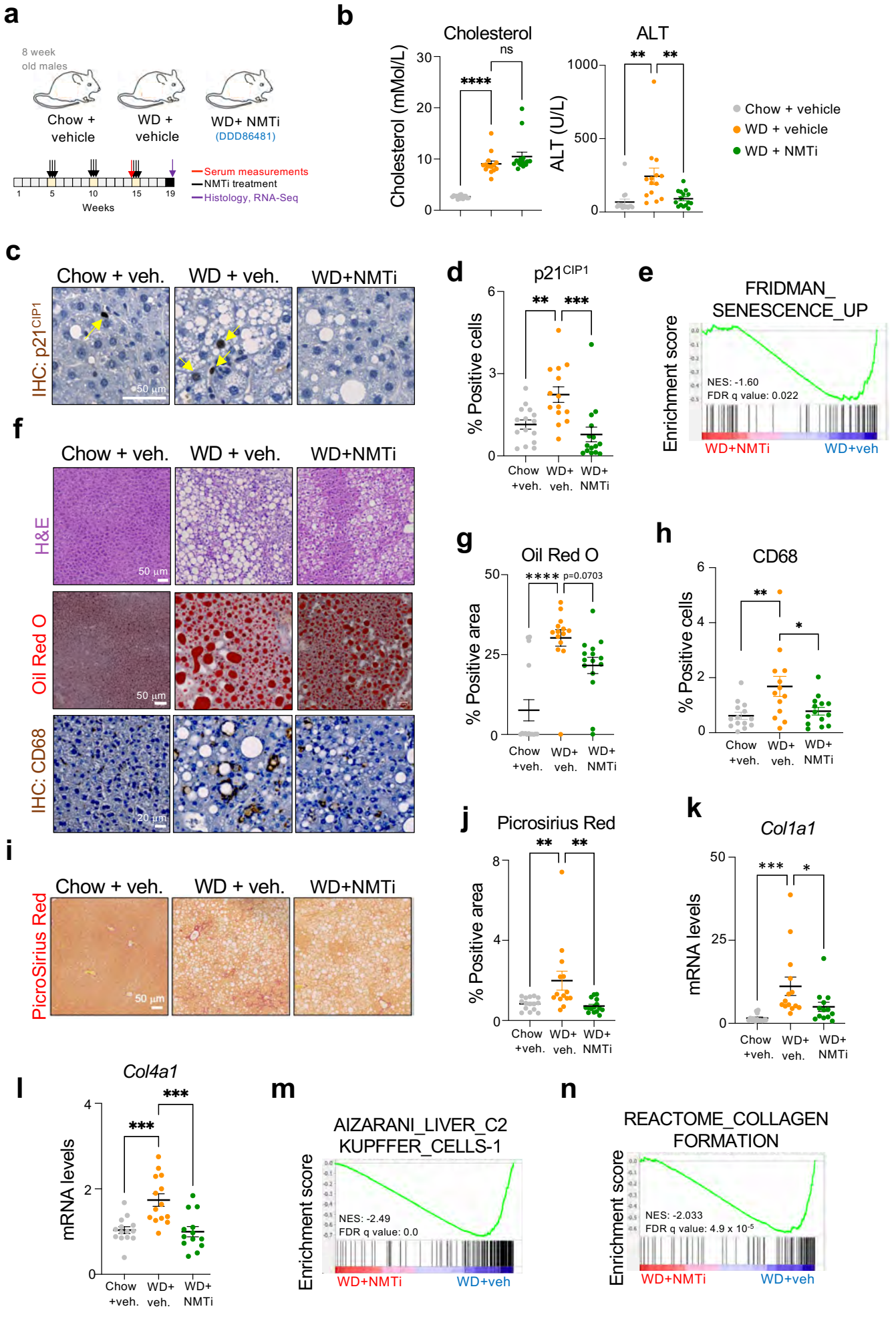
a
8 week old males
Chow + vehicle
WD + vehicle
WD+ NMTi (DDD86481)
Serum measurements
NMTi treatment
Histology, RNA-Seq
Weeks
b
Cholesterol
ALT
Cholesterol (mMol/L)
ALT (U/L)
ns
Chow + vehicle
WD + vehicle
WD + NMTi
c
Chow + veh.
WD + veh.
WD+NMTi
IHC: p21CIP1
d
p21CIP1
% Positive cells
e
FRIDMAN_ SENESCENCE_UP
Enrichment score
NES: -1.60
FDR q value: 0.022
WD+NMTi
WD+veh
f
H&E
Oil Red O
IHC: CD68
g
Oil Red O
% Positive area
p=0.0703
h
CD68
% Positive cells
i
PicroSirius Red
j
Picrosirius Red
% Positive area
k
Col1a1
mRNA levels
l
Col4a1
mRNA levels
m
AIZARANI_LIVER_C2 KUPFFER_CELLS-1
NES: -2.49
FDR q value: 0.0
n
REACTOME_COLLAGEN FORMATION
NES: -2.033
FDR q value: 4.9 x 10-5

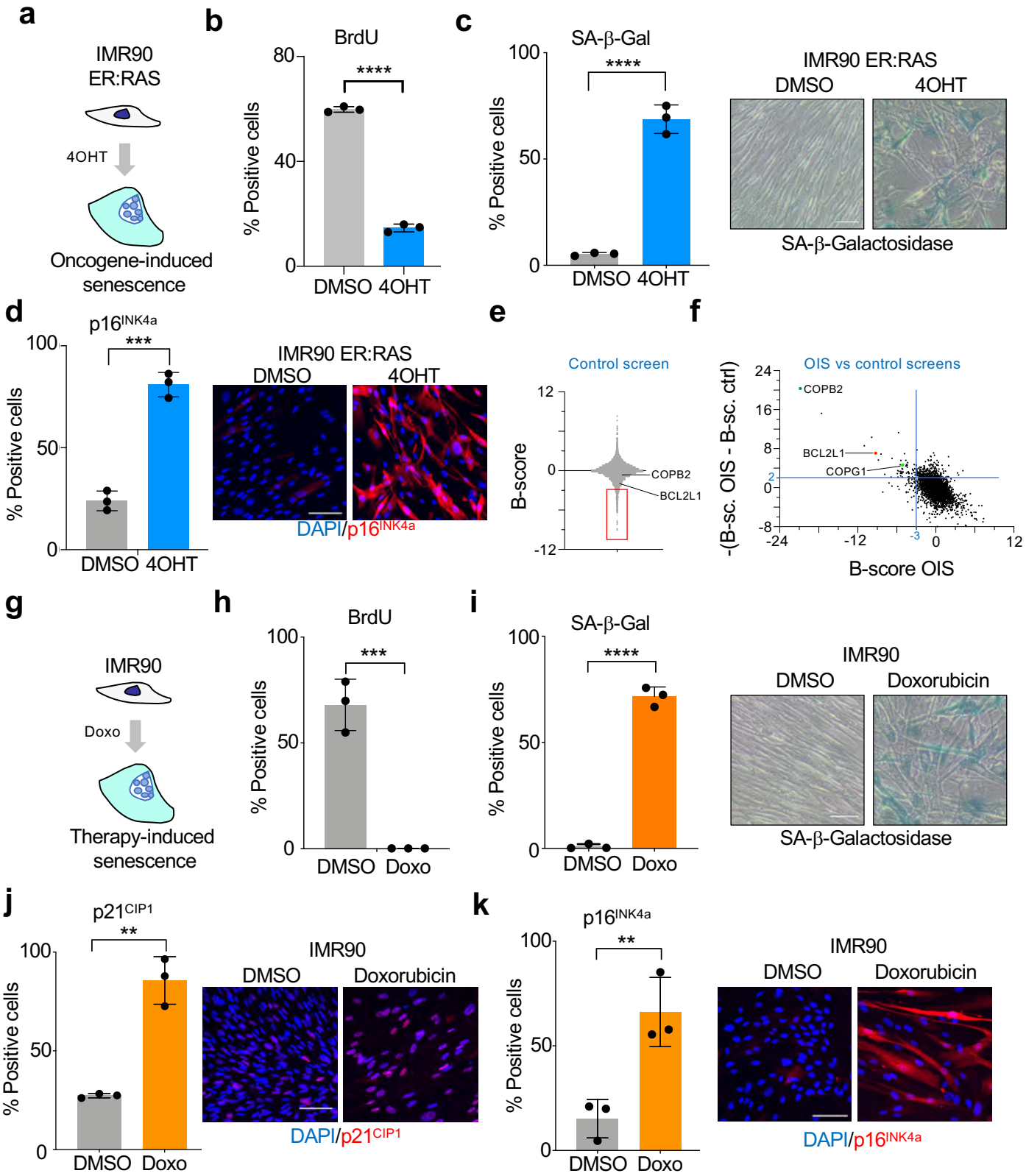
a
IMR90
ER:RAS
4OHT
Oncogene-induced
senescence
b
BrdU
% Positive cells
80
40
0
****
DMSO 4OHT
c
SA-β-Gal
% Positive cells
100
50
0
****
DMSO 4OHT
IMR90 ER:RAS
DMSO
4OHT
SA-β-Galactosidase
d
p16INK4a
% Positive cells
100
50
0
***
DMSO 4OHT
IMR90 ER:RAS
DMSO
4OHT
DAPI/p16INK4a
e
Control screen
B-score
12
0
-12
COPB2
BCL2L1
f
OIS vs control screens
-(B-sc. OIS - B-sc. ctrl)
24
16
8
2
0
-8
-24
-12
-3
0
12
COPB2
BCL2L1
COPG1
B-score OIS
g
IMR90
Doxo
Therapy-induced
senescence
h
BrdU
% Positive cells
100
50
0
***
DMSO Doxo
i
SA-β-Gal
% Positive cells
100
50
0
****
DMSO Doxo
IMR90
DMSO
Doxorubicin
SA-β-Galactosidase
j
p21CIP1
% Positive cells
100
50
0
**
DMSO Doxo
IMR90
DMSO
Doxorubicin
DAPI/p21CIP1
k
p16INK4a
% Positive cells
100
50
0
**
DMSO Doxo
IMR90
DMSO
Doxorubicin
DAPI/p16INK4a

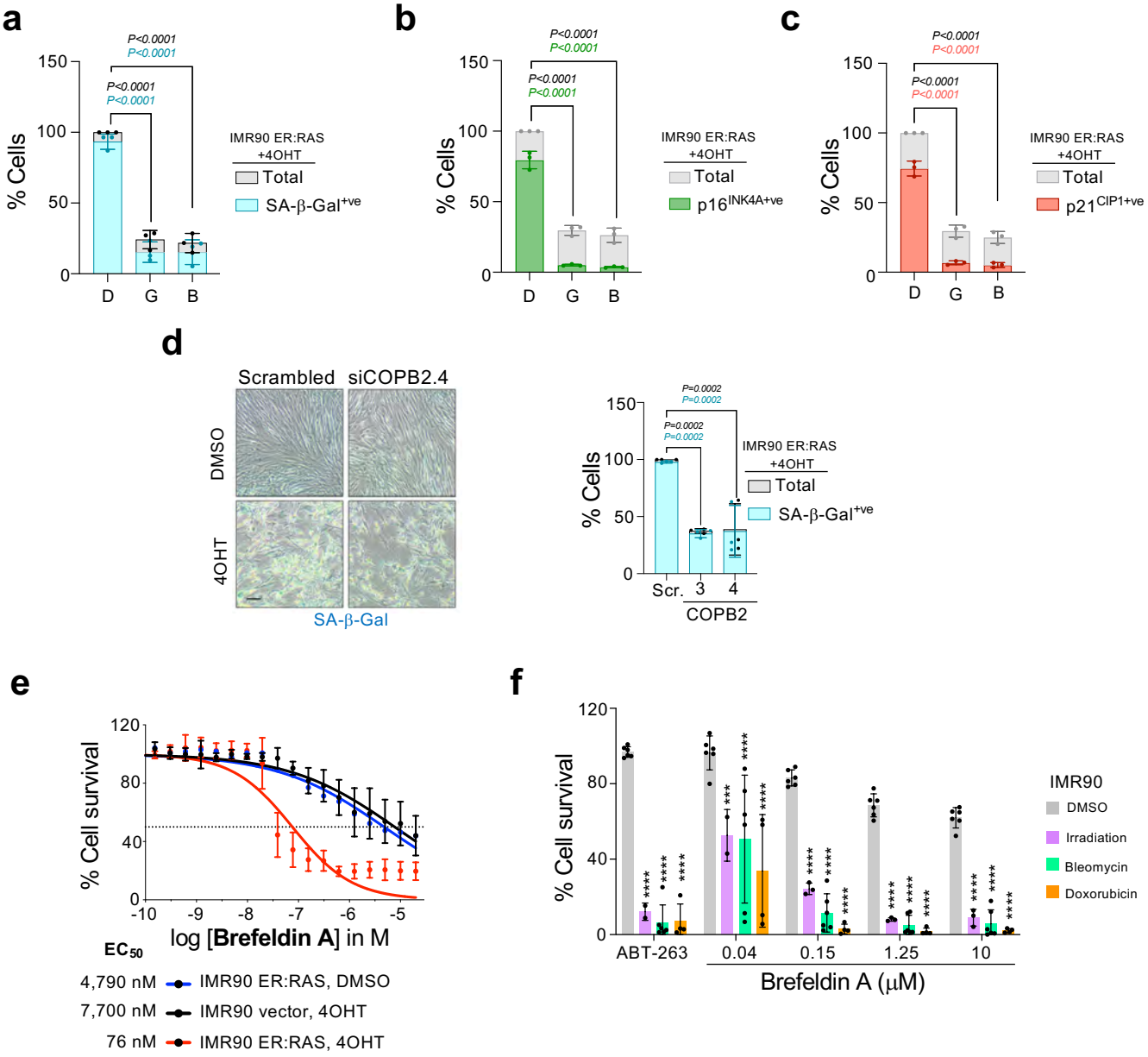
a
b
c
d
e
f
% Cells
IMR90 ER:RAS
+4OHT
Total
SA-β-Gal+ve
p16INK4A+ve
p21CIP1+ve
P<0.0001
P<0.0001
D
G
B
Scrambled
siCOPB2.4
DMSO
4OHT
SA-β-Gal
P=0.0002
Scr.
3
4
COPB2
% Cell survival
log [Brefeldin A] in M
EC50
4,790 nM
IMR90 ER:RAS, DMSO
7,700 nM
IMR90 vector, 4OHT
76 nM
IMR90 ER:RAS, 4OHT
IMR90
Irradiation
Bleomycin
Doxorubicin
ABT-263
0.04
0.15
1.25
10
Brefeldin A (μM)

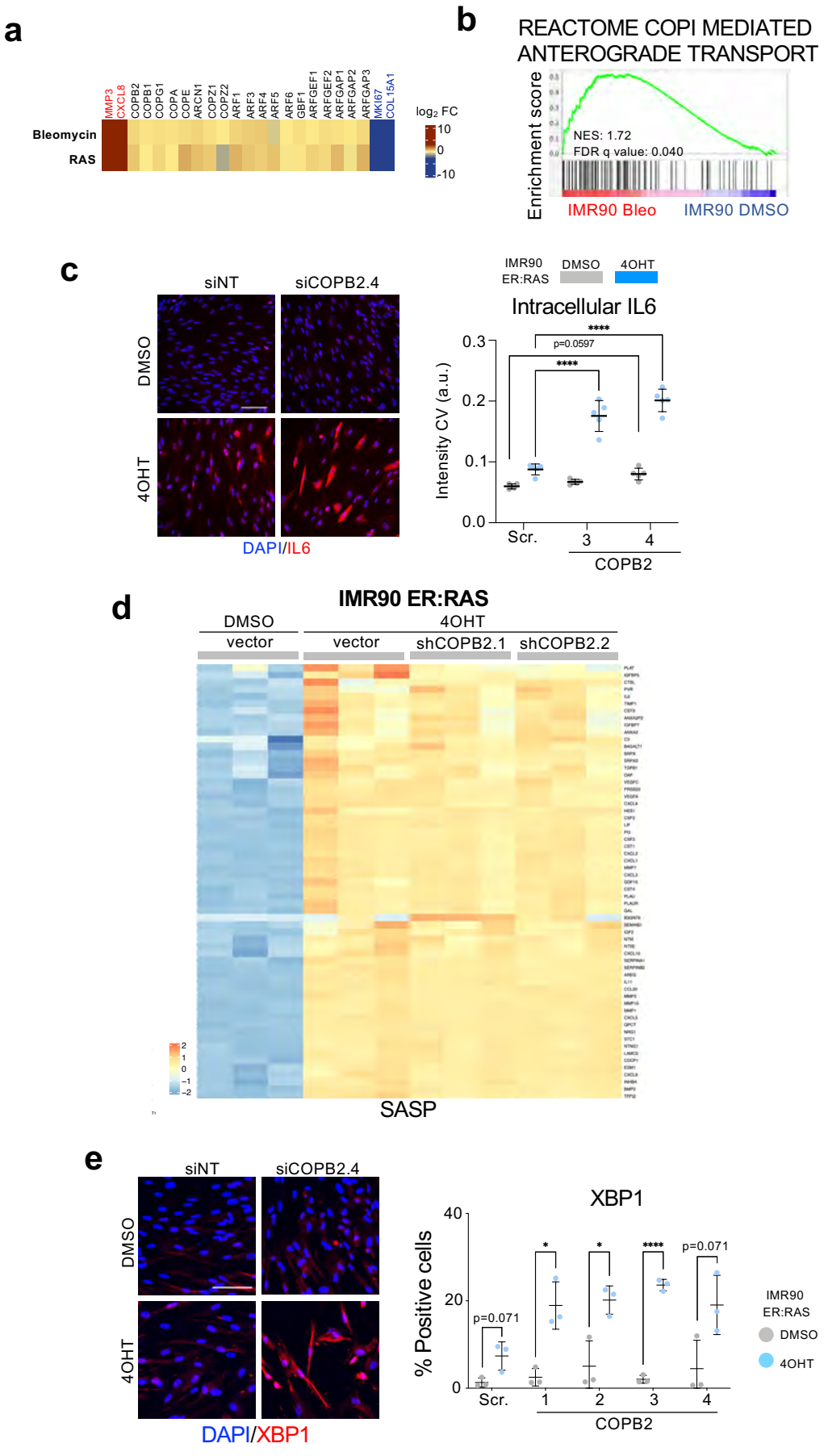
a
MMP3
CXCL8
COPB2
COPB1
COPG1
COPA
COPE
ARCN1
COPZ1
COPZ2
ARF1
ARF3
ARF4
ARF5
ARF6
GBF1
ARFGEF1
ARFGEF2
ARFGAP1
ARFGAP2
ARFGAP3
MKI67
COL15A1
Bleomycin
RAS
log2 FC
10
0
-10
b
REACTOME COPI MEDIATED ANTEROGRADE TRANSPORT
Enrichment score
NES: 1.72
FDR q value: 0.040
IMR90 Bleo
IMR90 DMSO
c
siNT
siCOPB2.4
DMSO
4OHT
DAPI/IL6
IMR90 ER:RAS
DMSO
4OHT
Intracellular IL6
Intensity CV (a.u.)
0.3
0.2
0.1
0.0
p=0.0597
****
****
Scr.
3
4
COPB2
d
IMR90 ER:RAS
DMSO
4OHT
vector
vector
shCOPB2.1
shCOPB2.2
2
1
0
−1
−2
SASP
e
siNT
siCOPB2.4
DMSO
4OHT
DAPI/XBP1
XBP1
% Positive cells
40
20
0
p=0.071
*
*
****
p=0.071
Scr.
1
2
3
4
COPB2
IMR90 ER:RAS
DMSO
4OHT

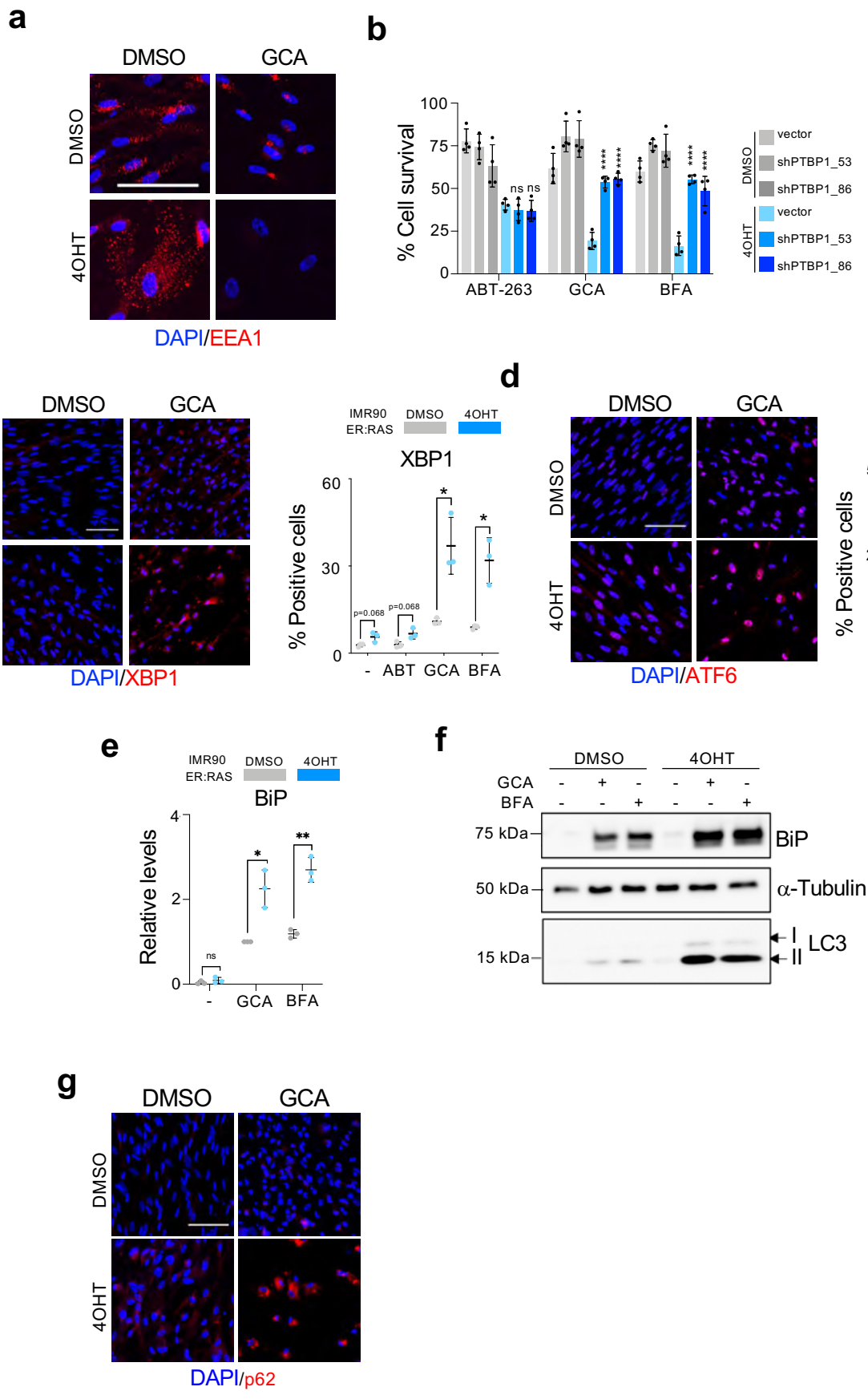
a
DMSO
GCA
DMSO
4OHT
DAPI/EEA1
b
% Cell survival
100
75
50
25
0
ns ns
****
****
****
****
ABT-263
GCA
BFA
DMSO
4OHT
vector
shPTBP1_53
shPTBP1_86
vector
shPTBP1_53
shPTBP1_86
c
DMSO
GCA
DMSO
4OHT
DAPI/XBP1
IMR90 ER:RAS
DMSO
4OHT
XBP1
% Positive cells
60
30
0
p=0.068
p=0.068
*
*
-
ABT
GCA
BFA
d
DMSO
GCA
DMSO
4OHT
DAPI/ATF6
IMR90 ER:RAS
DMSO
4OHT
ATF6
% Positive cells
50
25
0
ns
ns
**
**
-
ABT
GCA
BFA
e
IMR90 ER:RAS
DMSO
4OHT
BiP
Relative levels
4
2
0
ns
*
**
-
GCA
BFA
f
DMSO
4OHT
GCA - + - - + -
BFA - - + - - +
75 kDa
BiP
50 kDa
α-Tubulin
15 kDa
I
II
LC3
g
DMSO
GCA
DMSO
4OHT
DAPI/p62

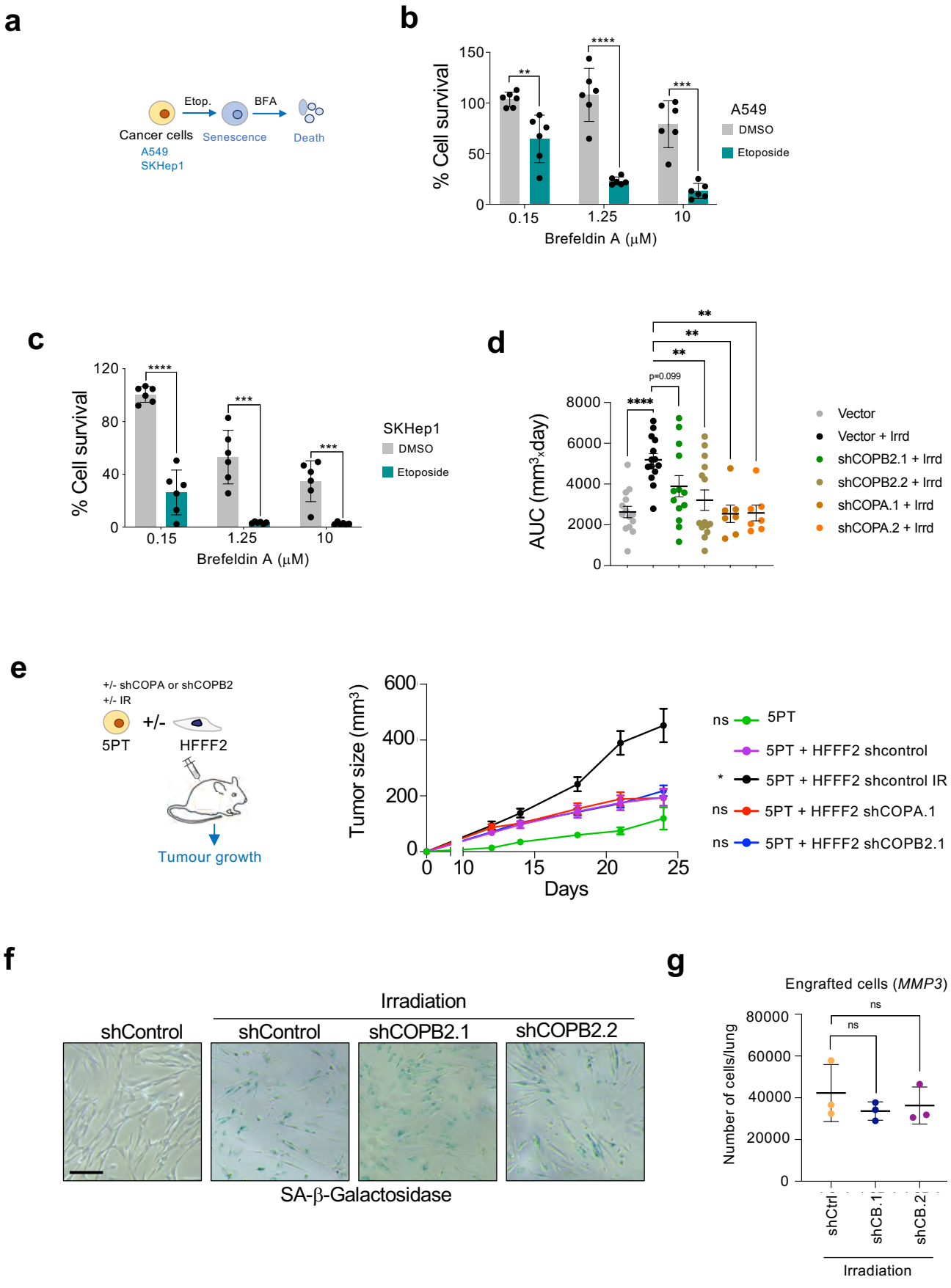
a
Etop.
BFA
Cancer cells
A549
SKHep1
Senescence
Death
b
% Cell survival
Brefeldin A (μM)
A549
DMSO
Etoposide
c
% Cell survival
Brefeldin A (μM)
SKHep1
DMSO
Etoposide
d
AUC (mm³xday)
p=0.099
Vector
Vector + Irrd
shCOPB2.1 + Irrd
shCOPB2.2 + Irrd
shCOPA.1 + Irrd
shCOPA.2 + Irrd
e
+/- shCOPA or shCOPB2
+/- IR
5PT
HFFF2
Tumour growth
Tumor size (mm³)
Days
ns 5PT
5PT + HFFF2 shcontrol
* 5PT + HFFF2 shcontrol IR
ns 5PT + HFFF2 shCOPA.1
ns 5PT + HFFF2 shCOPB2.1
f
Irradiation
shControl
shControl
shCOPB2.1
shCOPB2.2
SA-β-Galactosidase
g
Engrafted cells (*MMP3*)
Number of cells/lung
shCtrl
shCB.1
shCB.2
Irradiation

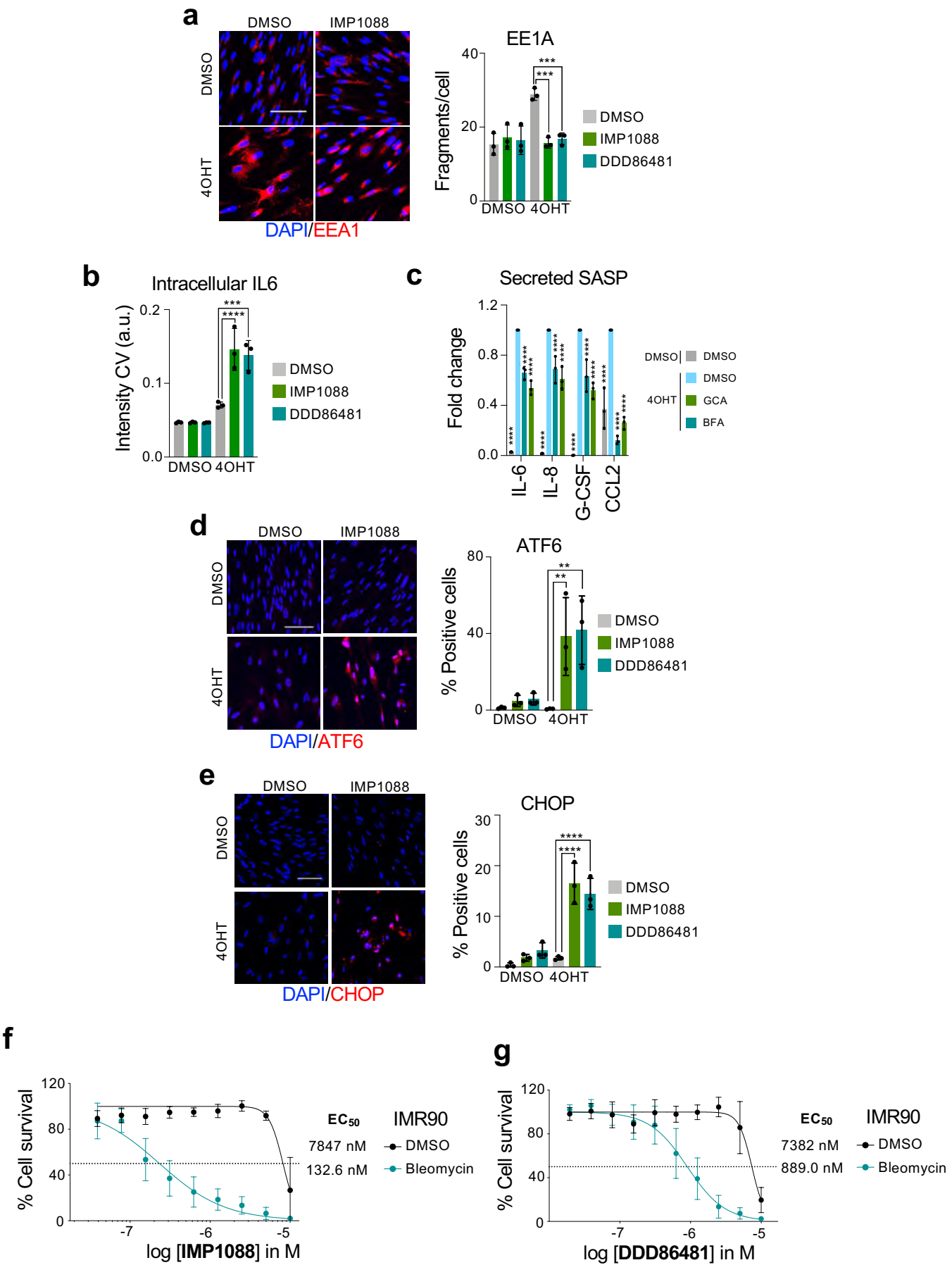
a
DMSO
IMP1088
DMSO
4OHT
DAPI/EEA1
EE1A
Fragments/cell
40
20
0
DMSO 4OHT
***
***
DMSO
IMP1088
DDD86481
b
Intracellular IL6
Intensity CV (a.u.)
0.2
0.1
0.0
DMSO 4OHT
***
****
DMSO
IMP1088
DDD86481
c
Secreted SASP
Fold change
1.2
0.8
0.4
0.0
IL-6
IL-8
G-CSF
CCL2
DMSO
DMSO
DMSO
4OHT
GCA
BFA
d
DMSO
IMP1088
DMSO
4OHT
DAPI/ATF6
ATF6
% Positive cells
80
40
0
DMSO 4OHT
**
**
DMSO
IMP1088
DDD86481
e
DMSO
IMP1088
DMSO
4OHT
DAPI/CHOP
CHOP
% Positive cells
30
20
10
0
DMSO 4OHT
****
****
DMSO
IMP1088
DDD86481
f
% Cell survival
120
80
40
0
-7
-6
-5
log [IMP1088] in M
EC50
IMR90
7847 nM
DMSO
132.6 nM
Bleomycin
g
% Cell survival
120
80
40
0
-7
-6
-5
log [DDD86481] in M
EC50
IMR90
7382 nM
DMSO
889.0 nM
Bleomycin

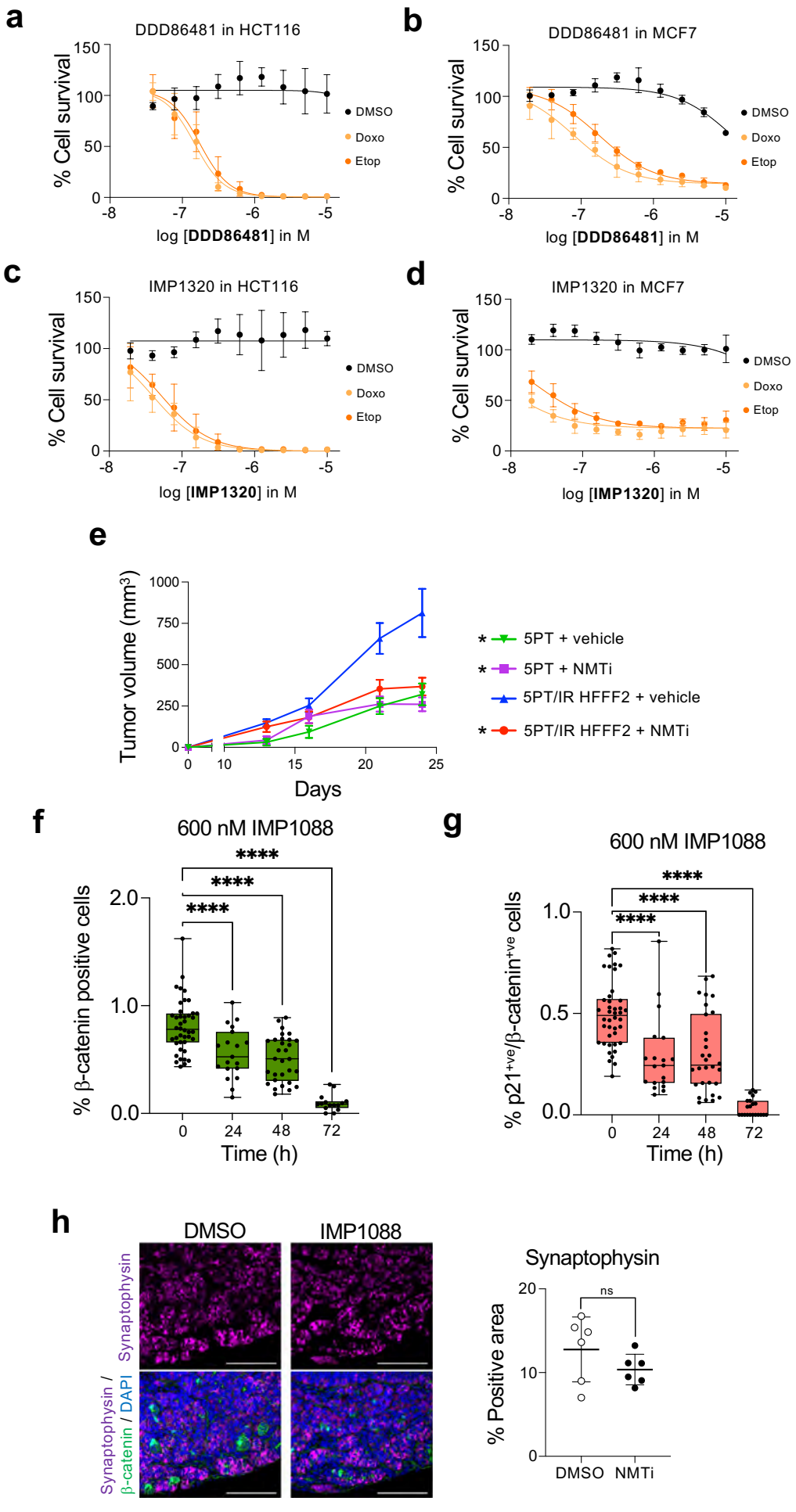
a
DDD86481 in HCT116
% Cell survival
log [DDD86481] in M
DMSO
Doxo
Etop
b
DDD86481 in MCF7
c
IMP1320 in HCT116
log [IMP1320] in M
d
IMP1320 in MCF7
e
Tumor volume (mm³)
Days
5PT + vehicle
5PT + NMTi
5PT/IR HFFF2 + vehicle
5PT/IR HFFF2 + NMTi
f
600 nM IMP1088
% β-catenin positive cells
Time (h)
****
g
% p21+ve/β-catenin+ve cells
h
DMSO
IMP1088
Synaptophysin
Synaptophysin / β-catenin / DAPI
Synaptophysin
% Positive area
ns
DMSO
NMTi

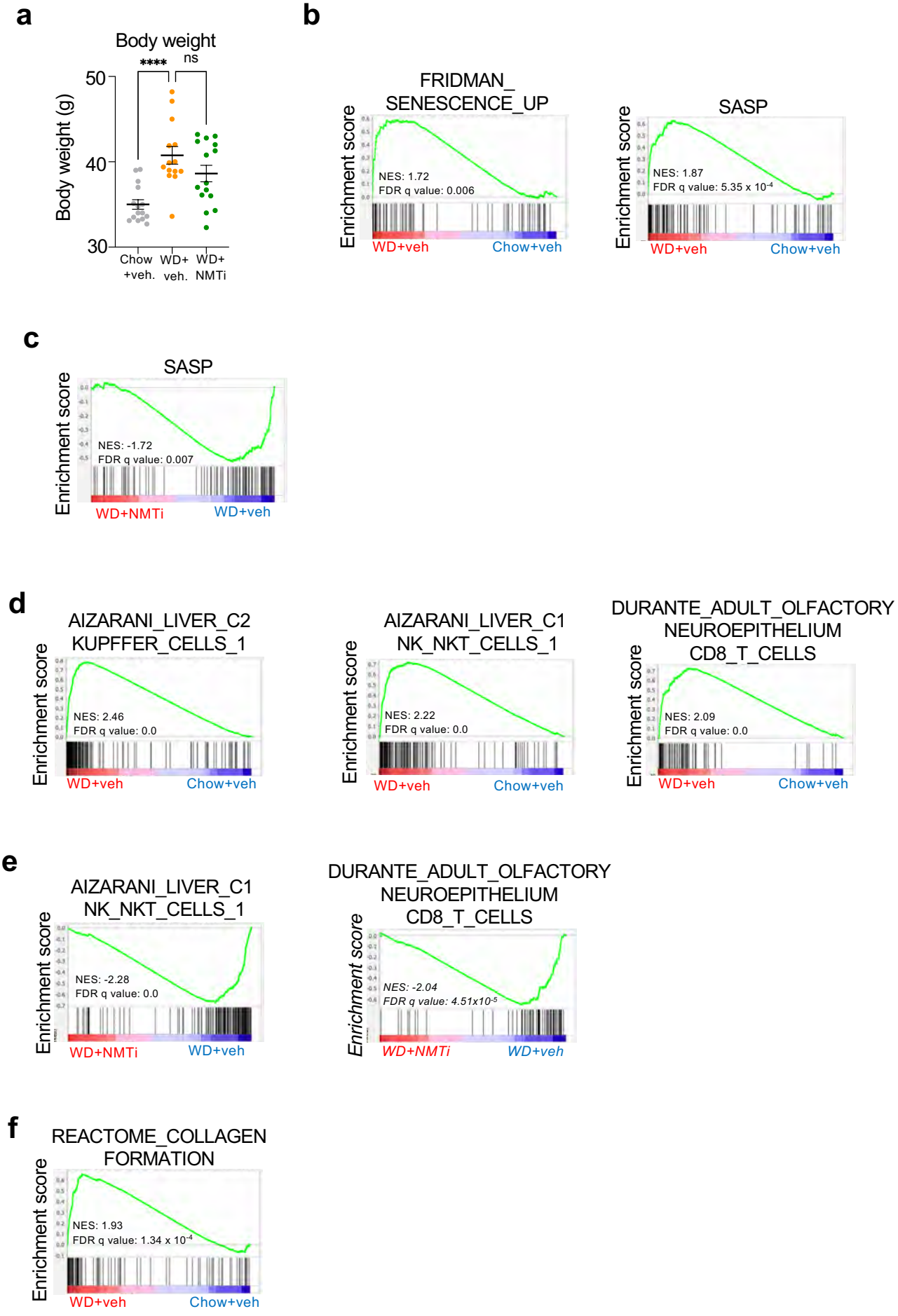
a
Body weight
****
ns
Body weight (g)
50
40
30
Chow +veh.
WD+ veh.
WD+ NMTi
b
FRIDMAN_ SENESCENCE_UP
Enrichment score
NES: 1.72
FDR q value: 0.006
WD+veh
Chow+veh
SASP
Enrichment score
NES: 1.87
FDR q value: 5.35 x 10-4
WD+veh
Chow+veh
c
SASP
Enrichment score
NES: -1.72
FDR q value: 0.007
WD+NMTi
WD+veh
d
AIZARANI_LIVER_C2 KUPFFER_CELLS_1
Enrichment score
NES: 2.46
FDR q value: 0.0
WD+veh
Chow+veh
AIZARANI_LIVER_C1 NK_NKT_CELLS_1
Enrichment score
NES: 2.22
FDR q value: 0.0
WD+veh
Chow+veh
DURANTE_ADULT_OLFACTORY NEUROEPITHELIUM CD8_T_CELLS
Enrichment score
NES: 2.09
FDR q value: 0.0
WD+veh
Chow+veh
e
AIZARANI_LIVER_C1 NK_NKT_CELLS_1
Enrichment score
NES: -2.28
FDR q value: 0.0
WD+NMTi
WD+veh
DURANTE_ADULT_OLFACTORY NEUROEPITHELIUM CD8_T_CELLS
Enrichment score
NES: -2.04
FDR q value: 4.51x10-5
WD+NMTi
WD+veh
f
REACTOME_COLLAGEN FORMATION
Enrichment score
NES: 1.93
FDR q value: 1.34 x 10-4
WD+veh
Chow+veh

SUPPLEMENTAL INFORMATION for

COPI vesicle formation and *N*-myristoylation are targetable vulnerabilities of senescent cells

Domhnall McHugh, Bin Sun, Carmen Gutierrez-Muñoz, Fernanda Hernández-González, Massimiliano Mellone, Romain Guiho, Imanol Duran, Joaquim Pombo, Federico Pietrocola, Jodie Birch, Wouter W. Kallemeijn, Sanjay Khadayate, Gopuraja Dharmalingam, Santiago Vernia, Edward W. Tate, Juan Pedro Martínez-Barbera, Dominic J. Withers, Gareth J. Thomas, Manuel Serrano, and Jesús Gil

Including 17 Supplemental Figures and their legends

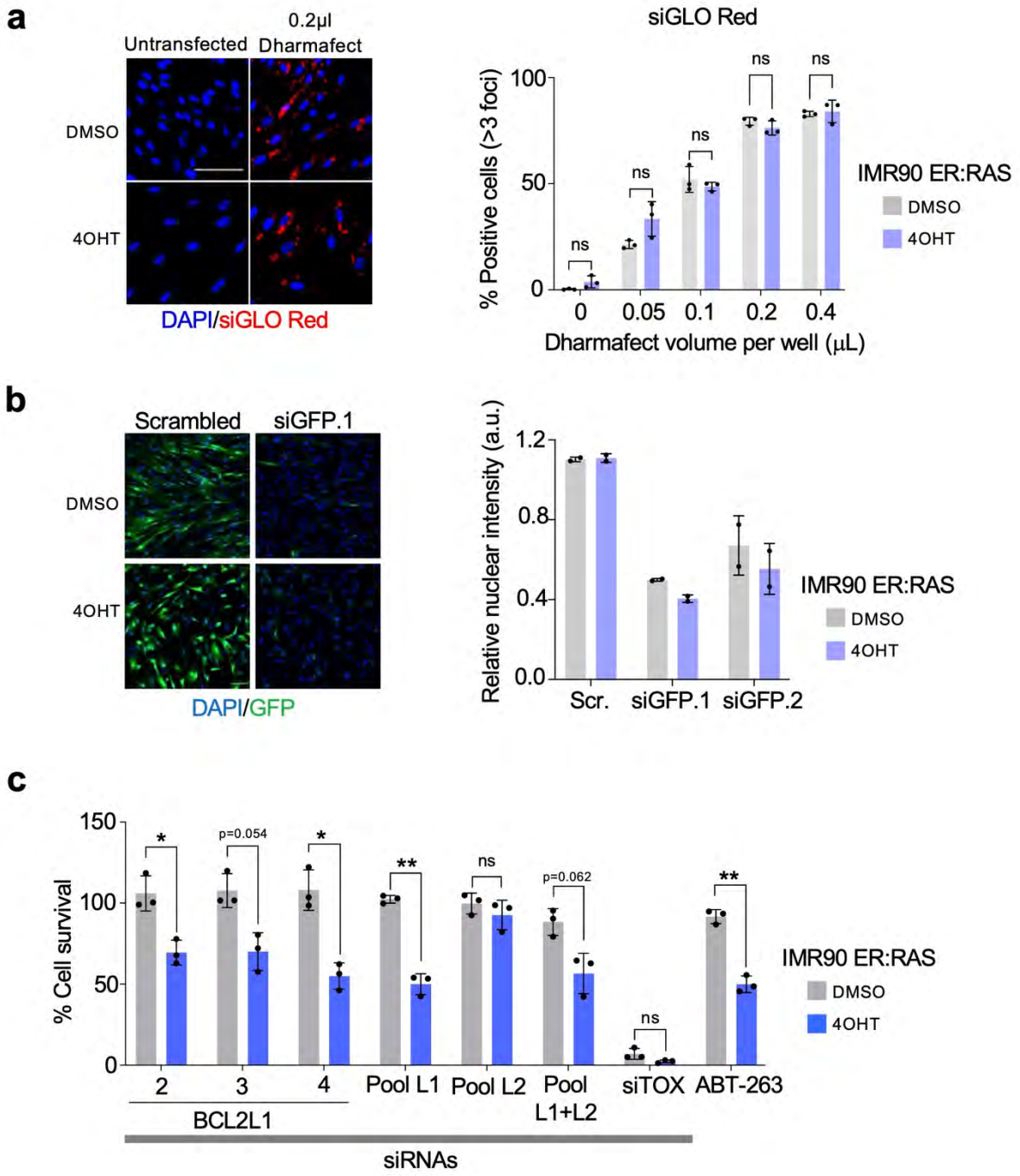

Supplemental Figure 1. Setting up RNAi screens for senolytic targets.a, Quantification of the percentage of cells with 3 or more cytoplasmic foci of fluorescent siGLO Red (Right) in control (DMSO) or senescent (4OHT) IMR90 ER:RAS cells 72h after reverse transfection at day 6 after senescence induction. Cells were transfected with varying volumes of Dharmafect 1 per well. Representative IF images are shown (left). (n=3). Scale bar, 100µm. **b,** Quantification of GFP nuclear intensity (right) relative to un-transfected control for control (DMSO) or senescent (4OHT) IMR90 ER:RAS cells 72h after reverse transfection with GFP siRNAs on day 6 post-

senescence induction cells. (n=2) Representative IF images shown (left). Scale bar, 100μm. **c,** Survival of control (DMSO) or senescent (4OHT) IMR90 ER:RAS cells 72h after reverse transfection with the indicated siRNAs on day 6 post-senescence induction. Pools of 4 individual siRNAs targeting BCL2L1 (pool L1), BCL2L2 (pool L2), or 4 siRNAs each against BCL2L1 and BC2L2 (pool L1+L2) were used. Treatment of cells with 1μM ABT-263 for 72 h starting 6 days after senescence induction was used as a senolytic control (ABT-263). (n=3). Data throughout the figure is represented as mean±SD. Statistical tests were performed using unpaired, student's t-test with holm-Šídák correction for multiple comparisons.

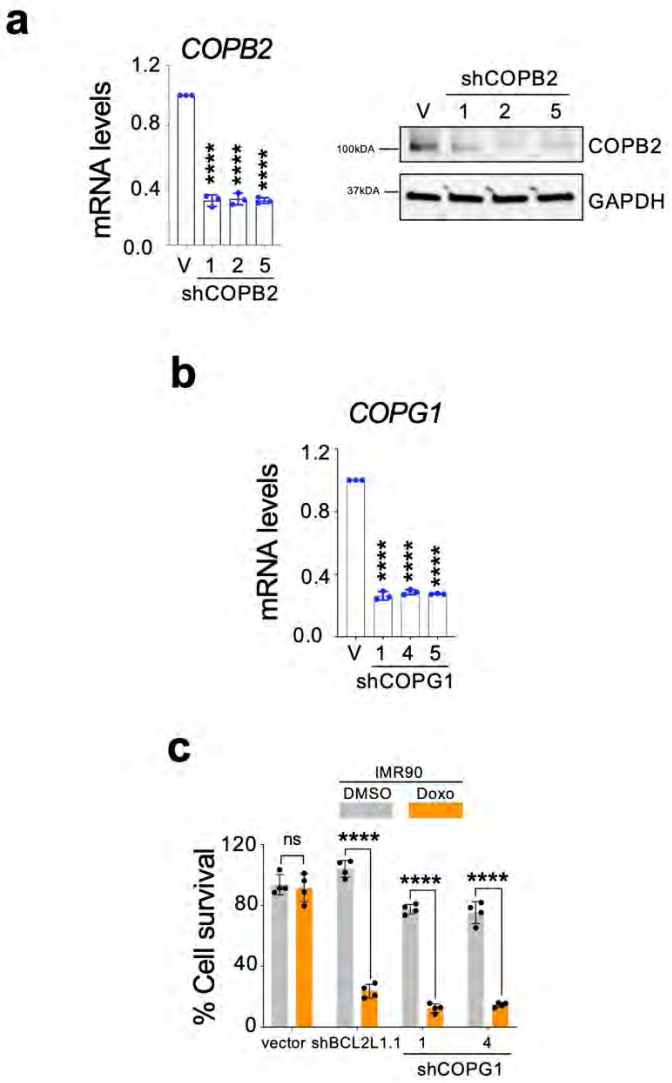

Supplemental Figure 2. Knockdown of COPB2 and COPG1 using shRNAs. a, Levels of COPB2 after knockdown with three independent shRNAs. (Left) qRT-PCR (n=3) One-way ANOVA, Dunnett's correction. (Right) Panel showing immunoblots representative of two independent experiments. Immunoblot of GAPDH is included as a loading control. **b,** Levels of COPG1 after knockdown with three independent shRNAs. (n=3). One-way ANOVA, Dunnett's correction. **c,** Quantification of cell survival of control (DMSO) and doxorubicin-induced senescent (Doxo) cells. (n=4) Unpaired Student's t-test. Data represented as mean±SD.

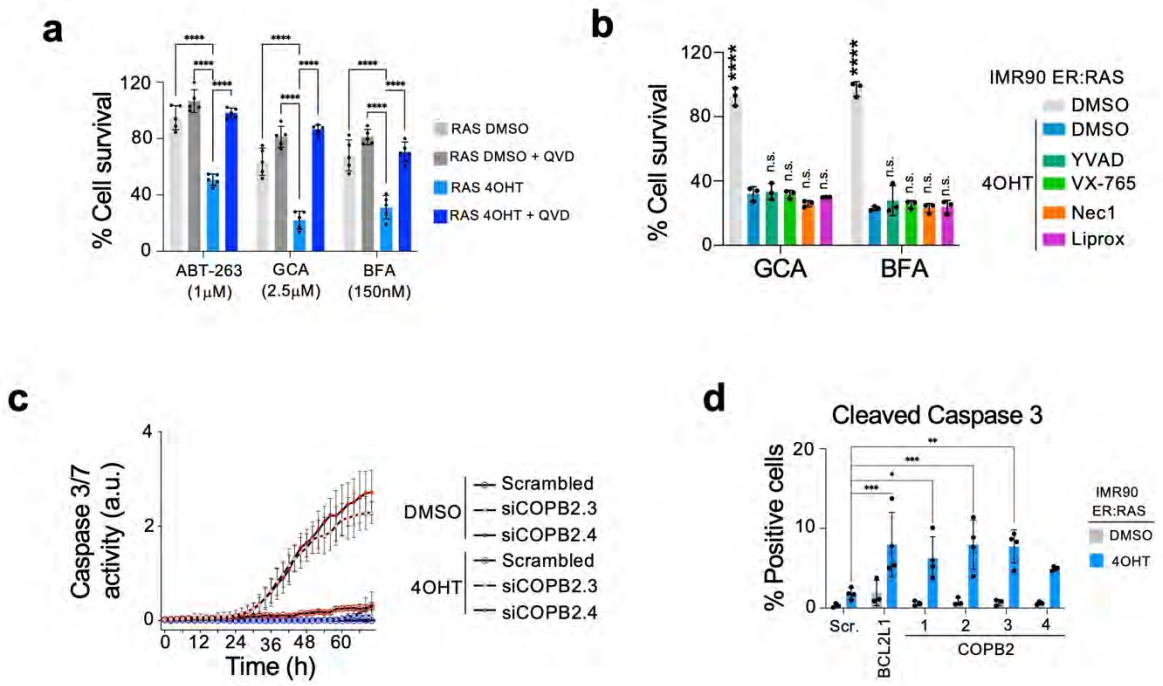

Supplemental Figure 3. COPI inhibition causes apoptosis in senescent cells. a, Quantification of percentage cell survival of control (DMSO) or senescent (4OHT) IMR90 ER:RAS cells treated in parallel with 20 μM of pan-caspase inhibitor (Q-VD-OPh) and either 1μM ABT-263, 2.5μM golgicide A (GCA) or 150nM brefeldin A (BFA) for 72h. (n=5). Ordinary Two-way ANOVA, Dunnett's Correction**. b,** Quantification of percentage cell survival of senescent (4OHT) treated in parallel with inhibitors to inhibit pyroptosis (10μM Z-YVAD-FMK, 20μM VX-765), necroptosis (10μM Nec-1) or ferroptosis i (1μM Liproxstatin) and either 2.5μM golgicide A (GCA) or 150nM brefeldin A (BFA) for 72h. (n=3). Comparisons are to the corresponding senescent cells treated with DMSO (blue bars). Ordinary Two-way ANOVA, Dunnett's correction. **c,** Caspase-3/7 activity in control (DMSO) or oncogene-induced senescent (4OHT) cells after reverse transfection with COPB2 siRNAs 6 days after senescence induction (n=2). **d,** Quantification of cells positive for cleaved caspase 3 as assessed by IF analysis (n=4). Unpaired, two-tailed, Student's t-test. Data is represented throughout the figure as mean ± SD.

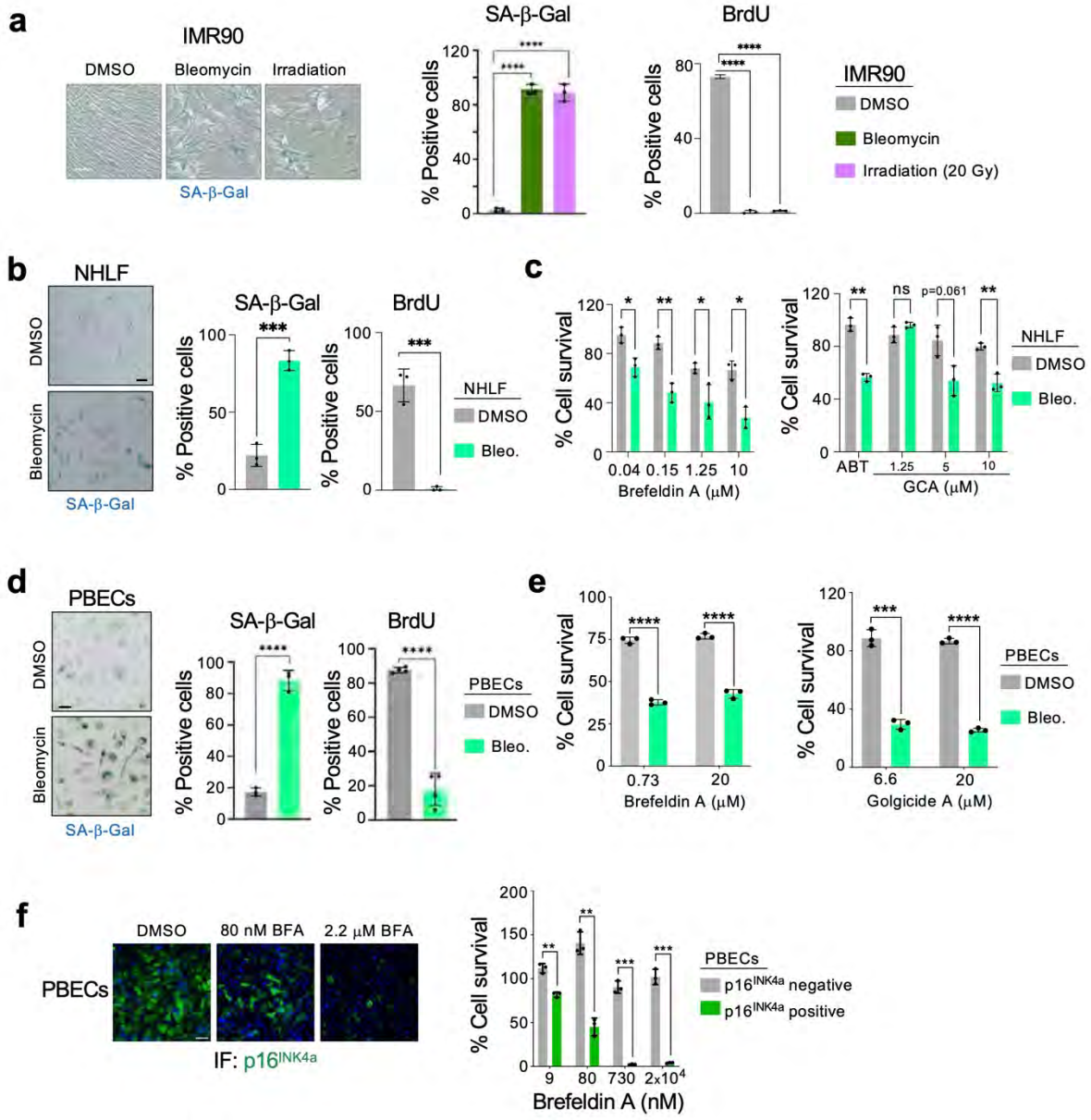

Supplemental Figure 4. GBF1 inhibitors are senolytic. a, Induction of senescence by bleomycin and irradiation in IMR90 cells. Quantification of the percentage of IMR90 cells positive for SA-β-gal staining (middle) or BrdU incorporation (right) 6 days after treatment of cells with 33 μM bleomycin or 20Gy Irradiation. (n=3). Representative image of SA-β-gal staining shown (left). Scale bar, 100μm. One-way ANOVA, Dunnett's correction. **b,** Bleomycin-induced senescence in NHLF cells. Quantification of the percentage of NHLF cells positive for SA-β-gal staining (middle) or BrdU incorporation (right) 6 days after treatment of cells with 50 μg/ml bleomycin (n=3). Representative image of SA-β-gal staining shown (left). Scale bar, 50μm. Unpaired, two-tailed Student's t-test. **c,** Percentage cell survival in either control (DMSO) or bleomycin-treated (Bleo) NHLF cells 72h after treatment on day 7 with brefeldin A (left)

or golgicide A (GCA, right). (n=3). Unpaired, two-tailed. Student's t-test. **d,** Bleomycin-induced senescence in PBECs. Quantification of the percentage of PBECs staining positive for SA-β-gal activity (middle) or BrdU incorporation (right) 6 days after treatment with 100ng/ml bleomycin (n=3). Representative image of SA-β-gal staining shown (left). Scale bar, 50μm. Unpaired, two-tailed. Student's t-test. **e,** Percentage cell survival in either control (DMSO) or bleomycin-treated (Bleo) PBECs 72h after treatment on day 7 with brefeldin A (left) or golgicide A (GCA, right). (n=3). Unpaired, two-tailed. Student's t-test. Data is represented throughout the figure as mean±SD. **f,** Quantification of percentage cell survival in either PBECs staining negative ($p16^{INK4a}$ negative) or positive ($p16^{INK4a}$ positive) for $p16^{Ink4a}$ 72h after treatment with brefeldin A (n=3). Representative images of $p16^{INK4a}$ IFs are shown (left). Unpaired, two-tailed. Student's t-test.

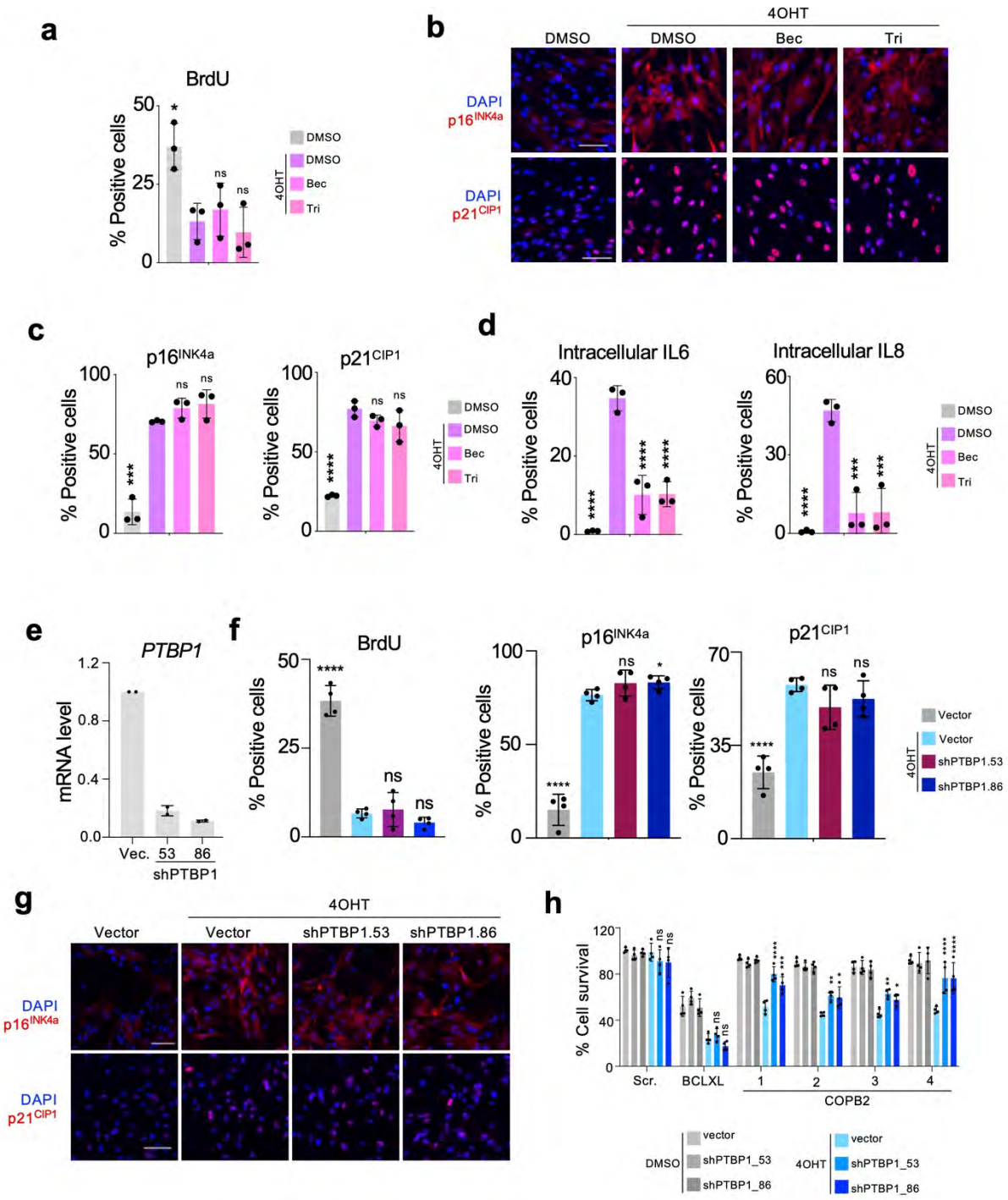

Supplemental Figure 5. Glucocorticoid treatment or PTBP1 depletion downregulate SASP without preventing the growth arrest associated with senescence. a Percentage of IMR90 ER:RAS cells positive for BrdU incorporation on day 6 post senescence induction. Cells were treated on day 4 with 10 μM beclomethasone (Bec) or on day 0 with 10 μM triamcinolone (Tri) (n=3). One-way ANOVA, Dunnett's correction. **b,** Representative immunofluorescence images of IMR90 ER:RAS cells treated with beclomethasone or triamcinolone, fixed and stained

6 days post-induction. Scale Bar, 100μm. **c,** Quantification of percentage cells positive for $p16^{INK4a}$ (left) and $p21^{CIP1}$ (right) on day 6 after senescence induction (n=3). Data represented as mean±SD. One-way ANOVA, Dunnett's correction.**d,** Percentage of cells positive for IL6 (Left) and IL8 (Right) on day 10 after senescence induction (n=3) One-way ANOVA, Dunnett's correction. **e,** Relative mRNA levels of PTPB1 on day 4 following transduction with shRNAs. (n=2). $p21^{CIP1}$**. f,** Percentage of cells positive for BrdU incorporation (left), $p16^{INK4a}$ (middle), or $p21^{CIP1}$ (right) on day 6 after senescence induction (n=4). Doxycycline was added on day 0 to induce shRNAs. One-way ANOVA, Dunnett's correction. **g,** Representative IF images of cells from the experiment described in e-f. Scale Bar, 100μm. **h,** SASP inhibition caused by the knockdown of PTBP1 prevents the senolysis induced by COPB2 depletion. Quantification of cell survival of senescent (4OHT) and control (DMSO) IMR90 ER:RAS cells infected with the indicated shRNAs (n=4). Data represented as mean±SD. *$p < 0.05$, **$p < 0.01$, ***$p < 0.001$. Statistical comparisons of 4OHT Vector vs. 4OHT shPTBP1 shRNAs are shown. Two-way ANOVA, Dunnett's correction. Data throughout the figure is represented as mean ± SD.

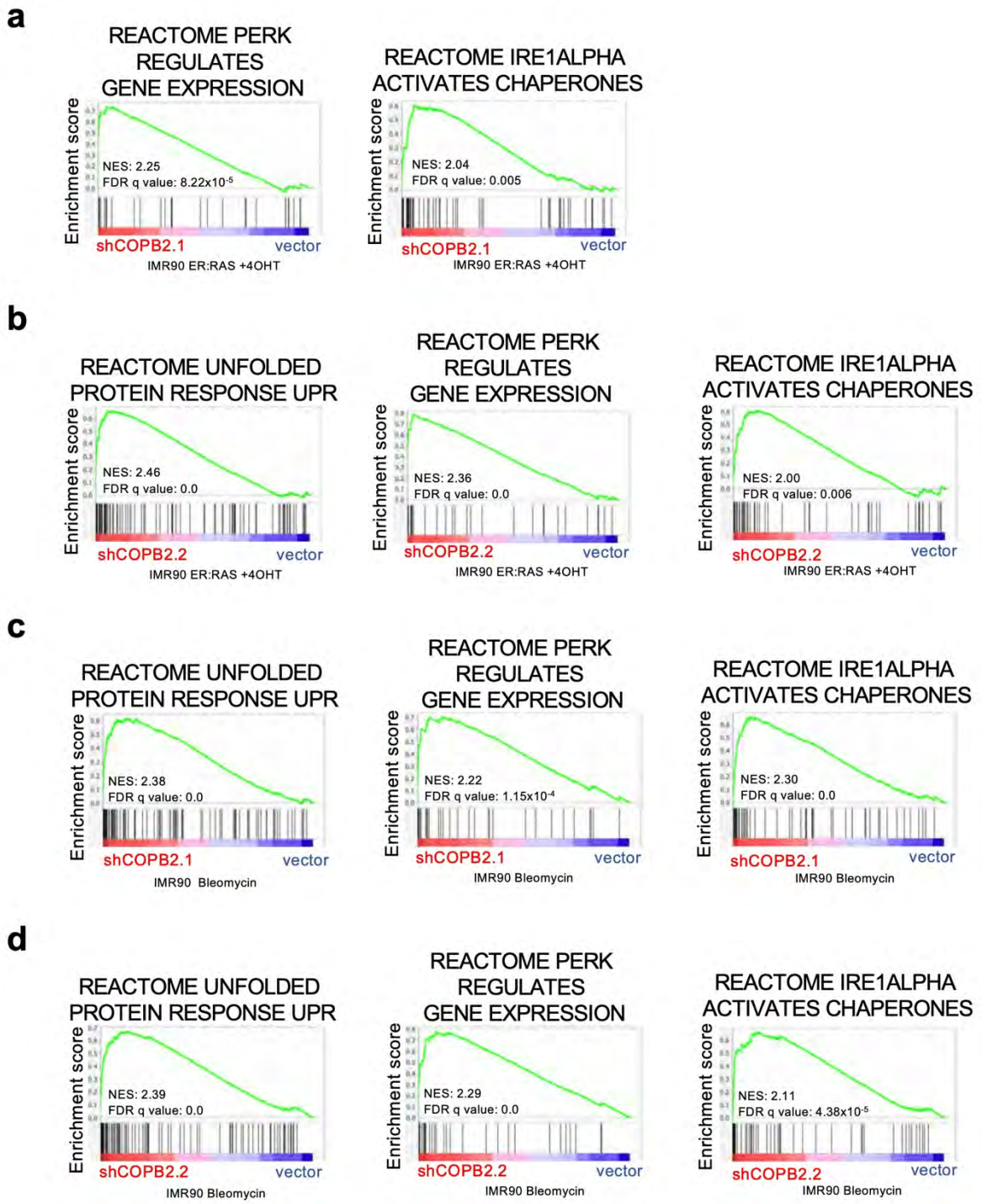

Supplemental Figure 6. COPB2 depletion activates the unfolded protein response. a-b, GSEA plot showing enrichment of the indicated signatures after COPB2 knockdown with either shCOPB2.1 (a) or shCOPB2.2 (b) in senescent IMR90 ER:RAS cells. **c-d,** GSEA plot showing enrichment of the indicated signatures after COPB2 knockdown with either shCOPB2.1 (a) or shCOPB2.2 (b) in IMR90 cells undergoing bleomycin-induced senescence. NES, normalized enrichment score; FDR, false discovery rate.

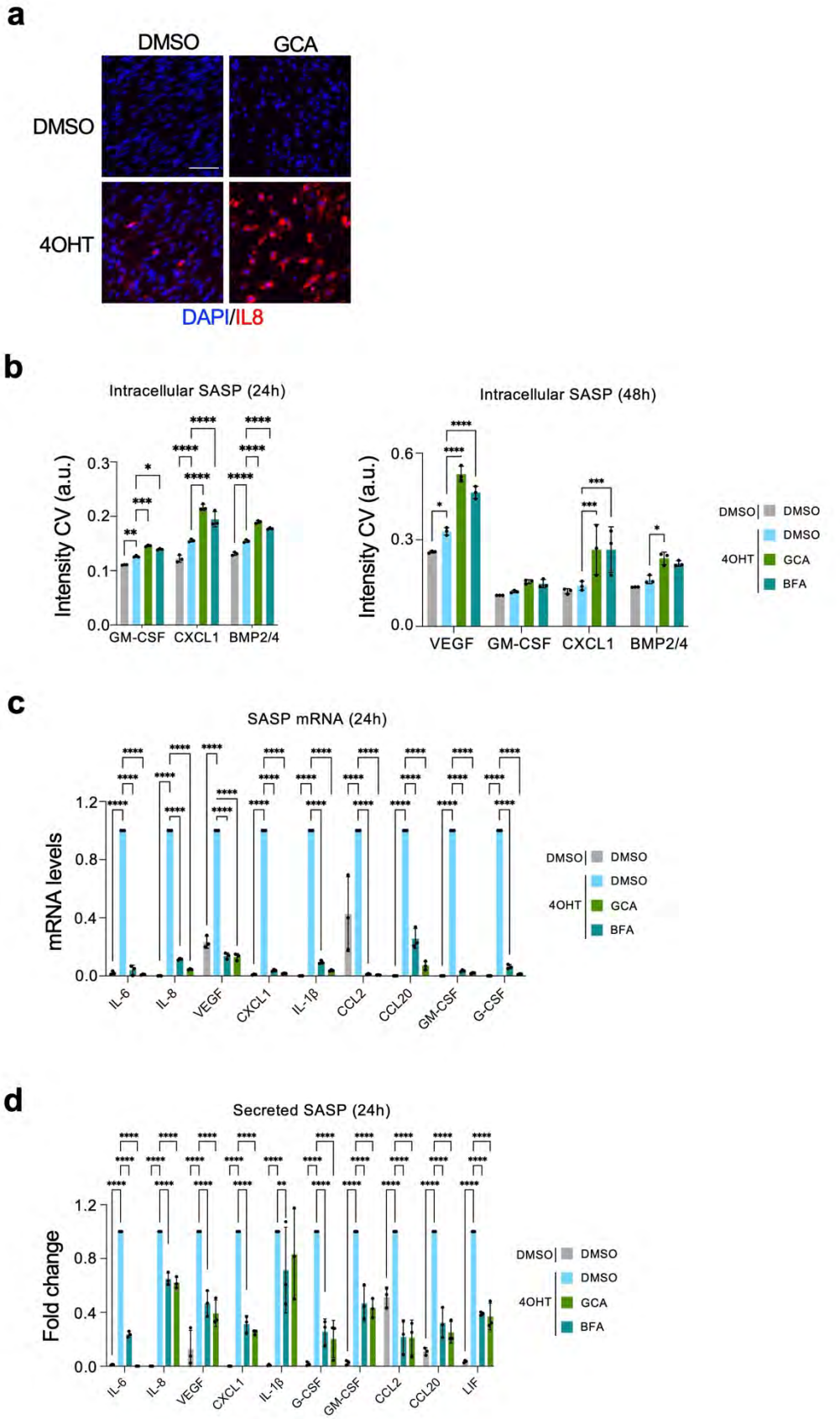

Supplemental Figure 7. Effect of GBF1 inhibitors on SASP production, secretion, and intracellular accumulation. a, Representative IF images showing IL8

staining of either control (DMSO) or senescent (4OHT) IMR90 ER:RAS cells, 48h after treatment with 1.25μM golgicide A (GCA). Scale bar, 100μm. **b,** Quantification of intracellular levels of SASP factors as assessed by IF at either 24h (left) or 48h (right) following treatment of day 7 IMR90 ER:RAS cells with either 1.25μM golgicide A (GCA) or 150nM brefeldin A (BFA). (n=3). Two-way ANOVA, Dunnett's correction. **c,** Quantification of mRNA levels for the indicated SASP factors 24h after treatment of day 7 IMR90 ER:RAS with either 1.25μM golgicide A (GCA) or 150nM brefeldin A (BFA). (n=3). Two-way ANOVA, Dunnett's correction. **d,** Fold change (referred to senescent cells) of secreted SASP levels 24h after treatment of day 7 IMR90 ER:RAS with either 1.25μM golgicide A (GCA) or 150nM brefeldin A (BFA). (n=3) as quantified by ELISA. Two-way ANOVA, Dunnett's correction. Data throughout the figure are represented as mean±SD.

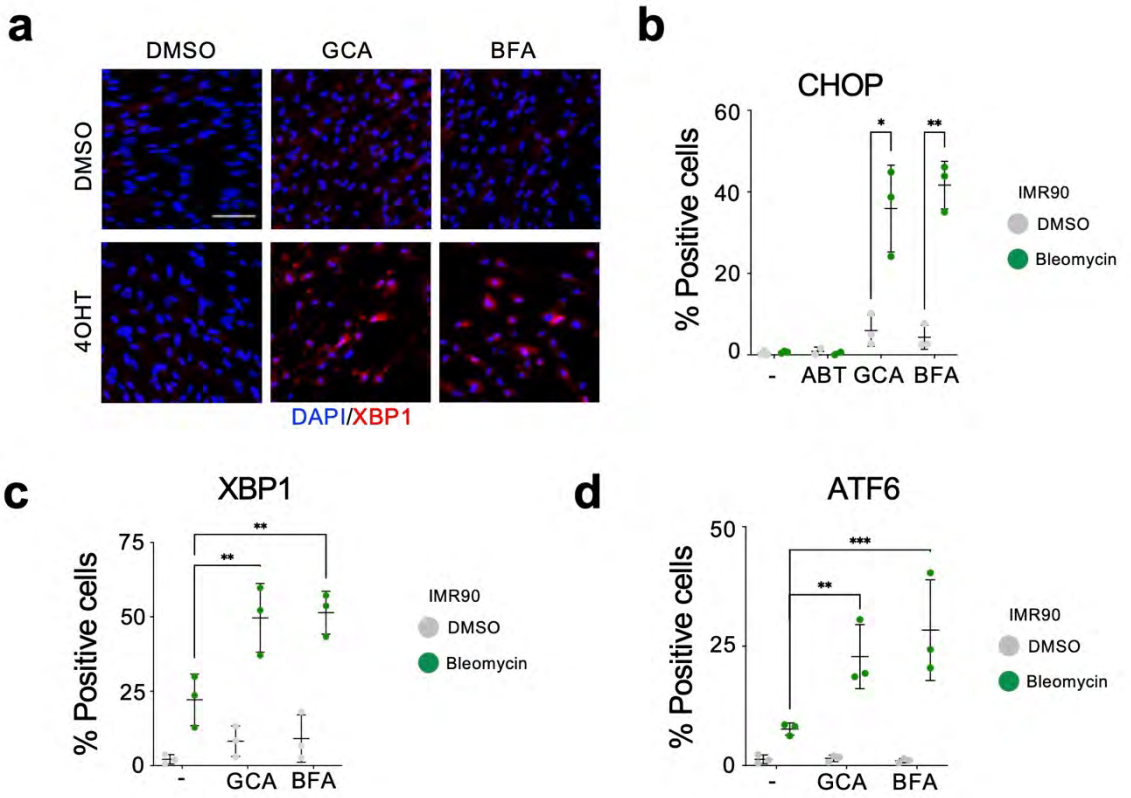

Supplemental Figure 8. COPI inhibition results in an unfolded protein response in cells undergoing bleomycin-induced senescence. a, Representative IF images of XBP1 staining in either control (DMSO) or senescent (4OHT) IMR90 ER:RAS cells treated with either 1.25μM golgicide A (GCA) or 150nM brefeldin A (BFA) for 48h. Scale bar, 100μm. **b-d,** Quantification of percentage of positive cells staining for nuclear CHOP (b), XBP1 (c), or ATF6 (d) in control (DMSO) or therapy induced senescent (Bleomycin) IMR90 cells treated on day 7 for 48h with either 1.25μM golgicide A (GCA) or 150nM brefeldin A (BFA) for 48h. (n=3, CHOP + ABT-263, n=2) Unpaired, two-tailed Student's t-test. Data represented as mean ± SD.

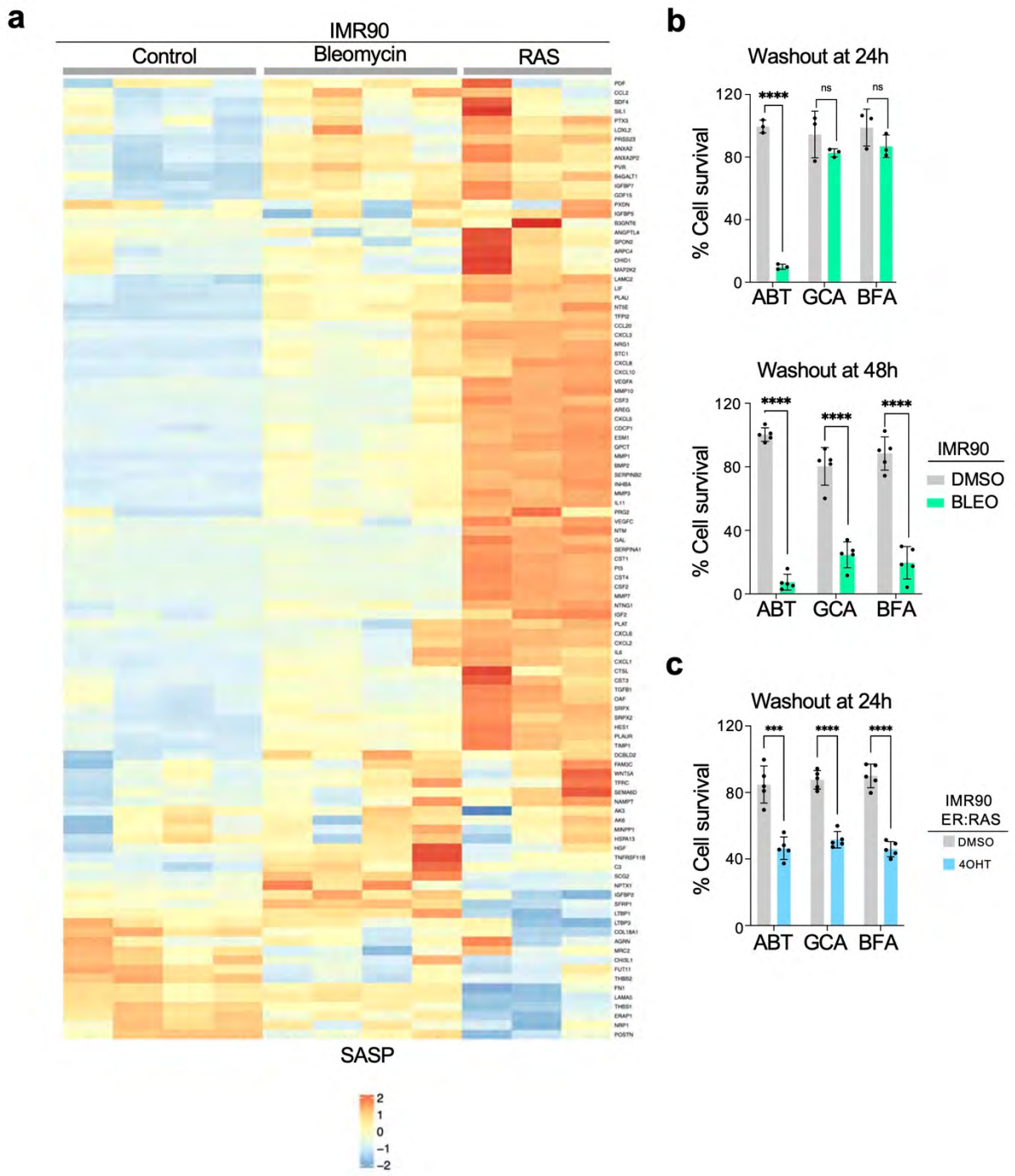

Supplemental Figure 9. Washout experiments with GBF1 inhibitors. a Heatmap showing expression of SASP factors in control (DMSO), oncogene-induced senescent (4OHT), and therapy induced senescence (BLEO) IMR90 cells. Data are shown as row z-score normalized. **b,** Percentage cell survival of control (DMSO) or bleomycin-treated (BLEO) IMR90 cells treated with 1μM ABT-263 (ABT), 2.5μM golgicide A (GCA) and 150nM brefeldin A (BFA) on day 7 post-induction for 24h (top) or 48h (bottom) followed by drug washout and fixation 72h after initial treatment. (n=5). Unpaired, two-tailed Student's t-test**. c,** Percentage cell survival of control (DMSO) or

senescent (4OHT) IMR90 ER:RAS cells treated with 1μM ABT-263 (ABT), 2.5μM golgicide A (GCA) and 150nM brefeldin A (BFA) on day 7 post-induction for 24h, followed by drug washout and fixation 72h after initial treatment. (n=5). Unpaired, two-tailed Student's t-test. Data represented as mean ± SD.

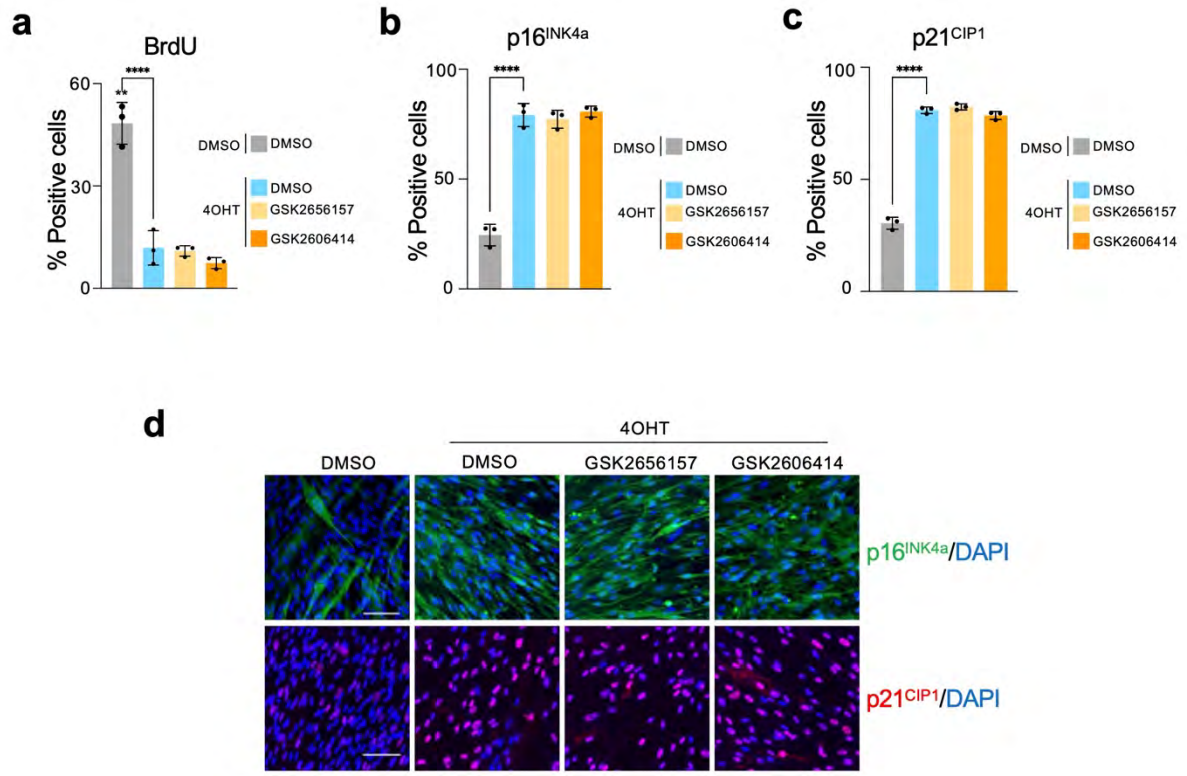

Supplemental Figure 10. Effect of PERK inhibitors on senescence. a-c, Quantification of BrdU (a), $p16^{INK4a}$ (b), and $p21^{CIP1}$ (c) staining by IF of either control (DMSO) or senescent (4OHT) IMR90 ER: RAS cells treated with either 1μM GSK2656157 or 1μM GSK2606414 on day 4 post senescence induction. Cells were fixed 6 days post senescence induction. (n=3) One-way ANOVA, Dunnett's Correction. Data represented as mean ± SD. **d,** Representative IF images of cells of the experiment described in a-c. Scale Bar, 100μm.

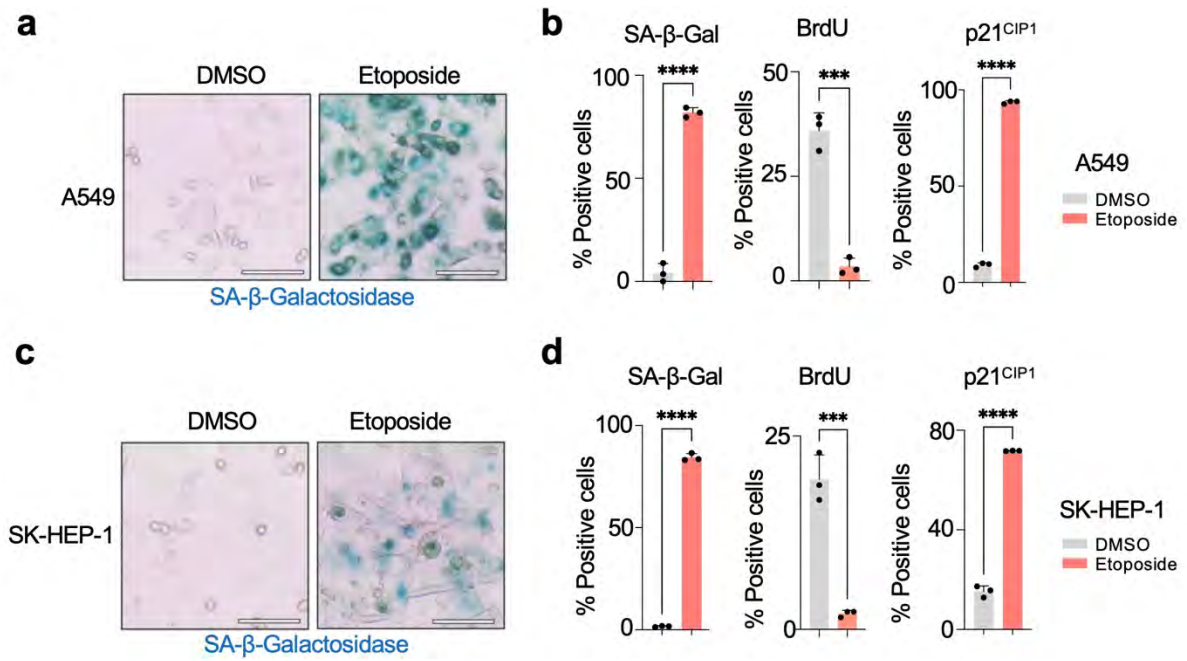

Supplemental Figure 11. Induction of senescence in A549 and SK-HEP-1 cells. **a,** Representative images of SA-β-gal staining in control (DMSO) or therapy-induced senescent (Etoposide) A549 cells 6 days after treatment with etoposide. Scale bar, 100μm. **b,** Quantification of percentage positive control (DMSO) or therapy induced senescent (etoposide) A549 cells for SA-β-gal staining (left), BrdU incorporation (middle) or $p21^{CIP1}$ staining s(right) on day 6. (n=3). Unpaired, two-tailed Student's t-test. **c,** Representative images of SA-β-gal staining in control (DMSO) or therapy-induced senescent (Etoposide) SK-HEP-1 cells 6 days after treatment with etoposide. Scale bar, 100 μm. **d,** Quantification of percentage positive control (DMSO) or therapy-induced senescent (Etoposide) SK-HEP1 cells for SA-β-gal staining (left), BrdU incorporation (middle) or $p21^{CIP1}$ staining s(right) on day 6. (n=3). Unpaired, Student's t-test. Data represented as mean ± SD.

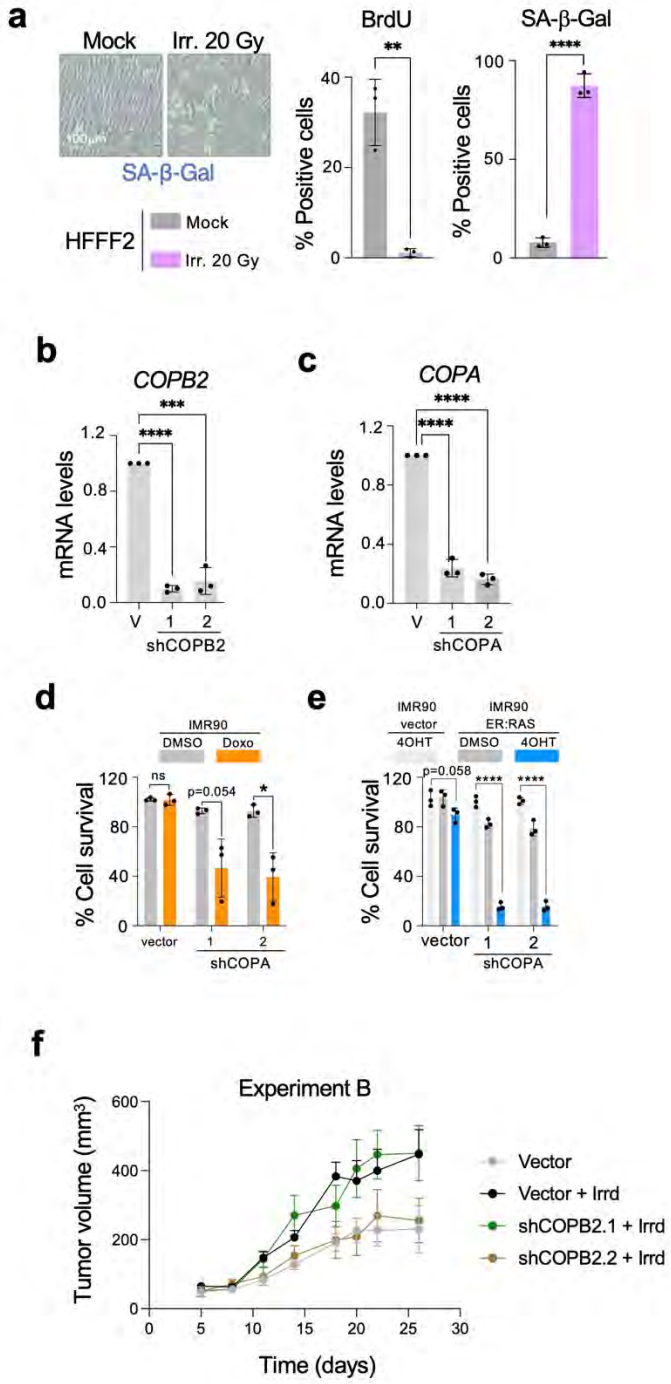

Supplemental Figure 12. Irradiation causes senescence in HFFF2 cells. a, Representative images of SA-β-gal staining (left) in either control (Mock) or irradiation-induced senescent (Irr. 20Gy) HFFF2 cells. Quantification of percentage cells positive for BrdU incorporation (middle) or SA-β-gal staining (right) is shown. (n=3). Unpaired, two-tailed Student's t-test. **b-c,** Relative mRNA levels of COPB2 (b) and COPA (c) following transduction of HFFF2 cells with the corresponding shRNAs again each. (n=3) One-way ANOVA, Dunnett's correction. **d,** Quantification of percentage cell survival in either control (DMSO) or therapy-induced senescent (Doxo). IMR90 cells

following transduction with inducible shRNAs against COPA. shRNAs were induced 7 days after induction of senescence and cells fixed 10 days after doxycycline addition. (n=3) Unpaired, two-tailed Student's t-test. **e,** Senolytic activity of COPA depletion during OIS in IMR90 ER: RAS cells (n=3). shRNAs were induced 7 days after induction of senescence and cells fixed 10 days after doxycycline addition. (n=3) Unpaired, two-tailed Student's t-test**. f,** Tumor growth curves of a second experiment (Experiment B) showing the tumour volume monitored over time (IR=irradiation). Data represented as mean ± SEM for all mice in each group. (n=7 per group). This experiment and the one shown in Fig 5e (Experiment A) were pooled in the analysis shown in Extended Data Figure 5d. Data represented as mean ± SD throughout the figure unless otherwise stated.

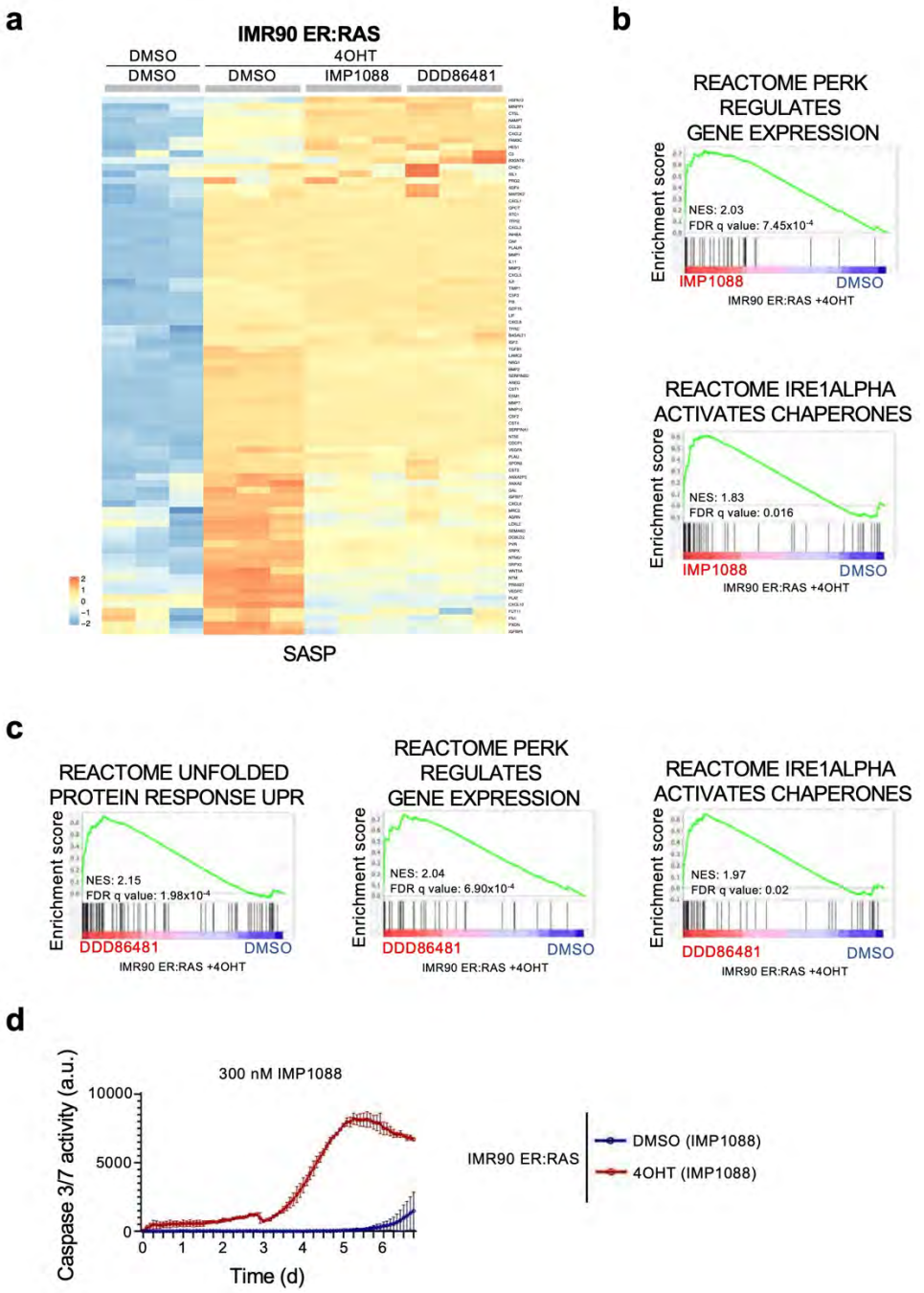

Supplemental Figure 13. NMT inhibitors are senolytic. a, Heatmap showing expression of SASP factors in either control (DMSO) or senescent (4OHT) IMR90 ER:RAS cells treated with 300nM IMP1088 or 1.5μM DDD86481. Data displayed as row-z-score normalized. **b-c,** GSEA plot showing enrichment of the indicated signatures in senescent cells treated with 300nM IMP1088 (b) or 1.5μM DDD86481 (c). NES, normalized enrichment score; FDR, false discovery rate. **d,** Caspase-3/7 activity in control (DMSO) or oncogene-induced senescent (4OHT) cells after treatment with DMSO or 300nM IMP1088. Measures start 7 days after senescence induction (n=2).

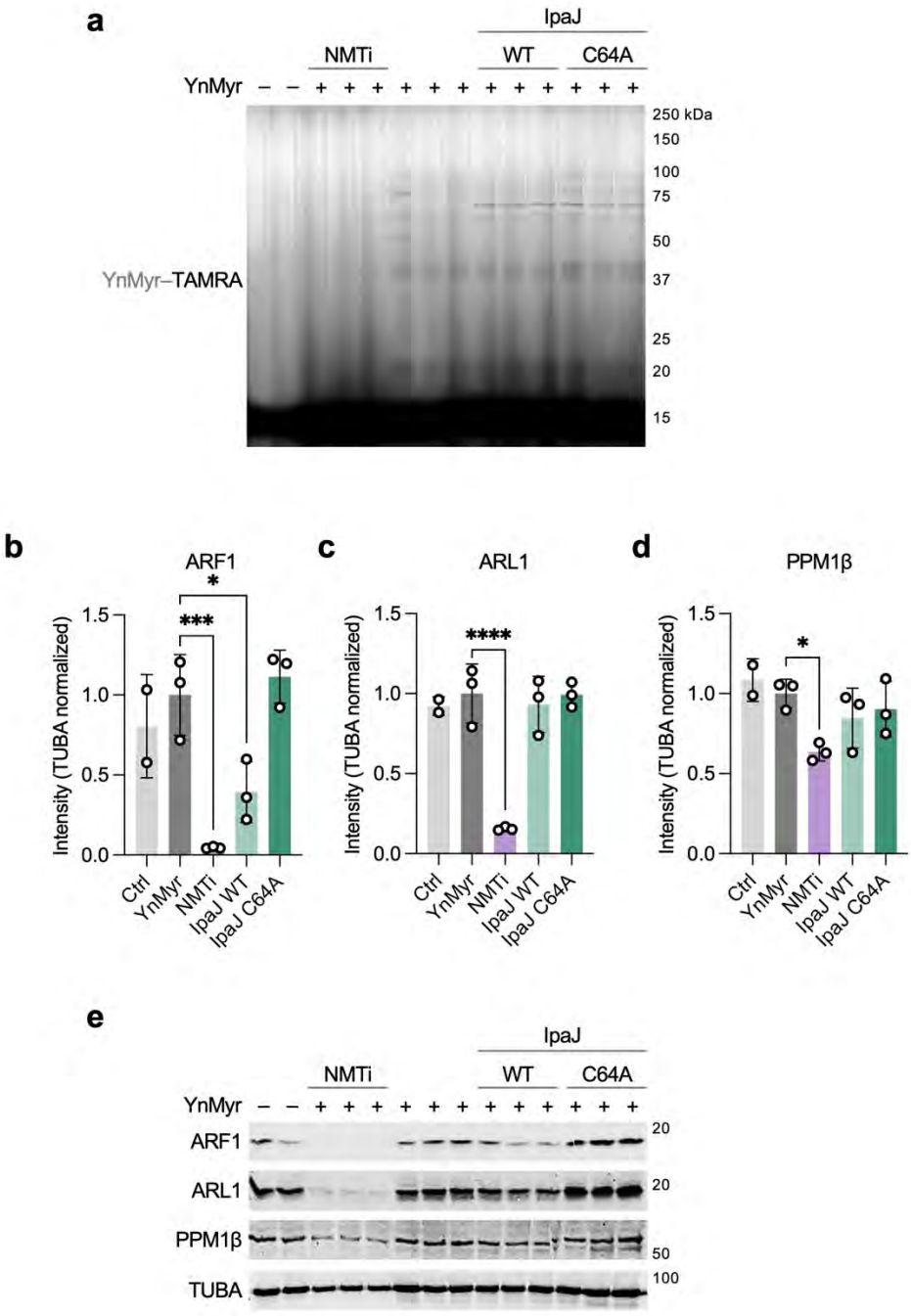

Supplemental Figure 14. Expression of IpaJ wt targets ARF1. a, In-gel visualization of the effect of NMTi (IMP-1088), IpaJ wild-type (WT), and inactive mutant (C64A) on N-myristoylation of proteins with YnMyr. **b-d,** Densitometric intensity quantified of ARF1 (b), ARL1 (c), and PPM1b (d) normalized to TUBA levels. Ordinary One-way ANOVA, Dunnett's correction. (n=2 independent samples for controls, n=3 independent samples for all other groups). Data represented as mean±SD. **e,** Immunoblots of ARF1, ARL1, PPM1B, and TUBA were used for the quantification shown in b-d. Immunoblot of TUBA is included as a sample processing control.

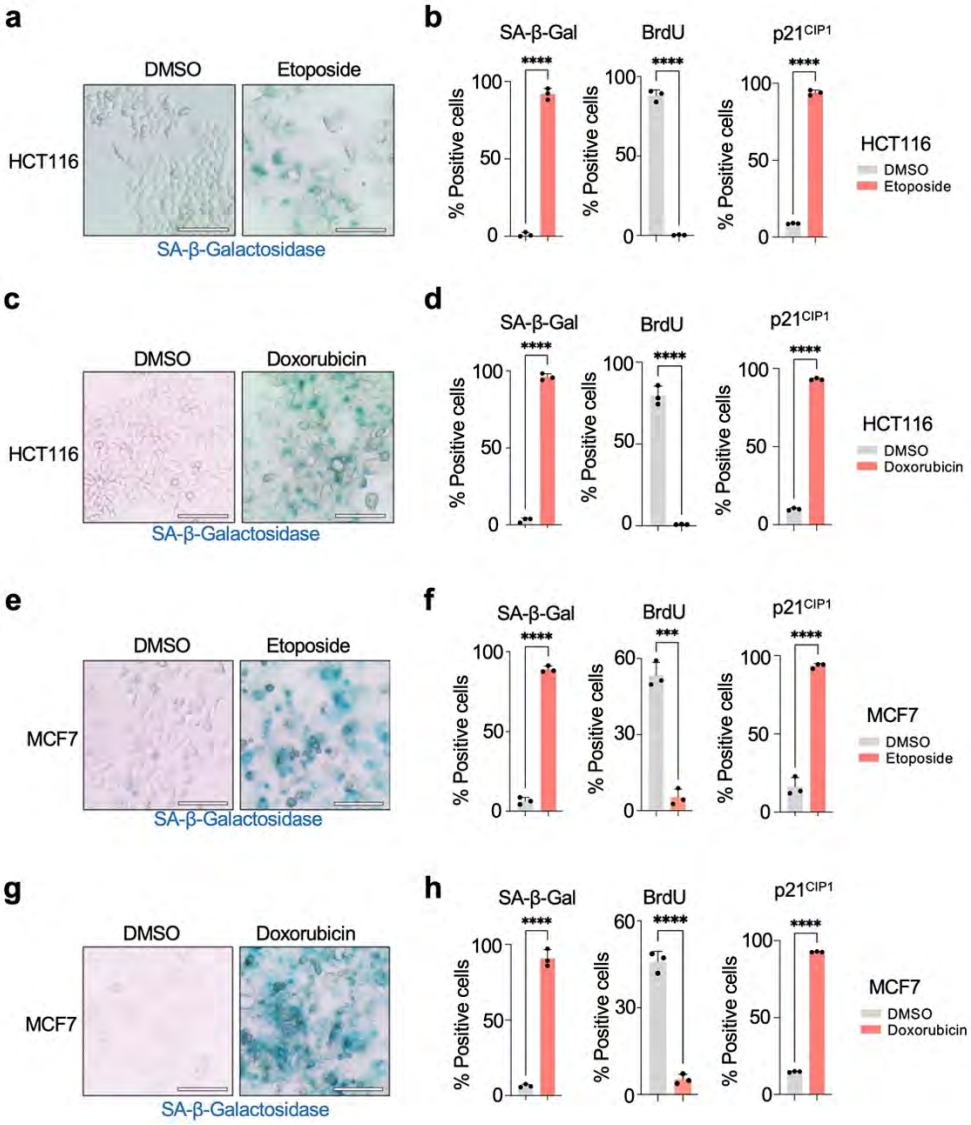

Supplemental Figure 15. Induction of senescence in HCT116 and MCF7 cancer cells. a, c, Representative images of SA-β-gal staining in HCT116 cells 6 days after treatment with DMSO (control, a and c), etoposide (a), or doxorubicin (c). Scale bar, 100μm. **b, d,** Quantification of percentage positive control (DMSO) or therapy-induced senescent (etoposide, b or doxorubicin, d) HCT116 cells for SA-β-gal staining (left), BrdU incorporation (middle) or $p21^{CIP1}$ staining (right) on day 6. (n=3). Unpaired, two-tailed Student's t-test. Data represented as mean±SD. **e, g,** Representative images of SA-β-gal staining in MCF7 cells 6 days after treatment with DMSO (control, e, and g), etoposide (e), or doxorubicin (g). Scale bar, 100μm. **f, h,** Quantification of percentage positive control (DMSO) or therapy-induced senescent (etoposide, f or doxorubicin, h) MCF7 cells for SA-β-gal staining (left), BrdU incorporation (middle) or $p21^{CIP1}$ staining (right) on day 6. (n=3). Unpaired, two-tailed Student's t-test. Data represented as mean ± SD.

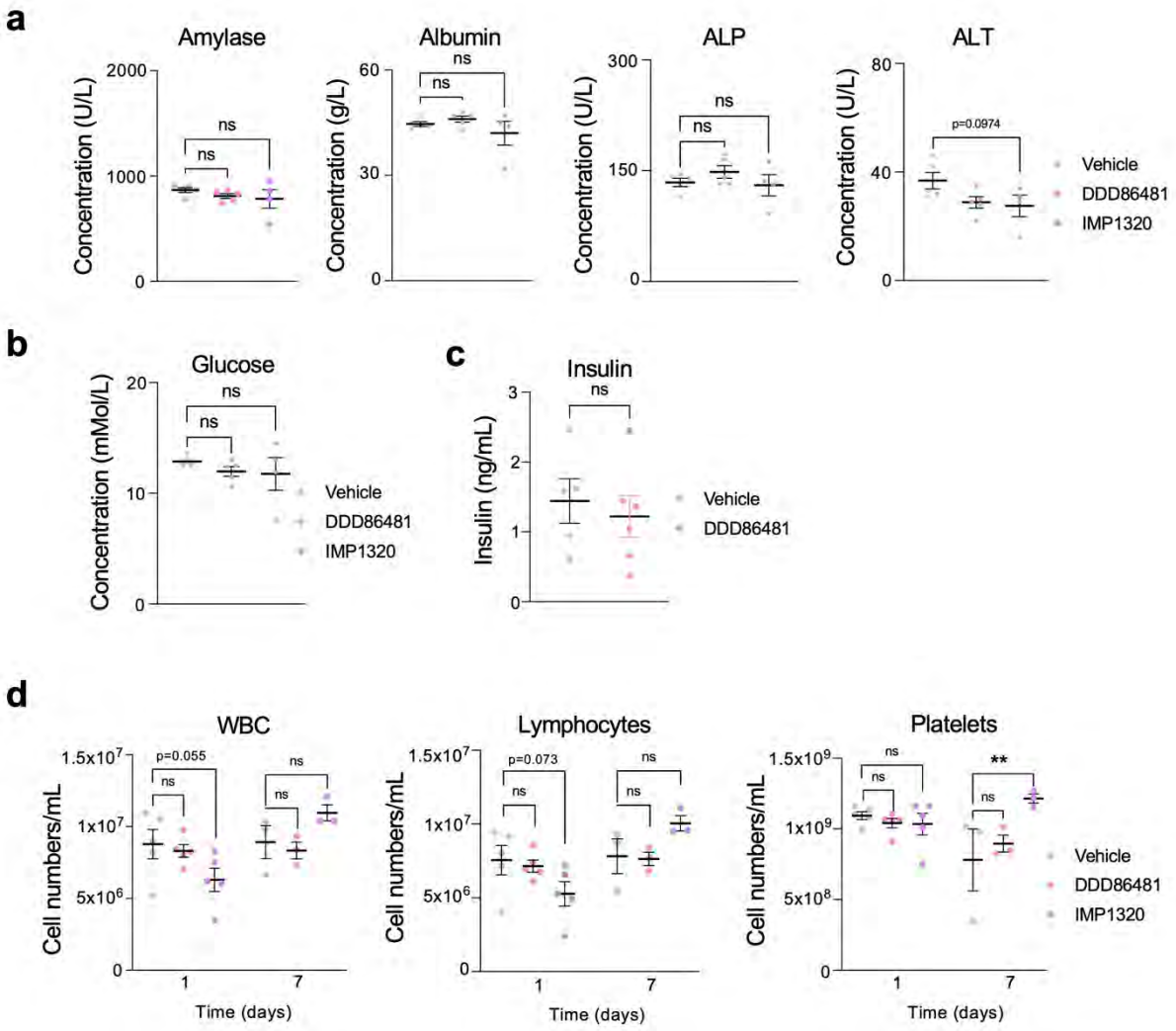

Supplemental Figure 16. NMTi are well tolerated *in vivo*. a Analysis of markers of liver function for C57/BL6 mice given 1 round of treatment with 10mg/kg DDD86481 or 25 mg/kg IMP1320. Blood was collected 7 days after. (n=5 mice for Vehicle and DDD86481, n=4 mice for IMP1320). One-way ANOVA, Dunnett's correction. **b,** Blood glucose levels for C57/BL6 mice given 1 round of treatment with 10mg/kg DDD86481 or 25 mg/kg IMP1320 and blood collected 7 days after. (n=5 mice for Vehicle and DDD86481, n=4 mice for IMP1320). One-way ANOVA, Dunnett's correction. **c,** Blood insulin levels for C57/BL6 mice given 1 round of treatment with 10mg/kg DDD86481 or 25 mg/kg IMP1320 and blood collected 7 days after. (n=5 mice for Vehicle, n=6 mice for DDD86481) Unpaired, Student's t-test. **d,** Blood cell counts for C57/BL6 mice given 1 round of treatment with 10mg/kg DDD86481 or 25 mg/kg IMP1320 and blood collected 1 and 7 days after. (n=3-5 mice per group). Two-way ANOVA, Dunnett's correction. Data represented as mean ± SD

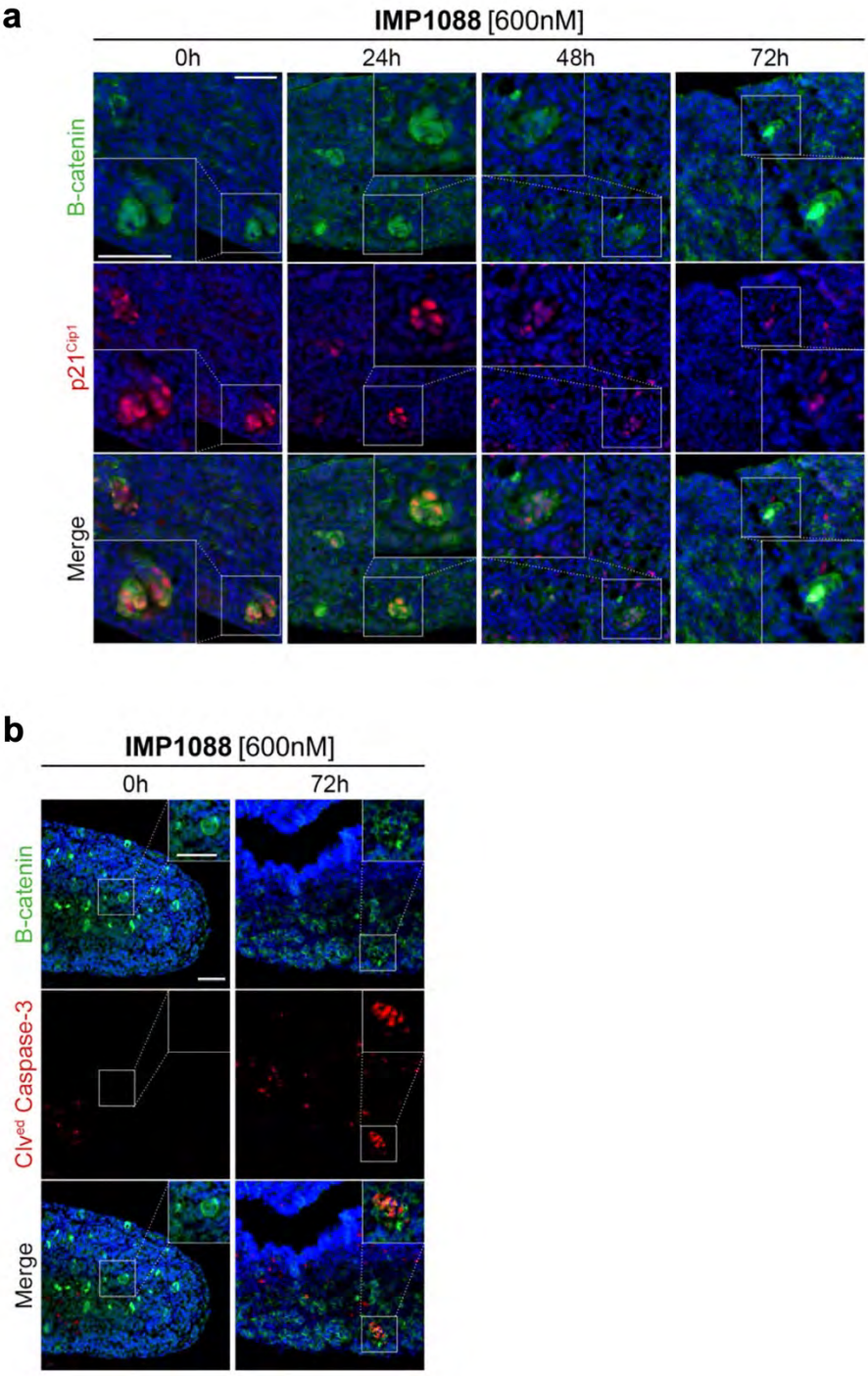

Supplemental Figure 17. Treatment with NMT inhibitors kills β-catenin-positive senescent clusters in a mouse model of adamantinomatous craniopharyngioma (ACP). a, Immunofluorescence staining against βcatenin (green) and $p21^{Cip1}$ (red). Main scale bar, 50μm - Insert scale bar, 40μm. **b,** Immunofluorescence staining against βcatenin (green) and cleaved caspase-3 (red) shows that an oncogene-induced senescent βcatenin-positive cluster of cells is undergoing apoptosis. Main scale bar, 50μm. Insert scale bar, 40μm.